Rochester Institute of Technology
RIT Digital Institutional Repository

Theses

1977

A digital signal processing system developed for the optimal use of high density magnetic storage media

Victor Hernandez

Follow this and additional works at: https://repository.rit.edu/theses

Recommended Citation
Hernandez, Victor, "A digital signal processing system developed for the optimal use of high density magnetic storage media" (1977). Thesis. Rochester Institute of Technology. Accessed from

This Thesis is brought to you for free and open access by the RIT Libraries. For more information, please contact repository@rit.edu.

A DIGITAL SIGNAL PROCESSING SYSTEM DEVELOPED FOR THE OPTIMAL USE OF HIGH DENSITY MAGNETIC STORAGE MEDIA

by

Victor M. Hernandez

A Thesis Submitted

in

Partial Fulfillment

of the

Requirements for the Degree of

MASTER OF SCIENCE

in

Electrical Engineering

Approved by:

Prof. Harvey E. Rhody
(Thesis Advisor)

Prof. Illegible Signature

Prof. Swaminathan Madhu

Prof. James E. Palmer
(Head of Dept.)

DEPARTMENT OF ELECTRICAL ENGINEERING
COLLEGE OF ENGINEERING
ROCHESTER INSTITUTE OF TECHNOLOGY
ROCHESTER, NEW YORK
JUNE, 1977

COPYRIGHT

Victor Manuel Hernandez

1977

To my wife and son

ACKNOWLEDGEMENT

I wish to thank Dr. William Feldman, Director of the Kodak Apparatus Division Research Laboratory, and Mr. Gareth Lloyd, Supervisor of the Electronics Research Team, for permitting the use of parts of the material in this report and for allowing the use of some of the facilities of the Research Laboratory.

I also would like to express my appreciation to Dr. Harvey Rhody, my thesis advisor, for his technical suggestions and consultation; Dr. Joseph Jastrzembski, for his support and advise; and Dianne, my wife, for her assistance in drafting and compiling this thesis.

G924297

TABLE OF CONTENTS

		Page
Acknowledgements		iv
Table of Contents		v
List of Figures		vii
List of Symbols		x
Abstract		xii
Historical Review		xiii
Chapter I	Introduction	1
Chapter II	Delta Modulation	5
	General Characteristics	6
	Quantizing Noise in Delta Modulation	10
	Hardware Implementaion	13
	Experimental Results	16
Chapter III	Encoding and Decoding	23
	General Considerations	24
	Selecting a Code	24
	AMC Encoding	27
	AMC Decoding	30
	Experimental Results	33
Chapter IV	Time Base Error	46
	Source of Error	47
	Analysis of Time Base Error	51

		Page
	The Perceptability of Flutter	58
	Hardware Description	62
	Experimental Results	73
Chapter V	The Channel	82
	Direct Record-Reproduce Process	83
	Bias	86
	High Frequency Response	91
	Analysis of Record-Reproduce Process	95
	Implementation of the Channel	100
	Experimental Results	101
	Total Available Channel Capacity	101
Chapter VI	Conclusion	113
	Summary of the Thesis	114
	Contributions of the Thesis	115
	Suggestions for Further Research	116
Appendix	Decoding Phase-Locked Loop	118
	General Considerations	119
	Specifications	121
	PLL Analysis	123
	Experimental Results	125
Bibliography		131

LIST OF FIGURES

Figure No.		Page
1	Theoretical Delta Modulator	7
2	Description of the Theoretical Delta Modulator	7
3	Slope limiting characteristics of Delta Modulation	12
4	Typical difference signal	12
5	Block diagram of a practical Delta Modulator	14
6	Delta Modulator	15
7	Output wave forms of the Delta Modulator circuit	18
8	Slope overloaded condition as it becomes progressively worse	19
9	Slope overloaded condition as it becomes progressively worse	20
10	Test set-up for Figure 11	21
11	Spectrum of the response of a Delta Modulator (a) to a 5 KHz Gaussian noise signal (b)	22
12	Description of the three most prominent codes for high-density digital recording	28
13	Power spectral density distribution of NRZ, Bi-phase, and Ampex-Miller codes	29
14	Ampex-Miller Encoder	31
15	Waveforms of an arbitrary NRZ-L code as it flows through the Ampex-Miller encoder	31
16	Ampex-Miller encoding board	32
17	Ampex-Miller decoder	34
18	Ampex-Miller code-decoder board	35
19	Typical waveforms of actual decoding circuit	36
20	Block diagram of actual AMC encoding, decoding, and synchronizing circuit	39

Figure No.		Page
21-A	Experimental results of Figure 20	40
21-B	Experimental Results of Figure 20	41
22	Test setup used to measure the spectral distribution of an Ampex-Miller encoded random binary sequence	42
23-A	Measured power spectrum for: 1. Binary random sequence 2. Sequence "a", Ampex-Miller encoded	43
23-B	Measured power spectrum for: 1. Binary random sequence 2. Sequence "a", Ampex-Miller encoded	44
24-C	Measured power spectrum for: 1. Binary random sequence 2. Sequence "a", Ampex-Miller encoded	45
24	Nationally standardized subjective flutter weights	59
25	Model of a digital time base corrector	61
26	Digital time base corrector block diagram	65
27	Address control logic	66
28	4096X1 Random access memory I and II with time-shared address	67
29	TBEG Write Clock PLL	68
30	Output PLL	69
31	TBEG Read Clock PLL	71
32	Flutter Transfer Function	75
33	Experimental setup used to study effects of flutter	76
34-A	Spectral degrading effects of flutter: a. Unfluttered spectrum	77
34-B	Spectral degrading effects of flutter: b. Fluttered spectrum	78
35	Block diagram of the experimental setup used to observe the flutter supressing effects of the TBC	79
36-A	Spectral comparison of a fluttered signal: a. Before it has been time base corrected	80

Figure No.		Page
36-B	Spectral comparison of a fluttered signal: b. After it has been time base corrected	81
37	Reproduce characteristics	85
38	A typical magnetization curve, or hysteresis loop	87
39	Head-to-tape transfer characteristics with no bias	88
40	Graphical representation showing how AC bias alternately transfers the signal from one linear section of the curve to the other	90
41	A graphical representation of gap effect	93
42	Impulse response, s(x), of the magnetic head as a function of the distance, (x)	98
43	The complete digital channel	102
44	Spectrum of the processed signal to be recorded on tape (Trace 1) resulting from a 5 KHz band limited gaussian noise input (Trace 2)	103
45	Test setup to measure the average playback power and average noise	108
46	A solution ot the channel capacity integral using the computer program "MACSYMA"	112
I-1	Decoding phase-locked loop	127
I-2	Phase-locked loop block diagram	128
I-3A	Step response of the phase-locked loop	129
I-3B	Step response of the phase-locked loop	130

LIST OF SYMBOLS

$a(t)$	Input signal to Delta Modulator
$\tilde{a}(t)$	Integrator output of the theoretical Delta Modulator
$\hat{a}(t)$	Low pass filter output of the theoretical Delta Modulator
AMC	Ampex-Miller code
B	Resultant induced magnetization on tape
BI-Φ-L	Bi-phase level
C_t	Theoretical channel capacity
$\Delta(t)$	A function of time which is equal to positive one when ε is positive and to negative one when ε is negative
dC	Differential channel capacity
dN	Differential noise power
dP	Differential signal power
E(%)	Channel efficiency
ε	A time function defined as the difference between $a(t)$ and $\hat{a}(t)$
f_x	Spacial frequency
f_r	Read clock frequency
f_w	Write clock frequency
$F_{pp}(\%)$	Peak-to-peak flutter in percent
FTF	Flutter transfer function
H	Magnetizing force
$H(s)$	Transfer function
K_o	Voltage control oscillator constant
K_ϕ	Phase detector constant
NRZ	Non-return-to-zero

NRZ-L	Non-return-to-zero-level
ω_n	Natural frequency
$P_i(t)$	Recurring series of impulses at the input of the theoretical Delta Modulator
$P_o(t)$	Recurring series of impulses at the output of the theoretical Delta Modulator
$r(x)$	Resultant field stored on tape
$R(f_x)$	Spacial transform of the tape resultant field
σ	The magnitude in volts of a quantum step of $\tilde{a}(t)$
$S(f_x)$	Spacial transform of the head impulse response
$s(x)$	Head impulse response
SNR	Signal-to-noise ratio
T	Time-delay
TBE	Time base error
TBEC	Time base error corrector
TBEG	Time base error generator
TD	Transition detector
ξ	Damping factor

ABSTRACT

High density data recording has traditionally been an essential factor in the development of communication and transmission systems. However, recently more sophisticated applications, including video recording, have necessitated refinements of this technology.

This study concentrates on the signal processing techniques used to inhance the packing density of stored data. A comparison of the spectral mapping characteristics of different codes illustrates that the need for equalization can be eliminated and that significant bandwidth reduction can be achieved.

Secondly, consideration is given to the deleterious effects of flutter, its associated effects on high density data recording, and the constraints imposed on the development of a time base corrector.

An analysis is made of the bandlimiting effect which results when the incoming data is convolved with the head impulse response. The bandwidth of the channel, the size of the head gap, and the velocity of the media are seen from this analysis to be intrinsically related.

These signal processing techniques are implemented, the channel capacity computed, and a significant channel efficiency achieved.

HISTORICAL REVIEW

Magnetic recording of information began with Valdemar Poulsen and his "Telegraphon" in 1893 in Denmark, although the basic idea was documented but apparently not built in 1888 by Oberlin Smith, an American. Since that time, great strides in the technology of materials, techniques of manufacture, and a constantly increasing need to record and store information have produced the highly complex magnetic tape recorders of today. As originally conceived, the recorder used steel wire spirally wound on a drum where a stationary transducer recorded or reproduced variations in magnetic flux into or from the wire as the drum rotated. Developments in magnetic materials and processes using steel ribbon tape, especially in Germany during the 1920-1930 era, resulted in several machines similar to present day configurations. In 1935, the first plastic tape was introduced by a recorder manufacturer, AEG of Germany. Tape recorders made in the United States (Brush Soundmirror) used steel ribbon tape until just after World War II. "Liberation" of several German-made tape recorders by the Allied Forces at the end of the war accounted for the beginning of magnetic tape recording as we know it today in the United States.

In spite of the difficulties in its use, wire recording had a pretty good foothold in this country by the end of World War II, where it was used in home entertainment, in the business world, and by the armed forces. By 1950, however, the many advantages of tape over wire were

widely accepted and wire recording became a thing of the past.

Following 1950, great improvements were made in audio recorder technology, and by 1955 stero recorders were available for home use. In the same period, instrumentation recorders moved up to 60-ips operation, 14 tracks on 1-inch tape, and 100-KHz response. By 1957 video recorders were on the market, and by 1959 instrumentation recorders were capable of 1-MHz response at 120-ips. In the 60's, home video recorders were available and instrumentation machines capable of 1-MHz at 60-ips were being built.

An integral part of the growth in tape recorder capabilities has been the great strides made in tape technology. From the paper-backed tapes of 1948 to the tensilized polyester tapes of today, many improvements have been made. Oxides, binder formulas, base materials, processing techniques, and exacting quality control standards have been combined to produce the high-resolution extremely smooth instrumentation computer and audio tapes in use today - all exhibiting many times the storage capacity available 15 years ago.

Today's magnetic recorders are capable of many orders of magnitude better performance than the 1893 models, but they still use the same basic magnetic principles; only the materials, techniques and requirements have changed over the years.

Standardization

A standard in the field of telemetry for guided missiles was established in 1948 by the Committee on Guided Missiles of the Research and Development Board (RDB), Department of Defense, and was thereafter

revised and extended as a result of periodic reviews of the standard by the committee's working group on Telemetering of the Panel on Test Range Instrumentation. The last official RDB revision of the standards was published as RDB report MTRI 204/6, dated November 8, 1951. Since the termination of the Research and Development Board, new standards have been prepared by the Inter-Range Instrumentation Group (IRIG). The steering committee representing IRIG and the Department of Defense test ranges has assigned the task of promulgating new or revised telemetry standards to the Telemetry Working Group (TWG). The importance of magnetic tape recording to range instrumentation and its widespread use in telemetry operations long ago led to its inclusion in these standards. IRIG Telemetry Standards, document number 106-69, dated March, 1971, represents the latest such document. Copies of the document may be obtained from the Defense Ducumentation Center for Scientific and Technical Information, Cameron Station, Alandria, Virginia (22314), or Secretariat, Range Commanders Council, White Sands Missile Range, New Mexico, 88002.

CHAPTER I

INTRODUCTION

INTRODUCTION

Historically, it has been the practice of manufacturers of tape recorders, whether they be audio, video, digital, or instrumentation recorders, to equalize the record-reproduce channel in order to match it to the information spectrum, thereby maximizing transmission efficiency. This often results in severe nonlinearities, causing cross modulation components within the information bandwidth, which then have to be suppressed. The new suppressor distorts the channel and, therefore, the channel must be re-equalized. This becomes an iterative process which degrades the signal-to-noise ratio of the overall system. The ultimate effect of this equalization process is unnecessary bulky and expensive electronics.

In addition, the practical problems associated with the head-to-tape interface and the generation of a pseudo-uniform tape motion can become limiting factors degrading signal-to-noise, bandwidth, and linearity. Often it is necessary to record the incoming information at some specific rate, generally dictated by other constraints in the system and to then play it back at a different rate. This is typically the case when the information in question is of a much higher bandwidth than the available channel bandwidth through which it must be transmitted. In this instance, the information would have to be transmitted at a lower rate, giving rise to a new set of channel characteristics which would, again, require re-equalization. In order to restructure the original information, it is necessary to maintain a record of the specific rates involved. To further complicate the problem, this must be done in the

presence of time base error. This error has severe degrading effects on the reproduced signal.

In this study, these problems are considered in great detail, solutions are formulated, and a complete channel incorporating these solutions is implemented. In addition, a series of experiments illustrate the results. The thesis has been organized in the following manner:

Chapter I - Delta Modulation

A delta modulator was selected to digitize the incomming data primarily for two reasons: First, the characteristics of the delta modulator response are relatively well suited for the specific choice of input signals involved. Secondly, this modulator, in conjunction with the proper encoder, has a unique synchronizing characteristic. A circuit realization of this subsystem was developed and its characteristics verified experimentally.

Chapter II - Encoding and Decoding

Several codes are studied and the specific spectral mapping characteristics of these codes are determined. Additionally, the self-clocking properties of these codes are analyzed and developed. Finally, based on these observations, a specific code is chosen and the required encoding, decoding and carrier extracting functions are implemented.

Chapter III - Time Base Error

In this chapter, the cause of timing errors are briefly reviewed, and a detailed study of the spectral degrading effects of flutter is presented. A time base generator and corrector is developed, and a series of experiments are performed to illustrate the results.

Chapter IV - The Channel

A discussion of the characteristics of the record-reproduce process is presented and a theoretical analysis of the recording process is made. From this study, significant results are obtained. In addition, the completed channel, with all sub-systems interconnected, is presented. Finally, the channel capacity is computed and compared to the actual results.

CHAPTER II

DELTA MODULATION

DELTA MODULATION

Delta modulation is a technique by which an analog signal can be encoded into binary digits. This technique has the advantage that the electronic circuitry required for modulation at the transmitter and, particularly, for demodulation at the receiver, is much simpler than the corresponding hardware needed for other modulation techniques.

A delta modulation system is shown in Fig.1. The input generator furnishes a regularly recurring series of impulses $P_i(t)$. These impulses, as well as a signal $\Delta(t)$, are received by the modulator. The modulator output $P_o(t)$ is the input train $P_i(t)$ multiplied by +1 or -1, depending solely on the polarity of $\Delta(t)$. The multiplication is by +1 if $\Delta(t)$ is positive and by -1 if $\Delta(t)$ is negative.

$P_o(t)$ is applied to an integrator having output $\tilde{a}(t)$ which approximates the input signal $a(t)$. Signals $\tilde{a}(t)$ and $a(t)$ are compared. The output of the comparator is:

$$\varepsilon = a(t) - \tilde{a}(t)$$

Fig. 2 shows the operation of this modulator. Arbitrary initial values are designated for $a(t)$ and $\tilde{a}(t)$. Since initially $a(t)$ is greater than $\tilde{a}(t)$, the output impulse of the modulator is positive. The integrator output is a positive step. This waveform pattern continues until $\tilde{a}(t)$ is greater than $a(t)$ and $\Delta(t)$ is negative; the next impulse in the modulator output is of negative polarity.

$P_o(t)$ is the output. In practice, these impulses are pulses and are widened to increase the energy in the transmitted bit. $P_o(t)$ transmits, in coded form, information about the difference between the

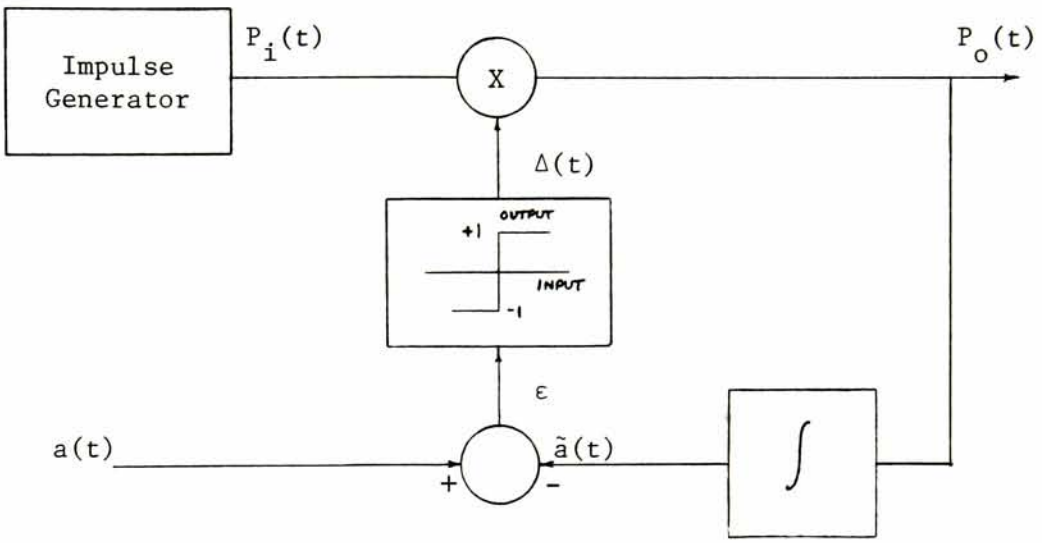

Fig.1 Theoretical Delta Modulator

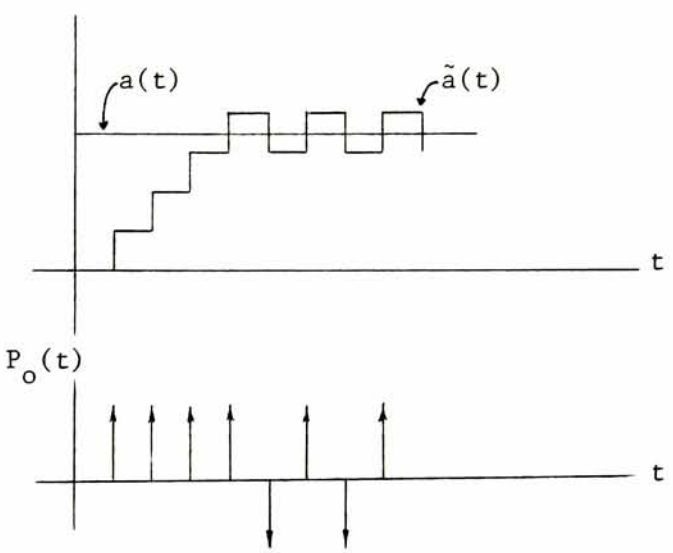

Fig.2 Description of the Theoretical Delta Modulator

two waveforms $a(t)$ and $\tilde{a}(t)$. Hence the name delta modulation.

The waveform $\tilde{a}(t)$ may be reconstructed using an integrator at the transmitter. In order to smooth the signal so that it better follows the original $a(t)$, the integrator may be followed by a low-pass filter. Since this filter provides an approximate measure of integration, the receiver integrator can be eliminated. The output of the filter is $\hat{a}(t)$ which differs from the transmitter input $a(t)$ only because of the stepwise approximation of delta modulation and because of errors due to noise in the receiver quantizer.

Since it is not necessary in reality to have a transmitter integrator that is a precise integrator, an RC low-pass filter (quasi-integrator) is sufficient.

The fixed step in $\tilde{a}(t)$ causes a limitation of delta modulation which is not found in other pulse-modulation schemes; the result is overloading when the signal changes too rapidly.

When the amplitude of the modulating baseband signal exceeds the range of the active devices used to process the signal, all modems (including delta modulation) overload. In addition, however, delta modulation is subject to another form of overload not encountered in other modems. This overload is exhibited when the modulating signal changes between samplings by an amount greater than the size of a step. Therefore, this type of overload is determined by the slope of the modulation signal rather than by its amplitude.

In Fig.3a, signal $a(t)$ is changing nearly as rapidly as the modulator can follow. In Fig.3b, the signal retains the same peak-to-peak amplitude but increases the slope (rate of rise). However, in both

cases, the slope of the modulator output increases at the same rate. Therefore, $\tilde{a}(t)$ does not follow $a(t)$ in this region of increased slope, and the delta modulation system is said to be slope overloaded.

The largest amplitude the system can reproduce is one changing by one level or step every pulse interval so that the maximum signal power depends on the type of signal. If the magnitude of one quantum step is σ volts and the time between sampling instants is $1/f_s$ seconds, where f_s is the sampling frequency, then the maximum rate of amplitude which can be reproduced for a sinusoidal wave of angular frequency $\omega = 2\pi f$ and of amplitude A is as follows:

$$a(t) = A_{max} \sin(2\pi f t)$$

$$\frac{da(t)}{dt} = 2\ f A_{max} \cos(2\pi f t)$$

Max. Rate of Change: $$\left.\frac{da}{dt}\right|_{max} = 2\ f A_{max} = \sigma f_s$$

$$A_{max} = \frac{\sigma f_s}{2\ f}$$

Thus both the maximum amplitude and the number of distinguishable levels decrease with increase of frequency to be transmitted as evidenced by the fact that as the frequency increases, the number of comparisons in one cycle, which constitutes the maximum number of distinguishable levels, decreases.

In NTSC structured video, as well as in speech, this limitation is minimized because the higher frequencies contain less energy than the lower ones. Hence, this type of network is well adapted to the transmission of these signals. Experimental results show that if the amplitude of a signal does not exceed the maximum sine wave amplitude that

can be transmitted at 800 Hz, delta modulation can transmit a speech signal without overloading.

The quantizing noise can be decreased by increasing the pulse frequency. Generally speaking, the quality of transmission is improved in two ways by this increase: first, the number of steps can be increased so that signals of greater amplitude can be transmitted; and second, a corresponding change in the frequency spectrum of the noise will cause a further reduction of the quantizing noise in the low frequency band.

Quantizing Noise in Delta Modulation

In delta modulation the noise is produced by the difference signal $\Delta(t) = a(t) - \tilde{a}(t)$ which at the receiving end is smoothed by means of a low-pass filter. The difference signal, which is shown in Fig. 4, is usually non-periodic and therefore has a continuous frequency spectrum which can be shown to be uniform for frequencies which are small compared to the sampling frequency f_s.[1] It should be noted at this point that there there will be spectral lines at the sampling frequency and at its multiples, but that these will be rejected by the low-pass filter. The power of the quantizing noise received after the low-pass filter with cut off frequency $f_m = \omega_m/2\pi$ will thus be proportional to f_m. Similarly, it can be reasoned that the unfiltered noise power is inversely proportional to the sampling frequency. For if the pulse frequency is doubled, using the same value of σ for the height of one step, the new difference signal Δ will have the same total power in a frequency band twice as large as before. Consequently, the noise power in the

band from 0 to f_m will be reduced by a factor of two. In fact, it can be shown[2] that the quantized noise power N_o is approximately given by:

$$N_o = \frac{2}{3}\frac{f_m}{f_s}\sigma^2$$

The signal power in the calculation of signal-to-noise ratio is taken as the power of the sinosoidal tone, which is just below the overload point. In signals which have approximately uniform energy distribution, the signal-tone frequency should be the top frequency since the point just below overload is determined by the highest frequency. In signals with a non-uniform energy distribution, some other than the top frequency may be used; as mentioned earlier, the reference frequency of a speech signal is 800 Hz. Assuming a sinosoidal signal A sin(ωt), the maximum amplitude that can be transmitted without overloading is:

$$A = \frac{f_s\sigma}{2\pi f}$$

Therefore, the average signal power is:

$$S_o = \frac{A^2}{2}$$

$$= \frac{\left(\frac{f_s\sigma}{2\pi f}\right)^2}{2}$$

$$= \frac{f_s^{\,2}\ \sigma^2}{4\pi^2 f^2}\cdot\frac{1}{2}$$

Hence, the signal-to-noise is:

$$\frac{S_o}{N_o} = \frac{\frac{f_s^{\,2}\ \sigma^2}{8\pi^2\ f^2}}{\frac{2}{3}\left(\frac{f_m}{f_s}\right)\sigma^2}$$

Note: Refer to previous derivation of N_o (Above)

$$= \frac{3}{2}\cdot\frac{f_s^{\,3}}{8f_m}\cdot\frac{1}{\pi^2\ f^2}$$

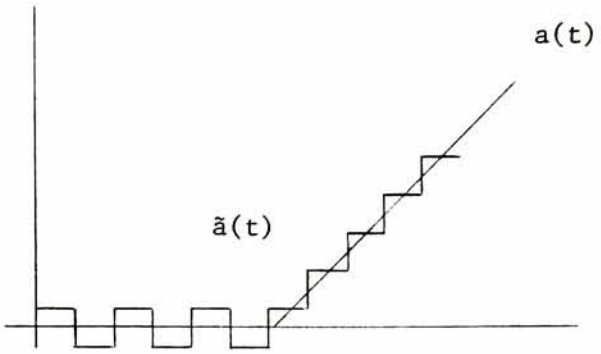

Fig.3a

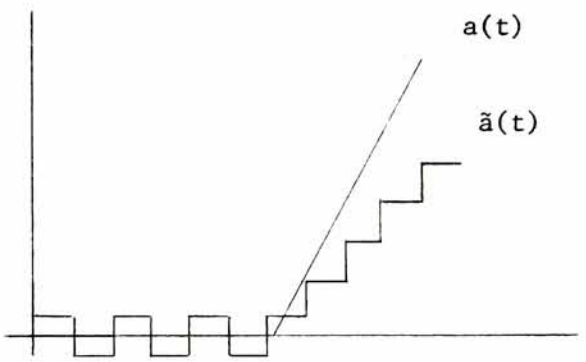

Fig.3b

Fig.3 Slope limiting characteristics of delta modulation

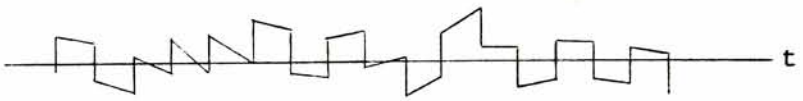

Fig.4 Typical difference signal

$$\frac{S_o}{N_o} = \frac{3}{16\pi^2} \frac{f_s^3}{f_m} \frac{1}{f^2}$$

Hardware Implementation

A block diagram of a practical delta modulator is shown in Fig.5. In this diagram the signal a(t) is sampled and held synchronously with $\tilde{a}(t)$. These two samples are then brought to a comparator, the output of which is the delta modulated code. This waveform is fed back, integrated, and amplified to become $\tilde{a}(t)$. Note that in this practical modulator, the pulse generated is, first of all, not an impulse but a square pulse of a duration no smaller than one f_s clock period. Secondly the integral of this waveform is not a step, but a ramp. This makes little difference due to the fact that this ramp is sampled with a narrow apature simultaneously with a(t) at the time of comparison.

The actual hardware implementation of this block diagram is shown in Fig.6. A description follows: The choice of the sample frequency will determine ultimately the frequency in the spectrum about which the overall channel signal energy will be located. To understand the reason for this particular choice of frequency, one must know something about the rest of the channel. This particular choice will be discussed later; at this point, it is sufficient to say that a signal of approximately 5 KHz can be adaquately sampled with a 15 KHz sample clock.

The 555 is the clock generator. The frequency generated here is 30 KHz, twice the sample frequency. By way of the D flip-flop (the 7474) and associated gates No.3, a 15 KHz negative-going narrow pulse is generated. This is the sample clock. The sample-and-hold (S/H) circuits for a(t) and $\tilde{a}(t)$ are the HA 2425 No.1 and No.2, respectively. The comparison is made by the LM 311, whose output is connected as a relatively low

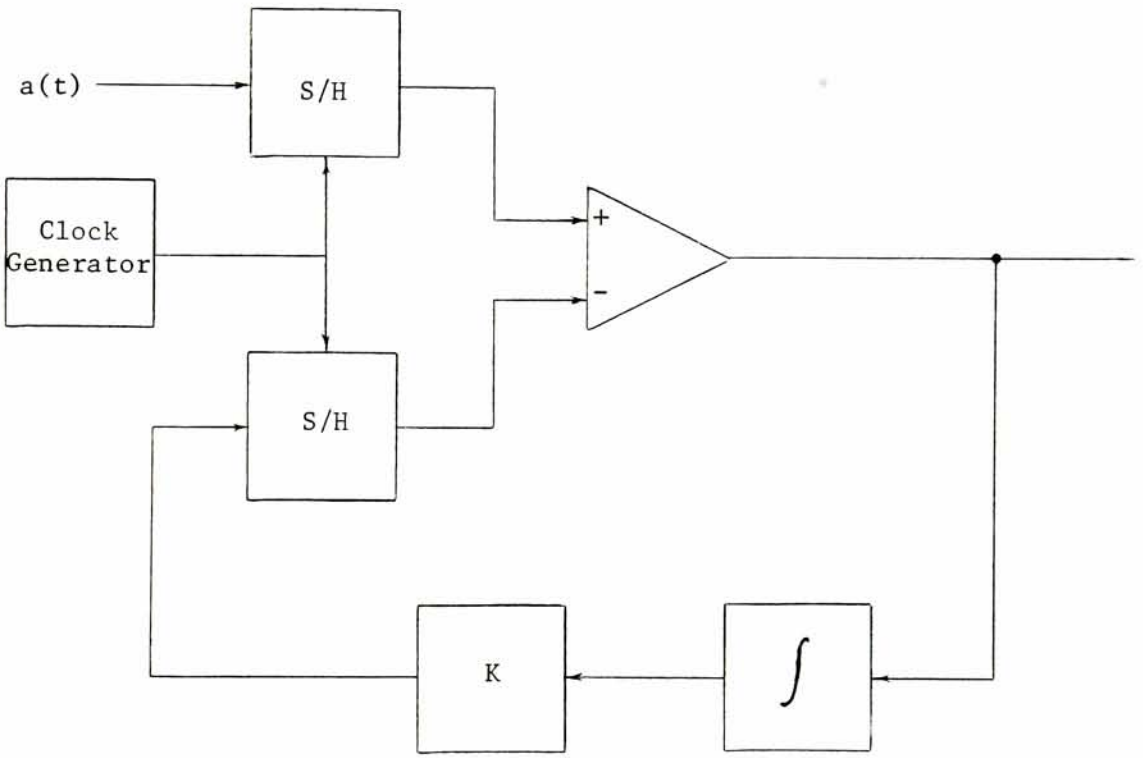

Fig.5 Block diagram of a practical delta modulator

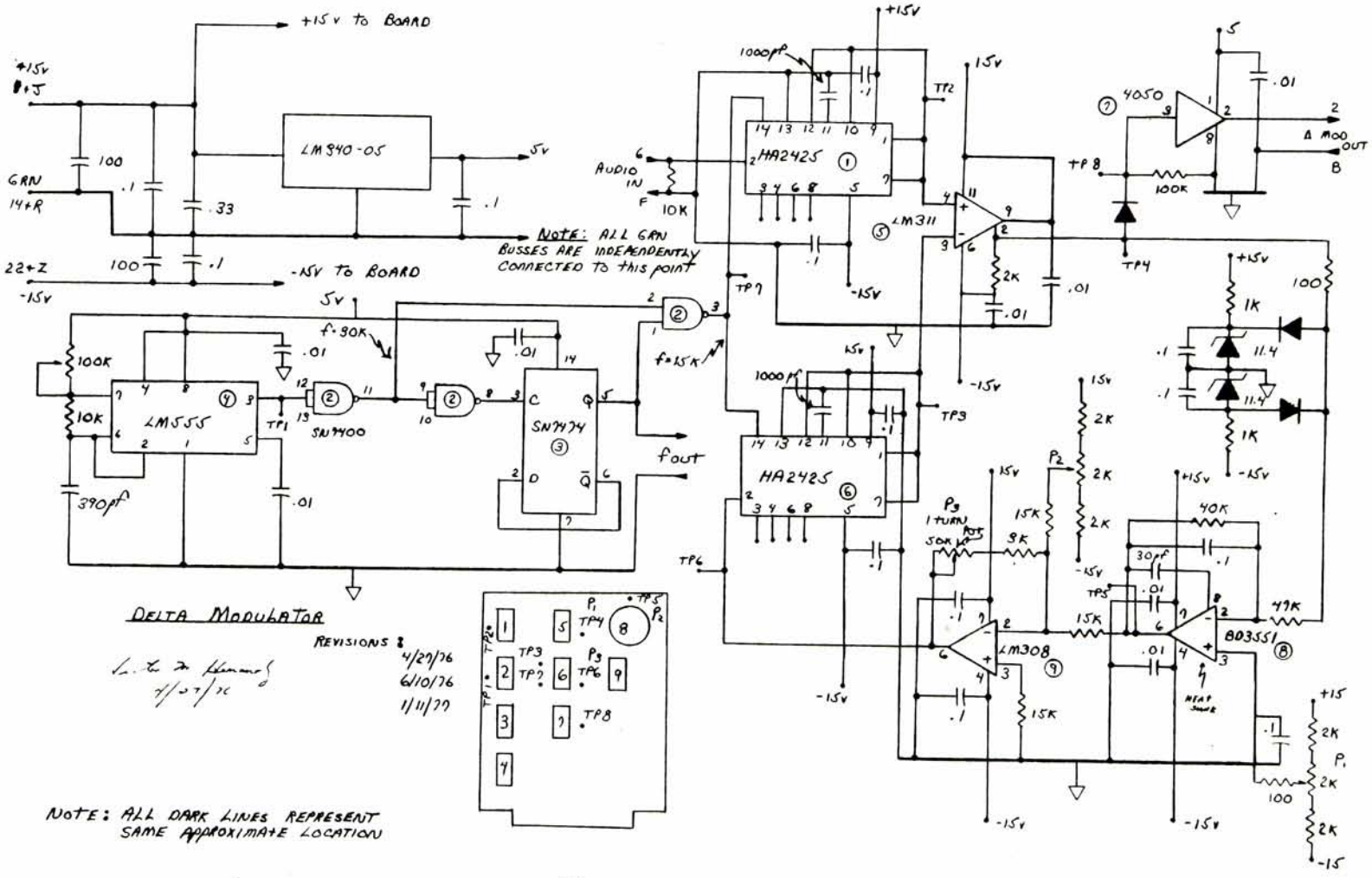
+15v to BOARD
+15v
GRN
14+R
22+Z
-15v
-15v to BOARD
LM340-05
5v
100
.1
.33
NOTE: ALL GRN BUSSES ARE INDEPENDENTLY CONNECTED TO this point
AUDIO IN
10K
HA2425
LM311
1000pf
TP2
TP3
TP4
TP5
TP6
TP7
TP8
4050
Δ MOD OUT
100K
LM555
SN7400
SN7474
f=90K
f=15K
fout
390pf
1K
11.4
LM308
BD3551
P1
P2
P3
1 TURN
50K
40K
30pf
47K
15K
9K
2K
DELTA MODULATOR
REVISIONS:
4/27/76
6/10/76
1/11/77
NOTE: ALL DARK LINES REPRESENT SAME APPROXIMATE LOCATION

Fig. 6

impedance linear buffer with a voltage swing of +15 to -15 volts. This signal is then reduced in amplitude to 12 volts by way of the diode matrix shown and fed to the integrator (BB 3551). The output of the integrator is then amplified by the LM 308 operational amplifier and fed to sample-and-hold No.2. It is at this point that the size of step σ is controlled. The buffer 4050 is there only to provide a TTL waveform with a high fan-out ratio.

Experimental Results

Fig.7 is a photograph of the actual results obtained. Here one can see the input to the delta modulator (Trace 1), the output (Trace 2) and the output of the integrator (Trace 3).

The next figures (Fig.8 and Fig.9) show the same waveform as in Fig.7 for slope overload conditions as this condition becomes progressively worse.

An analysis of a delta modulator to obtain its transfer function is difficult because it is a non-linear system. However, a relatively good observation of the magnitude distribution of this spectrum can be made by ensuring an adequate input signal. The magnitude of the highest frequency of interest in this signal must be chosen so as not to slope overload the modulation process and the frequency distribution chosen to be relatively flat in the region of interest. The magnitude of the spectral distribution of the delta modulator response to an input signal can be readily observed in the test shown in Fig.10. The input signal, a 5 KHz band limited Gaussian noise signal, was selected because of its relatively flat spectrum which does not exceed the Nyquist frequency of

the modulator itself. The spectral energy distribution for the input signal, as well as that of the response of the delta modulator, can be observed in Fig. 11.

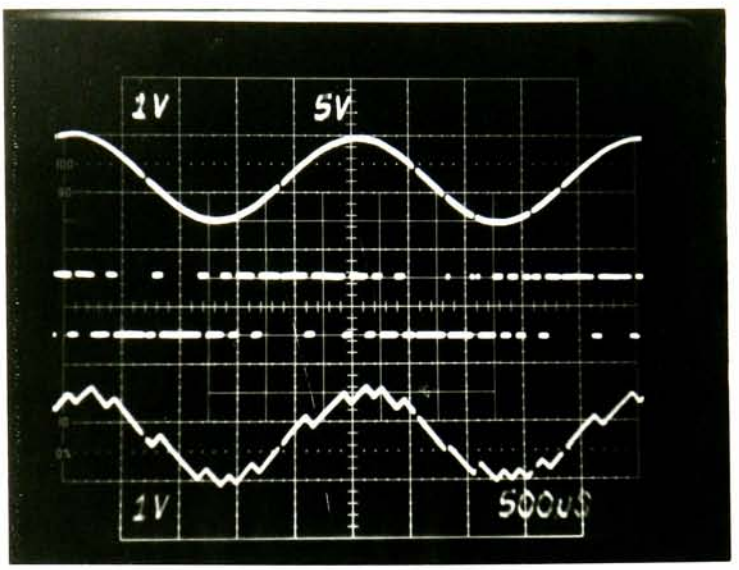

Trace 1 - Input to Delta Modulator
Trace 2 - Output of Delta Modulator
Trace 3 - Demodulator Output

Fig.7 Output Wave Forms of the Delta Modulator Circuit

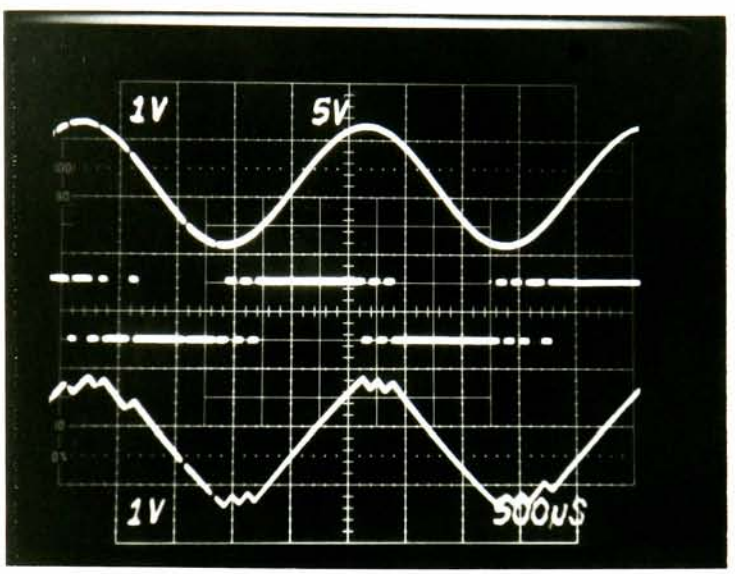

Trace 1 - Input to Delta Modulator
Trace 2 - Output of Delta Modulator
Trace 3 - Demodulator Output

Fig.8 Slope overloaded condition as it becomes progressively worse.

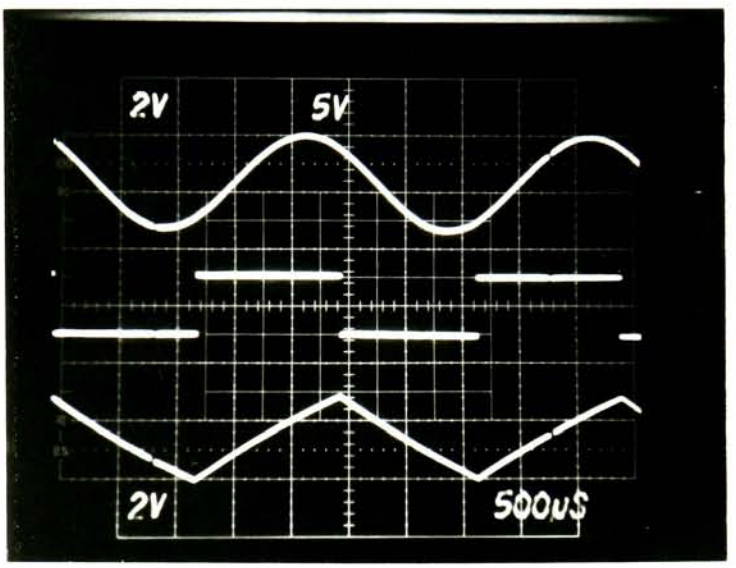

Trace 1 - Input to Delta Modulator
Trace 2 - Output of Delta Modulator
Trace 3 - Demodulator Output

Fig.9 Slope overloaded condition as it becomes progressively worse.

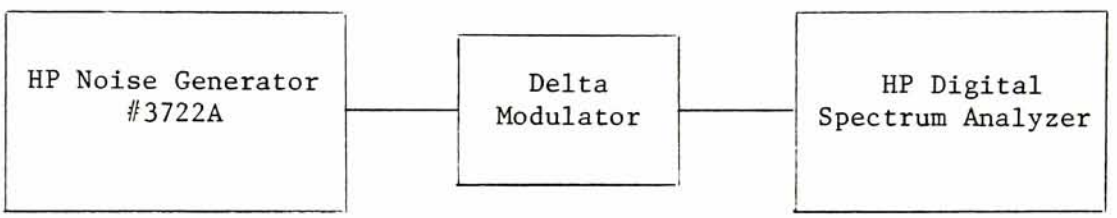

Fig.10 Test set up for Fig.11

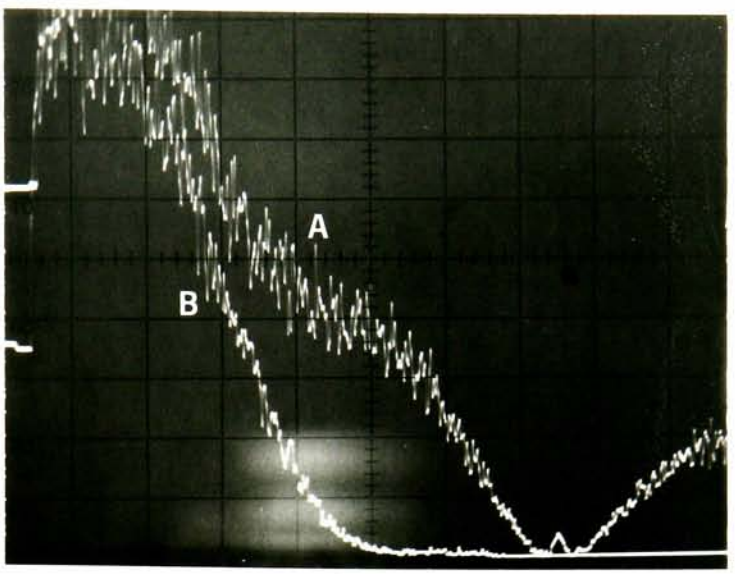

Specifications:

Input Signal: 5 KHz Gaussian Noise with amplitude = .1 volts chosen so as not to overload at 5 KHz

Delta Modulator Sample Rate = 15 KHz

σ = .2 volts/step

Analyzer Output:

Analyzer Settings	a	b
Resolution Bandwidth	300 Hz	300 Hz
Freq. Span per Division	2 KHz	2 KHz
Amplitude Ref. Level	-40 db	-30 db
Input Sensitivity	.1 volts	.2 volts

Fig.11 Spectrum of the response of a Delta Modulator (a) to 5 KHz Gaussian Noise (b)

CHAPTER III

ENCODING AND DECODING

ENCODING AND DECODING

For many applications, the recording of analog signals at bandwidths from 10 Hz to as high as 15 MHz with recording times of several minutes is important. Generally such signals are recorded either directly on magnetic tape or by an uncoded modulation method, usually FM. In this context, the term "coded modulation" is used to describe a process by which a particular modulated spectrum is modified, resulting in a new waveform. The capabilities of such analog systems may be insufficient in certain applications; for example: prior to recording, a noisy transmission channel requires conversion to pulse code modulation. This is particularly the case when the available bandwidth is limited.

The advantages of pulse code modulation, as well as delta modulation, over conventional analog redording on magnetic tape are the achievement of higher signal-to-noise ratio and the elimination of the degrading effects of flutter, time-base error, crosstalk, amplitude instability, poor low-frequency response (in direct recording mode), signal amplitudes exceeding dynamic range, and nonlinearities producing false output signals.

Selecting a Code

Once the analog signal has been converted to some non-return-to-zero format,the information must be transmitted through a channel having a particular spectral response which has, typically, been equalized to match the information spectrum of the input signal. However, it is also possible to transform the spectral distribution of the input signal to match that of the channel. If the proper choice of transforms is made,

some significant added advantages can be realized.

In addition, coding can be used to accomodate signals with dc content. If the original digital signal contains dc, or even long runs of unipolar pulses, the data must be encoded prior to recording; otherwise, the zero-signal level will drift and complicate the playback mechanism. Amplitude modulation, frequency modulation, or phase modulation may be used to correct this problem. However, it is desirable to employ a bandwidth-preserving process since the recording bandwidth is usually at a premium. In addition, if the proper choice of code is made, the clock may be derived from the reproduced digital signal itself.

Non-return-to-zero (NRZ) data codes are often used for digital data transmission because of their low bandwidth requirement. However, various incompatibilities exist between these codes and direct recorder systems. If the data were permitted to contain long run lengths of 1's or 0's, the low frequency response of the recorder would have to extend very close to dc to prevent distortion of the signal waveshape (baseline shifting). This effect could cause data loss. A second incompatibility is timing errors (pulse-to-pulse jitter) which reduces the ability to obtain a clock signal from the data. A clock can be extracted as long as the timing error does not surpass plus or minus one-half of one bit cell. However, if no signal transitions occur during long strings of 1's or 0's, the jitter may cause loss of clock information. A third limitation is system signal-to-noise ratio. Noise, like jitter, reduces the ability to extract a clock signal from the data. In any event, the clock will slip cycles relative to the input data, resulting in an increased error rate.

Fig.12 describes the three most important codes for high density digital recording: NRZ-L, BI-Φ-L and AMC.

It should be noted that due to the lack of transitions in the NRZ-L code during a continuous string of data 1's, there is no data correction signal before a following 1,0 transmission. Therefore, a number of bits may be incorrectly sensed if a single transition is missed.

In summary, the two most important drawbacks of NRZ codes are susceptibility to time-base errors and the requirement for dc response.

With Bi-phase level (BI-Φ-L) codes, a transition occurs for every clock period. Therefore there is no need for dc response since these are self-clocking codes. A wider bandwidth is required, however, than for NRZ codes.

The Ampex-Miller Code (AMC), or Delay Modulation Code, is a phase shift code which requires about half the bandwidth of the BI-Φ-L code while achieving reliable self-clocking. It is defined as follows: A one is represented by a transition in the middle of the bit cell. A zero has no transition unless it is followed by another zero, in which case there is a transition at the end of the first zero's bit cell. The selection of this format is arbitrary, and the definitions of data one and zero can be interchanged.

A quality factor often used to characterize the value of a particular code is the "packing density" which can be achieved with it in a recording format. In the literature, this term, packing density, is generally used to refer to the number of bits per square inch (cm) of tape. In a linear format, however, it is often quoted as the number of bits per inch (cm) of track. This is particularly the case when

the track width, as well as the number of tracks, is constant within the specific recording format.

The packing density achieved using the Ampex-Miller code is approximately twice that achieved with bi-phase codes. This is principally due to the fact that the power spectral energy distribution associated with the AMC code has most of its energy concentrated at a frequency approximately one-half the corresponding frequency associated with the bi-phase spectrum. Fig.13 clearly illustrates this point. In this figure, a comparison is made of the spectral content of a coded random bit sequence. Note the lower end of the AMC spectrum contains only a minimal amount of signal energy; thus, the run length of a bit pattern is unrestricted. The Ampex-Miller code spectrum best approximates the unequalized frequency response of record heads. Hence there is often no need for equalization.

Using AMC code, reliable packing densities five times higher than with NRZ-L have been achieved with the same error rate.[4] It is easy to accomplish time-base expansion or contraction; the only restriction is that the bit rate must not exceed the bandwidth capability of the encoding and decoding electronics and of the magnetic recording process itself.

AMC Encoding

The encoding electronics are relatively simple to implement. Fig.14 shows an AMC encoder. The data, in the form of a NRZ-L code, is latched to ensure synchronization with the clock. The output of the latch, as well as that of the clock, is brought to an exclusive "or" gate. It should be noted that the behavior of the exclusive "or" gate, in a very

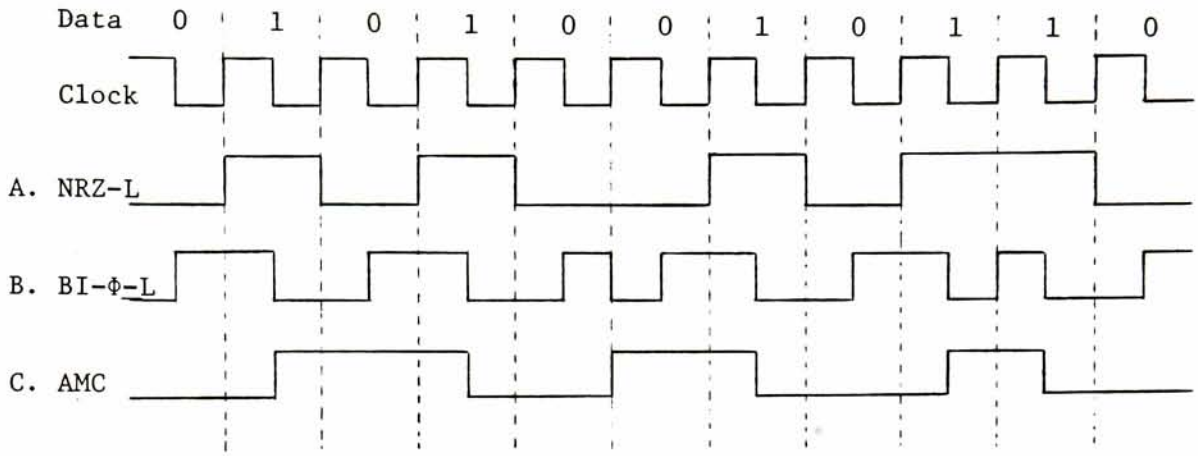

A. In non-return-to-zero-level (NRZ-L) Code, logic "1" and "0" can, for example, be represented by +5 and 0 volts. (On the tape, quasi-sinusoidal flux variations, corresponding to the coded waveform, are typical of any digital recording of this nature.) In this code, the highest possible frequency in the data is one-half that of clock and the lowest is zero, requiring dc response of the tape recorder.

B. Most feasible at lower densities and at low tape speeds, the bi-phase-level (BI-Φ-L) code uses successive "1" (at +5 volts, for example) and "0" (at 0 volts, for example) in a given data cell (time interval allotted for one data bit) to denote logic "1". Logic "0" is represented by a "0,1" succession within a data cell. In this code, the clock signal can be easily extracted from data, and the highest possible fundamental frequency of data stream exactly equals the rate. Since the fundamental frequency in the data cannot fall below one-half that of clock, low-frequency response of the tape recorder is usually of no concern.

C. Practical within a very wide range of tape speeds, the Ampex-Miller code (AMC) is characterized by transitions - in the middle of data cells containing a logic "1" and at the end of a data cell containing a logic "0", when followed by another data cell containing a logic "0". Lowest and highest possible fundamental frequencies in this code are 0.25 and 0.50 that of clock.

Fig.12 Description of the three most prominent codes for high-density digital recording:

A. Non-return-to-zero-level (NRZ-L)
B. Bi-phase-level (BI-Φ-L), or Manchester
C. Ampex-Miller (AMC), or Delayed Modulation Mark

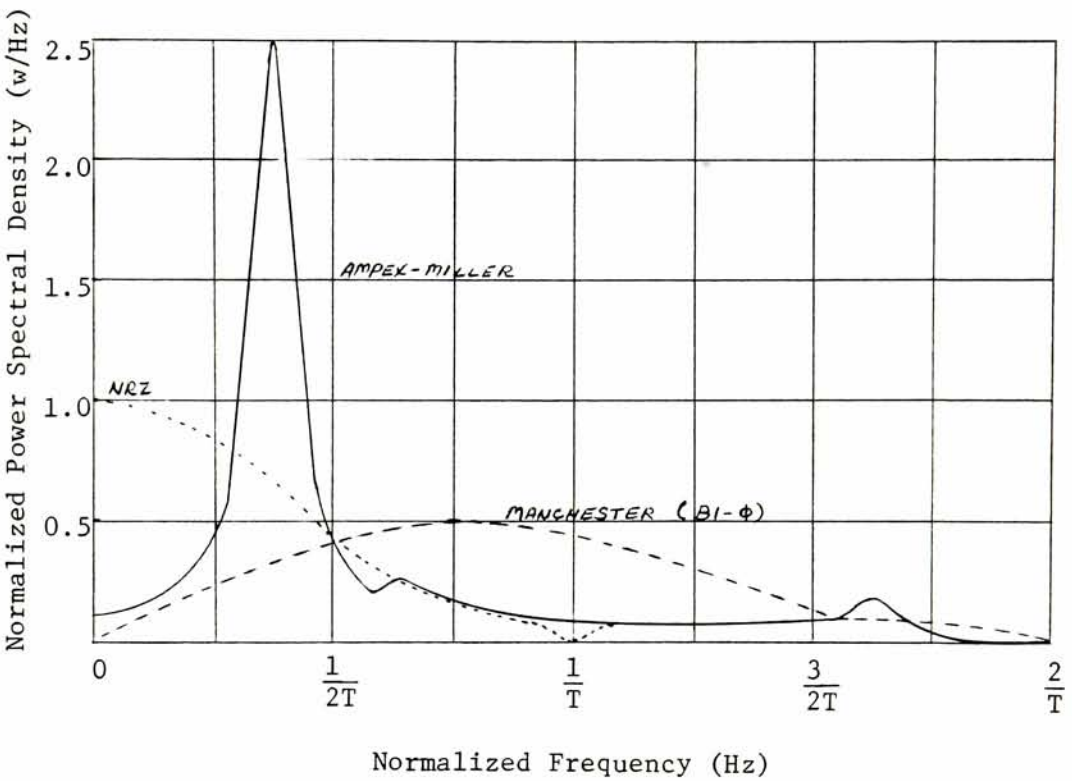

Fig.13 Power Spectral Density Distributions of NRZ, Bi-Phase, and Ampex-Miller Codes.

real sense, is the same as that of a saturated balanced modulator. Therefore, at this point we can consider the output of the gate as a hererodyne NRZ-L code to the carrier clock frequency. The resulting wave is called the BI-Φ-L code. At this point, the desired output can be obtained simply by driving a toggling flip-flop with the 1 to 0 transition of the BI-Φ-L code. Fig.15 illustrates an example of an NRZ-L code as it is Ampex-Miller encoded.

An actual hardware implementation of the encoder is shown in Fig.16. A description follows: The 7475 dual D flip-flop and exclusive OR gate #1 are the actual latch and bit synchronizer at the encoding input. At this point, delta modulated data is assured to be synchronized with the clock. The encoder, as previously described, follows with gate #2 and the 7476 JK flip-flop.

AMC Decoding

The decoding process is more complicated. A phase-locked loop (PLL) is required in order to extract the clock from the AMC code. The PLL is discussed in greater detail in Appendix I. However, we will assume that a frequency equal to twice the clock frequency is available in synchronism with the Ampex-Miller code. Fig.17 is a diagram of the decoder. A transition detector provides a narrow pulse at every data transition. This signal drives both the phase-locked loop and a "1 0 1" pattern detector. This pattern is used to synchronize the clock phaser so that the proper comparison may be made.

By observing the code, we notice that the 1 transitions always occur synchronously with the properly phased 90° clock. The desired decoding

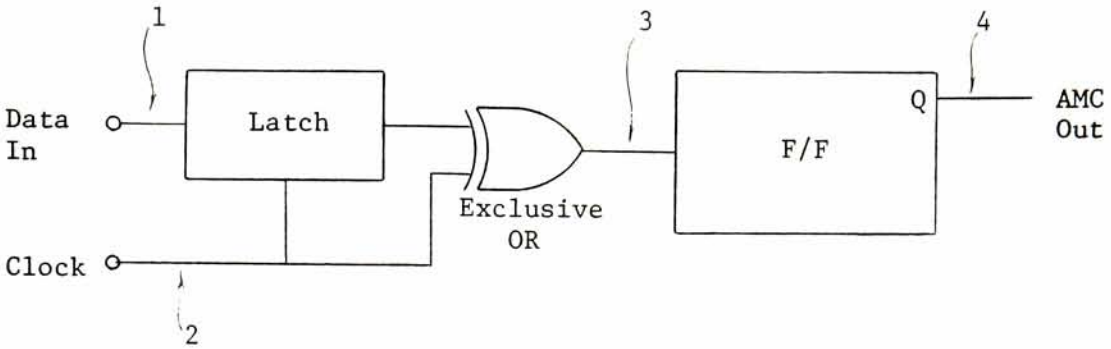

Fig.14 Ampex-Miller Encoder

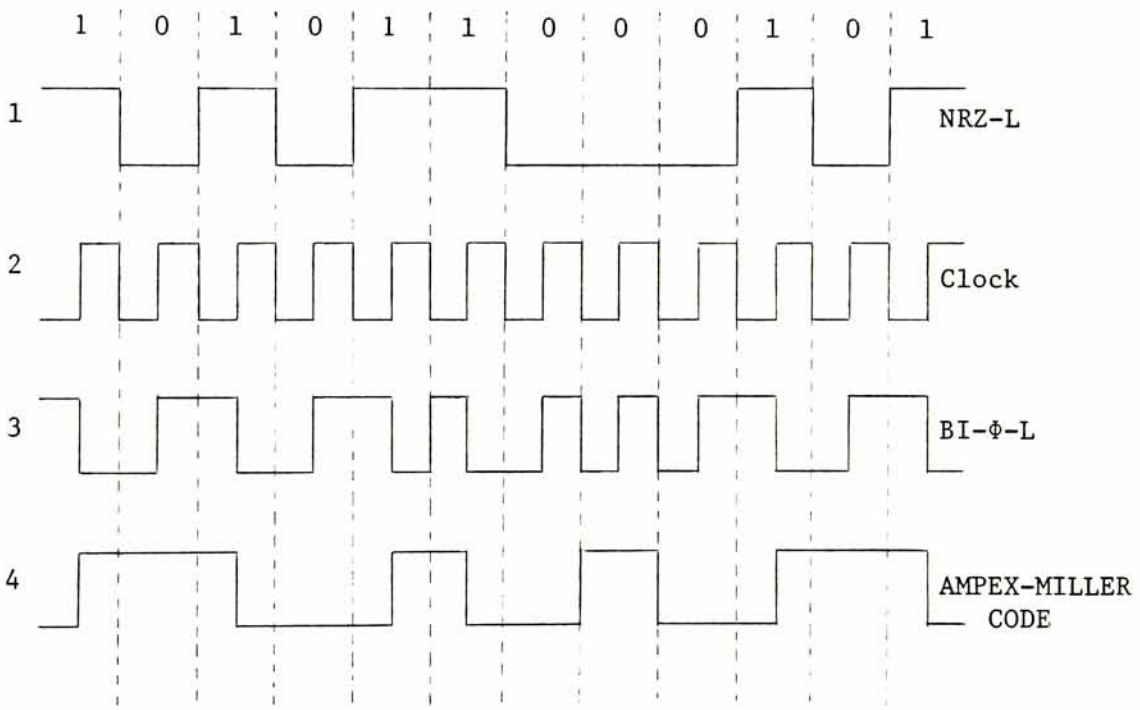

Fig.15 Waveforms of an arbitrary NRZ-L code as it flows through the Ampex-Miller Encoder

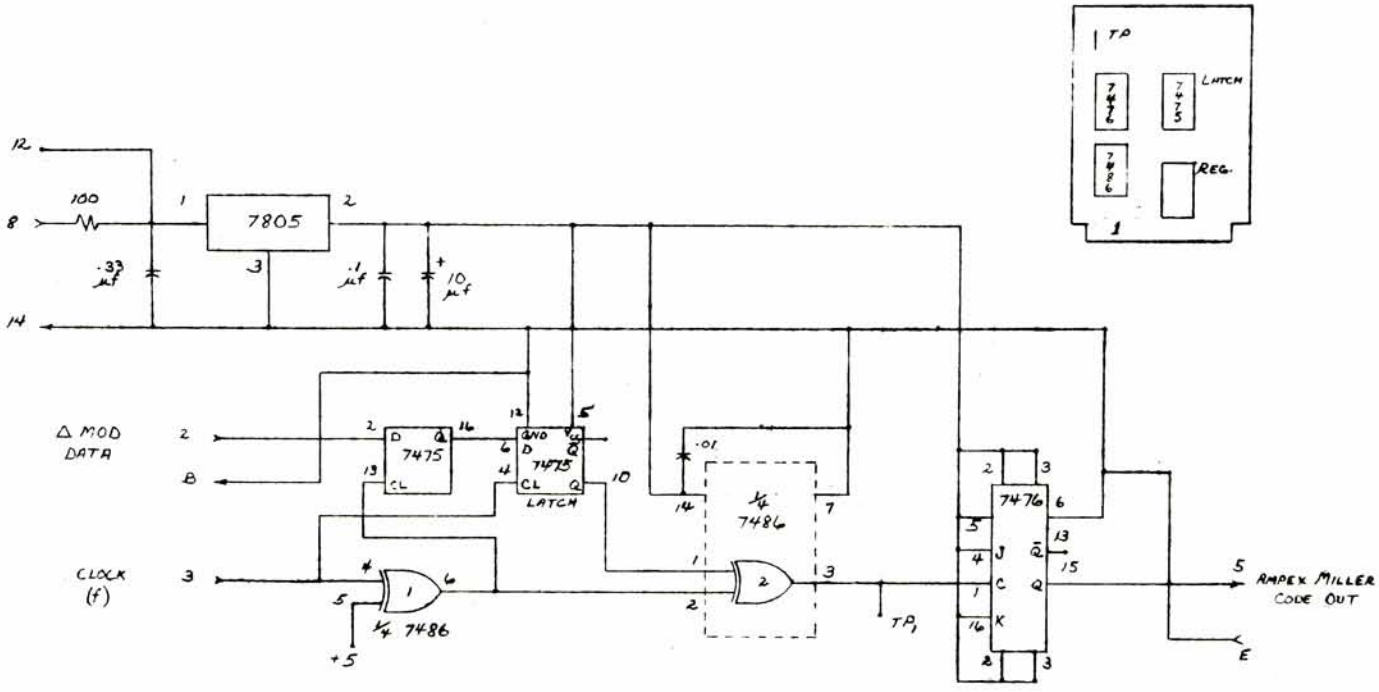

AMPEX-MILLER CODE
ENCODING BOARD

REVISIONS: 4/11/76
1/11/77

3/23/76

Fig. 16

logic functions can be obtained as well from observing the encoded input waveform and the desired results at the output of the decoder.

The important thing to notice is that the AMC code can be decoded provided that the starting and midpoint transitions of a bit period can be distinguished. This can be done by detecting the "1 0 1" pattern. When encoded, this sequence of bits results in the widest possible waveform the AMC code can have.

This particular combination of bits of the input data (1 0 1) will generate an AMC code with a pulse equal to four clock periods. By detecting the presence of one of these patterns, the clock phaser can be synchronized. Hence, the proper 0°, 90°, 180° and 270° clocks required for decoding can be generated.

The polarity of the clock while decoding data in the AMC format is verified and, if necessary, corrected each time the reset pattern occurs in the data. Strictly speaking, proper clock phasing between the long code elements cannot be guaranteed due to the ever-present possibility of signal dropouts. However, since the probability of a "one-zero-one" sequence occurring in data is quite high, loss of clock phasing in practice is rare and can only last for a very short period of time. Overall system error rates do not indicate this to be a serious problem with the Ampex-Miller code.

Experimental Results

The actual circuitry required for decoding is shown in Fig.18, and the associated waveforms for an arbitrarily chosen NRZ-L pattern are shown in Fig.19. Notice that the decoded NRZ-L output (the last waveform

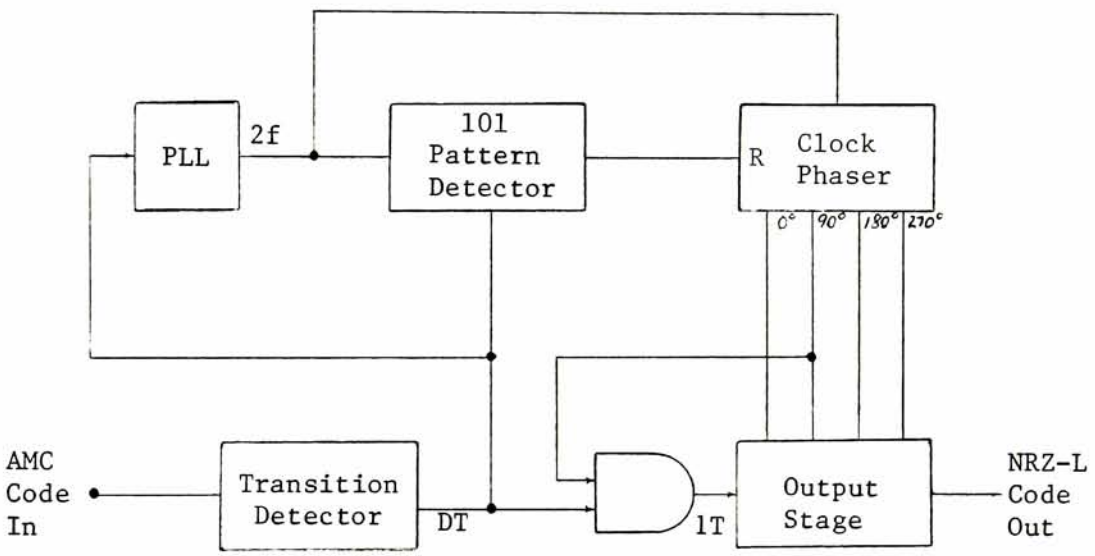

Fig.17 Ampex-Miller Decoder

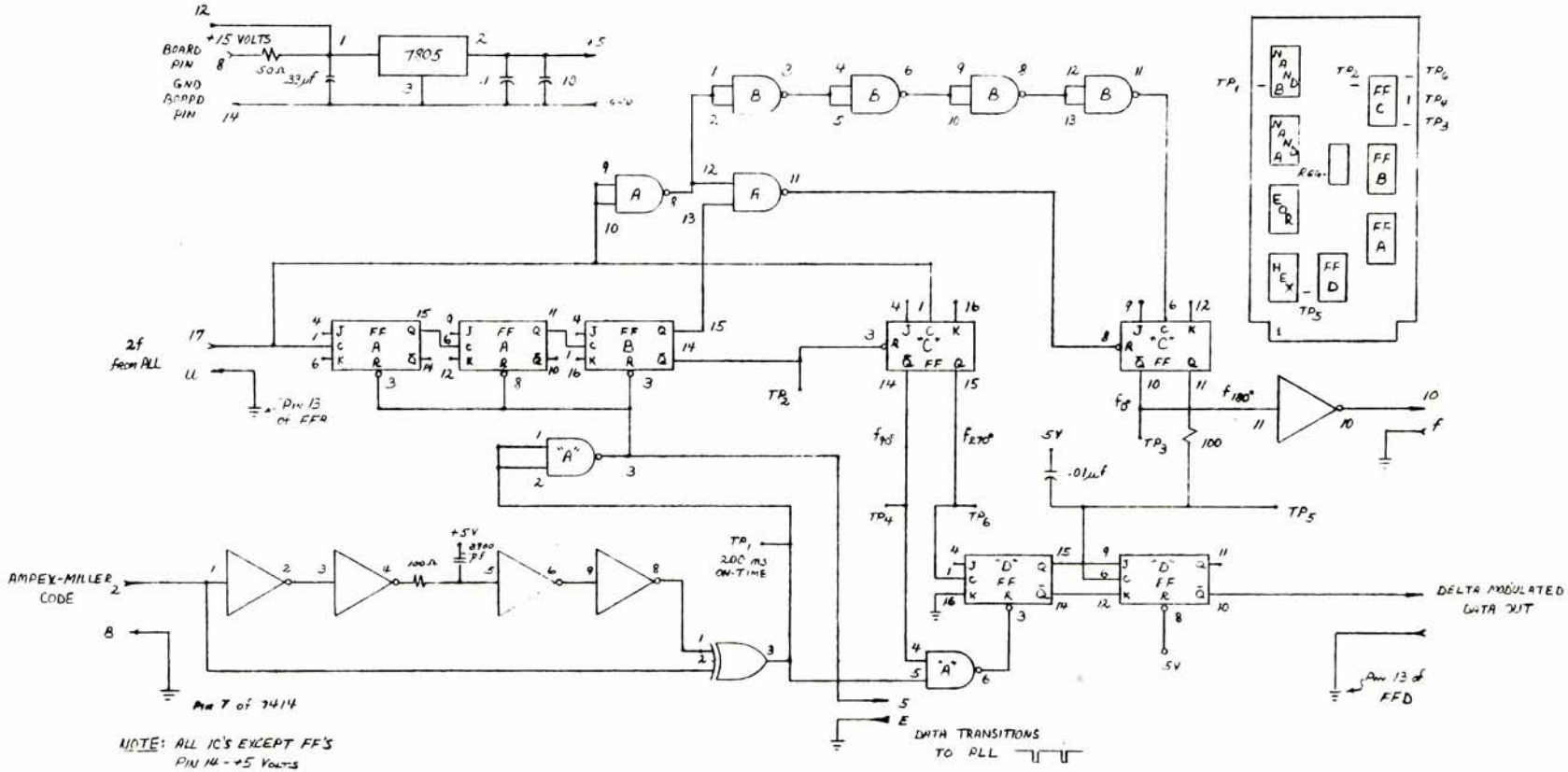

NOTE: ALL IC'S EXCEPT FF'S
PIN 14 - +5 VOLTS
PIN 7 - GND
BYPASS WITH .01μf CHARACITOR

PACKAGE 7476 - DUAL JK FLIP-FLOP WITH PRESET AND CLEAR
PACKAGE SN7414 - INVERTER
PACKAGE SN7486 - EXCLUSIVE OR
PACKAGE SN7400 - NAND GATE

AMPEX-MILLER CODE DECODER BOARD

3/24/76

REVISIONS: 3/31/76
6/11/76
1/12/77

Fig. 18

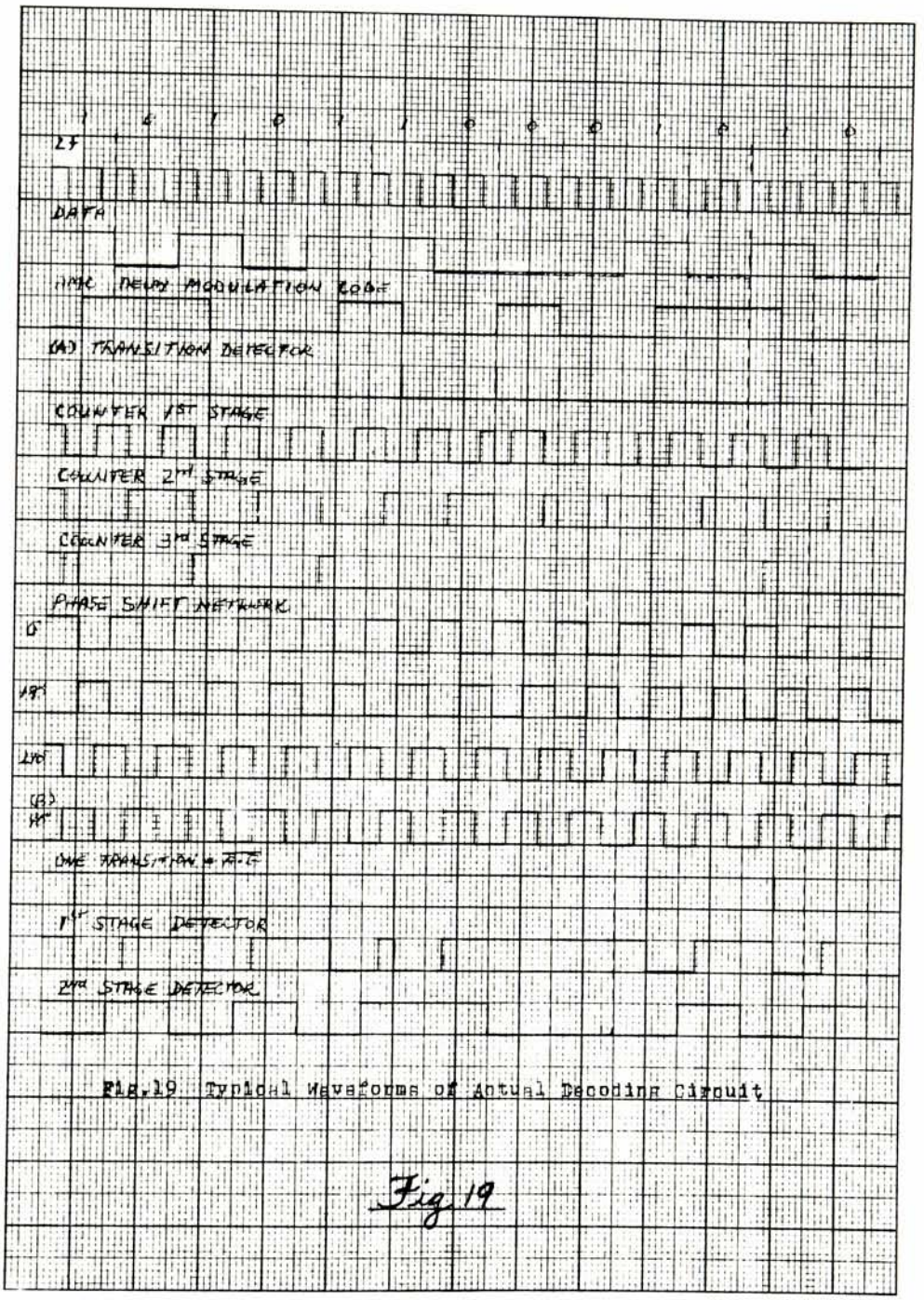

Fig.19 Typical Waveforms of Actual Decoding Circuit

Fig. 19

in Fig.19) is one f clock period delayed from the input.

Fig.20 is a block diagram of the actual encoding and decoding circuit, as well as the phase-locked loop, interconnected so that the encoding-decoding process may be observed. In this figure, the delta modulated data is the NRZ-L code. The clock is provided by the delta modulator. Fig.21 is a series of photographs depicting the results: trace 1 is the NRZ-L code input; trace 2 is the clock; trace 3 is the AMC encoded data at the output of the encoder; and trace 4 is the decoded NRZ-L code at the output of the decoder.

Fig.22 is a block diagram of the experimental setup used to measure the power spectral density distribution of a binary random sequence before and after it has been Ampex-Miller encoded. And Fig.23-A, B, and C are a series of photographs depicting the results. In each, one can see the spectrum of the input binary sequence to the encoder (1) and the spectrum of its Ampex-Miller encoded counterpart (2). In Fig.23-A, the input random sequence is a maximum length sequence made up of combinations of a 10msec clock period; in Fig.23-B, a 33.3μsec clock period was used, and in Fig.23-C a 10μsec clock period was used. The implication here is, of course, that the spectrum of the input sequence is increasingly wider. From Fig.23-A, B, and C it is interesting to note that the energy distribution is progressively approaching 5.625 KHz, which is 3/8 that of the bit rate (15 Kbits/sec), as the input spectrum becomes wider. On the other hand, the lowest and highest possible fundamental frequencies in the AMC code are 0.25 and 0.5 that of the clock. This can be readily noticed by encoding alternate "1 0" patterns resulting in 0.25 the bit

rate, and encoding a constant level which results in 0.5 bit rate. It should then not be surprising to find most of the energy concentrated half way between these two points - that is, at 3/8 the bit rate.

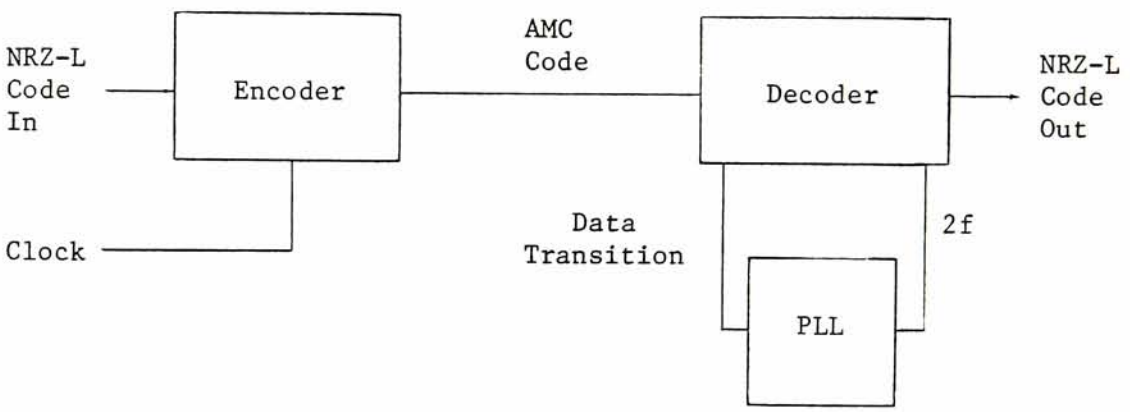

Fig.20 Block Diagram of Actual AMC Encoding, Decoding and Synchronizing Circuit

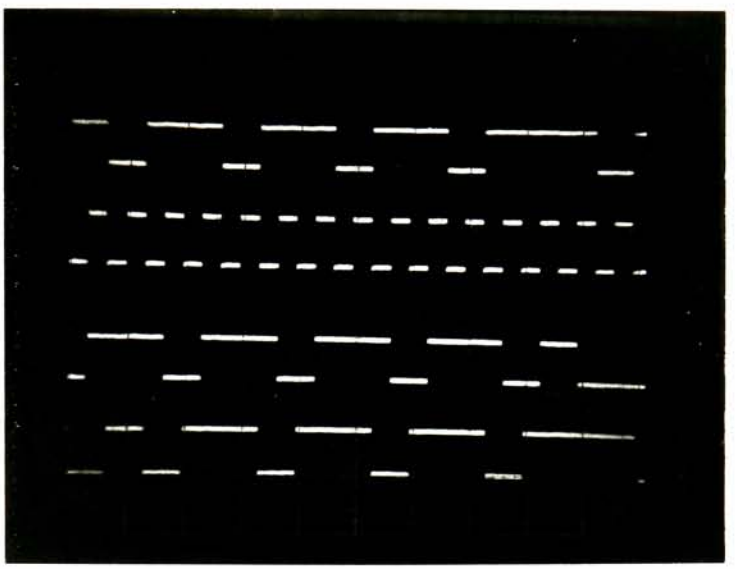

Vertical Sensitivity - 5 volts/cm
Horizontal Sensitivity - 100 μsec/div.

Trace 1 - NRZ-L Code In
Trace 2 - Clock Input to the Encoder
Trace 3 - Ampex-Miller Coded Input
Trace 4 - NRZ-L Decoded Output

Fig.21-A Experimental Results of Fig.20

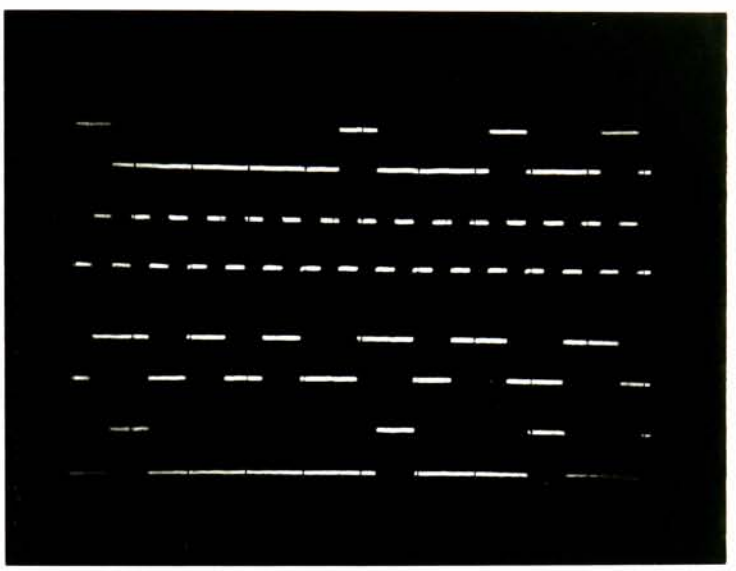

Vertical Sensitivity - 5 volts/cm
Horizontal Sensitivity - 100 μsec/div.

Trace 1 - NRZ-L Code In
Trace 2 - Clock Input to the Encoder
Trace 3 - Ampex-Miller Coded Input
Trace 4 - NRZ-L Decoded Output

Fig.21-B Experimental Results of Fig.20

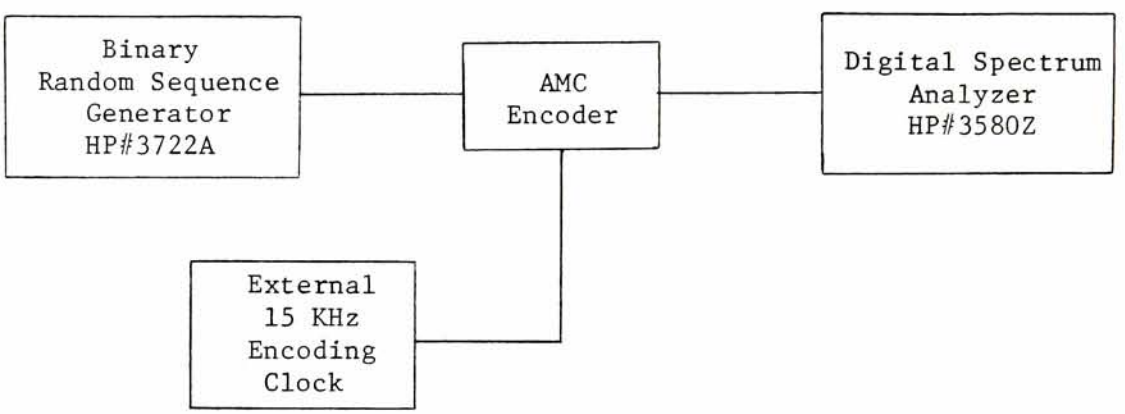

Fig.22 Test setup used to measure the spectral distribution of an Ampex-Miller encoded random binary sequence

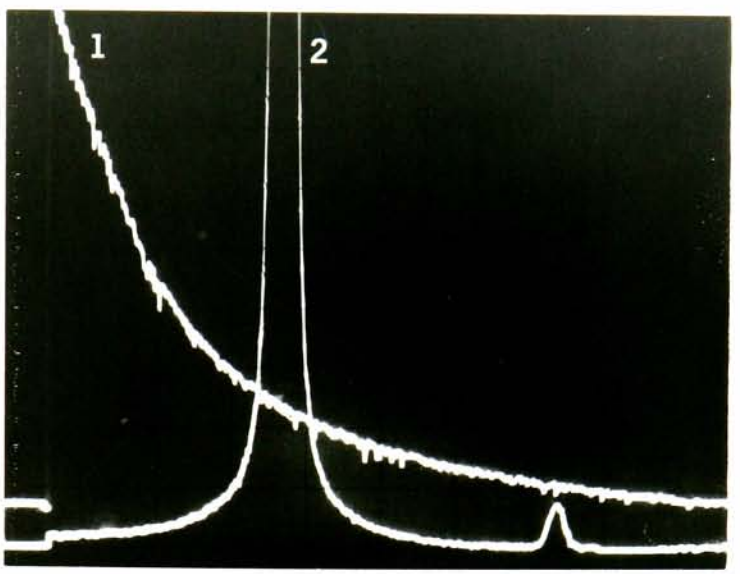

	1	2
Resolution Band Width	300 Hz	300 Hz
Frequency Scan/Div.	2 KHz/cm	2 KHz/cm
Amplitude Ref. Level	-40 db	-40 db
Input Sensitivity	.1 volt	.1 volt
Scan Time/Div.	50 sec/cm	
Input Code Ref.Clock	10 msec	

Note: f_{start} 0 Hz

Fig.23-A Measured power spectrum for:
1. Binary random sequence
2. Sequence "a", Ampex-Miller encoded

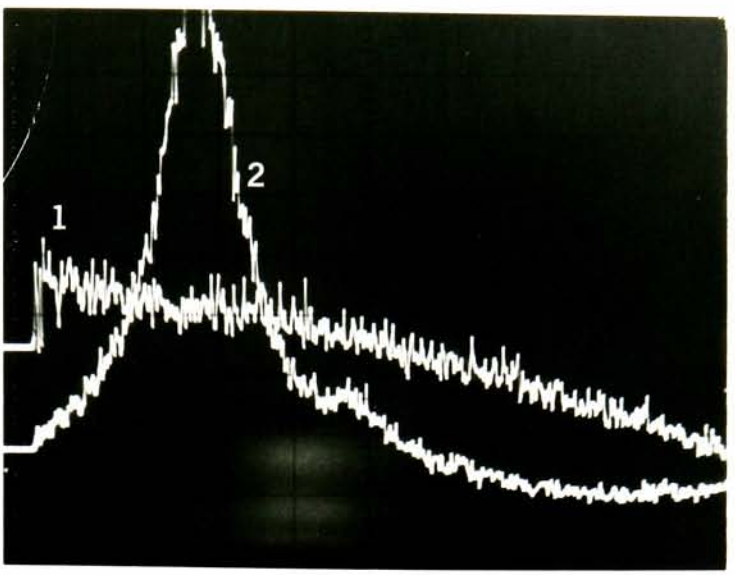

	1	2
Resolution Band Width	100 Hz	100 Hz
Frequency Scan/Div.	2 KHz/cm	2 KHz/cm
Amplitude Ref. Level	-20 db	-30 db
Input Sensitivity	2 volts	2 volts
Scan Time/Div.	100 sec/cm	
Input Code Ref.Clock	33.3 μsec	

Note: f_{start} 0 Hz

Fig.23-B Measured power spectrum for:
1. Binary random sequence
2. Sequence "a", Ampex-Miller encoded

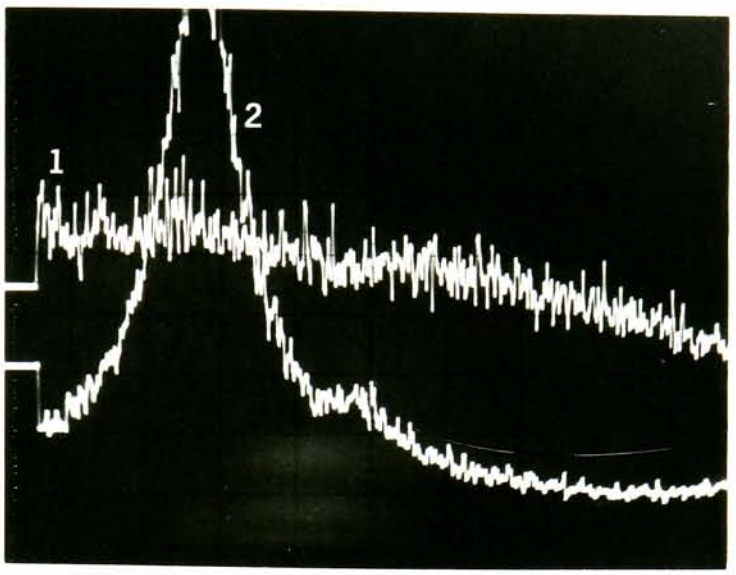

	1	2
Resolution Band Width	100 Hz	100 Hz
Frequency Scan/Div.	5 KHz/cm	2 KHz/cm
Amplitude Ref. Level	-30 db	-30 db
Input Sensitivity	1 volt	.2 volt
Scan Time/Div.	100 sec/cm	
Input Code Ref.Clock	10 μsec	

Note: f_{start} 0 Hz

Fig.23-C Measured power spectrum for:
1. Binary random sequence
2. Sequence "a", Ampex-Miller encoded

CHAPTER IV

TIME BASE ERROR

TIME-BASE ERROR

Source of Error

In ideal tape motion, the tape moves with precise, uniform velocity across the heads. Although improvements are being made, ideal motion is unattainable by tape transports. Servo systems can correct medium or long-term variations in average speed. Although some short-term deviations may be correctable by new, faster, low-inertia, high-torque capstans, complete elimination of flutter is not possible. Therefore, short-term variations must be accepted as inherent to recorders.

There are many causes of velocity variations. Among these are: reel eccentricities, pulsations of the torque motor, tape physical characteristics, vibrations due to friction as the tape passes over fixed guides or heads, mechanical run-out of rotating parts, power line voltage transients which may affect the motors, pinch rollers with surface deformations, sticky bearings, etc. The problem is further compounded by reels and reel drive assemblies which have varying velocities and a mass which is constantly changing.

The terms wow, flutter, and drift have been applied to short-term speed variations that are uniform across the tape. Flutter is applied to tape speed variations occurring at frequencies above 10 Hz; wow indicates variations between 0.1 Hz and 10 Hz; and drift (i.e., tape speed accuracy) denotes those below 0.1 Hz. However, the term "flutter" has been broadened to enclude all uniform speed variations from 0.1 Hz to 10 KHz, for instrumentation recorder applications. Time-base error

(TBE) and jitter are other terms that are also applicable to these same tape speed variations from a different viewpoint. These terms are used to refer to the time discrepancy between a signal reproduced by an ideal transport mechanism (constant speed) and a real one. Time-base error or jitter figures must specify the time during which they were measured; flutter must be stated in rms or peak-to-peak values over a specific band of frequencies.

A properly designed machine has a flutter spectrum composed of small discrete sinusoidal components and a uniformly distributed noise signal. It is difficult to obtain a definite measurement of flutter because noise is present. By recording a very stable sine wave reference and passing the reproduced signal through an FM discriminator, the flutter signal can be obtained. If the tape speeds were identical for both reproduction and recording, the signal generated would be constant. The discriminator will respond to any deviations in the reference tone frequency caused by differences in the two tape speeds. In instrumentation recorders, flutter is measured to at least 10 KHz, and the reference tone should be 5 to 10 times the maximum flutter frequency. Various other flutter measurement techniques are available. Flutter bridges which use a bridge type circuit that is tuned for a null at the reference frequency are also used.

The most widely used method of measuring flutter uses standard FM recording units. The FM record amplifier, with shorted input, is used to record a reference frequency; the FM reproduce unit is used to recover the average and instantaneous frequency variations of the reproduced signal.[8]

"Cumulative flutter" measurements are obtained by passing the flutter signal through a variable cutoff, low-pass filter and measuring the filter's output for increasing values of cutoff frequency.

Since the noise contribution in the flutter signal is basically uniform, the shape of the cumulative flutter curve will rise with frequency. At each point where some rotating component produces a discrete sinusoidal contribution, there will be a small step function in the cumulative curve. Many manufacturers publish curves of this type, but they are usually the averaged results of tests of many transports. Such curves do not show the steps mentioned above, nor the extremes that may be found in individual machines.

It is virtually impossible to obtain a precise rms value for flutter because the signal contains a dc component, a noise component, and many sinewave components. The rms value can be estimated at 1/6 to 1/4 of the peak-to-peak value. This is the usual approximation made in the literature and has been found experimentally to be relatively accurate.

There are many techniques used for measuring time-base perturbations caused by flutter. Basically they all involve comparison between a precise electronic time delay and the time-base represented by some length of tape. A reproduced pulse from the tape is used to initiate the electronic delay, and,some period of time later, a second pulse from the tape is compared with the electronically delayed pulse for time coincidence. The time mismatch between the two pulses then represents a time-base error attributable to tape speed variations. The equipment to accurately make such measurements is costly and not

readily available.

Flutter has several harmful effects on recorded data. Perhaps best known is the noise it produces in FM carrier recordings. A constant frequency carrier will be frequency modulated by tape speed variations and when the carrier is reproduced and discriminated the expected dc output will also include the noise of the unwanted modulation. When the carrier is modulated with a data signal, then this noise is added with the data in the demodulation process. Thus flutter's first order effect is to increase the noise level of the reproduced signal with a corresponding reduction in dynamic range. For a given percentage flutter, the ability of the flutter noise to interfere with the data signal is dependent on the deviation ratio of the FM carrier system being recorded.

Flutter disrupts the time-base of the reproduced signal in the direct record mode, causing the reproduced waveform to suffer broadening of its spectral components. A more detailed analysis of this topic follows.

The random nature of flutter is related to the physical characteristics of the tape as follows: The tape coating is granular in nature, and when this surface rubs on fixed surfaces, such as the heads, it will be subjected to a large number of very small impulse forces. These would be caused by the granular nature of the tape coating, variations in individual particle coefficients of friction, and minute imperfections in the surface contacting the head. The net effect is a forcing function which resembles shot noise. Because of the large number of possible resonances, the tape itself will respond to this

forcing function in a complex way. In view of the number and wide range of such possible resonances and the different damping of many of them, it is reasonable to suppose that the tape will greatly affect the spectral distribution of the forcing function over the range of frequencies normally encompassed in flutter measurements. As tape transports are improved by the elimination of periodic flutter components, a relatively low level of random flutter will remain distributed uniformly over the flutter spectrum. This is clearly apparent from flutter frequency analyses and the general shape of cumulative flutter curves published by manufacturers of tape transport equipment.

A driving impulse caused by a single particle will set up waves in the tape which travel in all directions; these will be reflected from the edges of the tape and from sections where the tape is in contact with parts of the tape transport. The velocity of such waves will be different in different directions, further complicating the pattern.

Consequently, in a machine so perfect that periodic flutter components are negligible, we should expect a background random flutter with an approximately uniform frequency spectrum. A portion of this flutter would be correlated in adjacent tracks, while the balance would be uncorrelated.

A relationship between sinusoidal flutter and time-base error can be obtained by observing the flutter waveform from two different points of view.

Let:

$$V_{carrier} = \cos \theta$$

$$\theta = \omega_c t + K \int f(t)\, dt$$

Instantaneous Frequency:

$$\omega_{inst.} = \frac{d}{dt}\theta$$

$$= \omega_c + K\, f(t)$$

Frequency Deviation:

$$\frac{\Delta\omega_{op}}{\omega_c} = \frac{\Delta f_{op}}{f_c}$$

$$= \frac{K}{\omega_c} \qquad \text{(a)}$$

Note: The usual definition of frequency deviation is: $|K\, f(t)|_{max}$. However, it is assumed f(t) has a unity peak value.

Let:

$$f(t) = \cos(\omega_F t)$$

where ω_F is the flutter frequency.

$$V_{carrier} = \cos\theta$$

$$= \cos\{\omega_c t + K \int f(t)\, dt\}$$

$$= \cos\{\omega_c t + \frac{K}{\omega_F}\sin(\omega_F t)\}$$

Phase Deviation:

$$\Delta\Phi_{op} = \frac{K}{\omega_F} \qquad \text{(b)}$$

Solving for K in equation (a) and (b) and equating, one can obtain:

$$\omega_f \Delta\Phi_{op} = \frac{\omega_c \ \Delta f_{op}}{f_c}$$

$$\Delta\Phi_{op} = \frac{\omega_c}{\omega_f} \ \frac{\Delta f}{f_c} \qquad \text{(c)}$$

Suppose this change in phase were generated by a perfectly linear delay line:

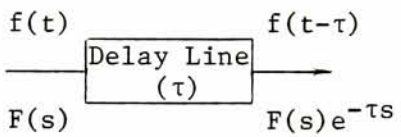

Setting $s = j\omega$,

$$V_{out}(j\omega) = F(j\omega) \ e^{-j\omega\tau}$$

$$= |V_{out}(j\omega)| \ e^{j\phi(\omega)}$$

Therefore,

$$\Delta\phi = -\omega\tau$$

It is obvious the delay τ and the phase of the output signal relative to the input signal are related as follows: For an input sinusoid of frequency ω_c,

$$\tau = \frac{1}{\omega_c} \Delta\Phi \qquad \text{(d)}$$

Equating (c) and (d),

$$\tau = \frac{1}{\omega_c} \frac{\omega_c}{\omega_f} \frac{\Delta f_{op}}{f_c}$$

$$\tau = \frac{1}{2\pi} \frac{1}{f_F} \frac{\Delta f_{op}}{f_c}$$

Flutter, however, is generally measured in peak-to-peak and percent, or in rms and percent.

Peak-to-peak and percent:

$$F_{pp}(\%) = 2 \frac{\Delta f_{op}}{f_c} \times 100$$

Therefore

$$\tau = \frac{1}{4\pi \times 100} \frac{1}{f_F} F_{pp}(\%)$$

This equation can be interpreted as the amount of time required to correct a particular quantity of flutter. Conversely, it can also be interpreted as the amount of time delay required to generate a particular quantity of flutter.

Consider, for example, a discrete delay line of a delay,

$$\tau = \frac{n}{f_o}$$

where n refers to the number of storage elements, and f_o refers to the rate at which the data travels through these elements.

Let

$$f_o = \overline{f}_o \{1 + K_o \cos(\omega_F t)\}$$

$K_o \overline{f}_o$ is the peak frequency deviation of f_o.

$\overline{f}_o$ is the average data rate .

$$\tau = \frac{n}{f_o}$$

$$= \frac{n}{\bar{f}_o\{1 + K_o \cos(\omega_F t)\}}$$

$$= \frac{n}{\bar{f}_o}\left(\frac{1}{1 + K_o \cos(\omega_F t)}\right)$$

$$= \frac{n}{\bar{f}_o}\{1 - K_o \cos(\omega_F t)\} \text{ , for } K_o << 1$$

Let the input signal,

$$V_{in}(t) = \cos(\omega_c t)$$

Then,

$$V_o(t) = \cos\{\omega_c(t - T_{total})\}$$

$$= \cos(\omega_c t - \omega_c T_{total})$$

$$= \cos\{\omega_c t - \frac{n\omega_c}{\bar{f}_o} + \frac{n\omega_c K_o}{\bar{f}_o} \cos(\omega_F t)\}$$

$$= \cos(\omega t - \Phi_{fixed} + K_\phi \Delta\Phi)$$

Instantaneous frequency out:

$$\omega_o = \frac{d}{dt}\{\Phi(t)\}$$

$$= \omega_c - \left(\frac{nK_o\omega_c\omega_F}{\bar{f}_o}\right) \sin(\omega_F t)$$

$$= \omega_c\{1 - \frac{nK_o\omega_F}{\bar{f}_o} \sin(\omega_F t)\}$$

$$\frac{\omega_o}{\omega_c} = 1 - \frac{nK_o\omega_F}{\overline{f}_o} \sin(\omega_F t)$$

$$\left.\frac{\omega_o}{\omega_c}\right|_{max} = 1 + \frac{nK_o\omega_F}{\overline{f}_o} \qquad \text{(e)}$$

Percent change in output frequency, $\Delta\%$:

$$\Delta\% = \frac{\omega_{out} - \omega_{in}}{\omega_{in}} \times 100$$

$$= \left(\frac{\omega_{out}}{\omega_{in}} - 1\right) \times 100$$

$$= \left(\frac{\omega_o}{\omega_{in}} - 1\right) \times 100 \qquad \text{(f)}$$

Substituting equation (e) in (f):

$$\Delta\% = \left(1 + \frac{nK_o\omega_F}{\overline{f}_o} - 1\right) \times 100$$

$$= \frac{nK_o\omega_F}{\overline{f}_o} \times 100 \qquad \text{(g)}$$

It should be noted the term:

$$\Delta\% = \frac{\omega_o - \omega_{in}}{\omega_{in}} \times 100$$

$$= \frac{\Delta f}{f} \times 100$$

which is flutter in percent peak-to-peak.

The significance of equation (g) becomes evident when trying to find the amount of flutter that would be generated (or, for that matter, corrected) by such a delay system. Let for example:

$$n = 2048$$

$$\bar{f}_o = 50 \text{ KHz}$$

$$K_o = .05 \text{ (i.e., 5\% change in clock rate)}$$

$$\omega_F = 2\pi(10 \text{ Hz}) \text{ rad/sec}$$

The percent change in output frequency can then be found using:

$$\Delta\% = \frac{nK_o\omega_F}{\bar{f}_o} \times 100$$

$$= \frac{(2048)(.05)(2\pi)(10)}{(50 \times 10^3)} \times 100$$

$$= 12.8\%$$

Therefore, for a 1 KHz tone input, the output frequency would vary from 1,128 Hz to 872 Hz at a 10 Hz rate. This interesting effect is not only observable, but also audible.

The subjective effects of audio flutter have been measured, standardized, and are readily available in the literature. The original national standards were first published by the Journal of Audio Engineering Society, Volume 19, pages 859-861 (November 1971).

Because the preceptibility of frequency variations depends on the variation frequency,[9] the measurements are performed with a weighting filter which approximates the ear/brain mechanism. This particular combination of weights have been found to give measured values of flutter which predict the subjective evaluations made by listening panels. Fig.24 shows the standard curve used to determine the subjective effects of audio flutter components. In the case of video recorders, as well as computer data recorders, flutter is always considered in peak percent.

When considering the desired parameters of a time base corrector, particular emphasis should be given to the flutter bandwidth to be corrected. In video, for example, the lowest frequency which needs to be corrected is the fastest frequency that the reproducing video system's AFC will respond to. In other words, there is no need to correct flutter components which are tracked by the displaying raster. This is particularly important when, by observing equation (g), one notes the fact that the lower the flutter frequency of interest, the larger the amount of memory (n) needed for the same percent flutter ($\Delta\%$). On the other hand, the upper cutoff frequency of a video time base corrector is chosen for one of two reasons: either no significant mechanism flutter is expected in this frequency region, or flutter there shows up primarily as a small loss in resolution. In an audio time base corrector, however, the frequencies are chosen to suppress the flutter components which lie in the preceptible region of Fig.24. From this figure, it can be noted that the flutter region which appears to be most

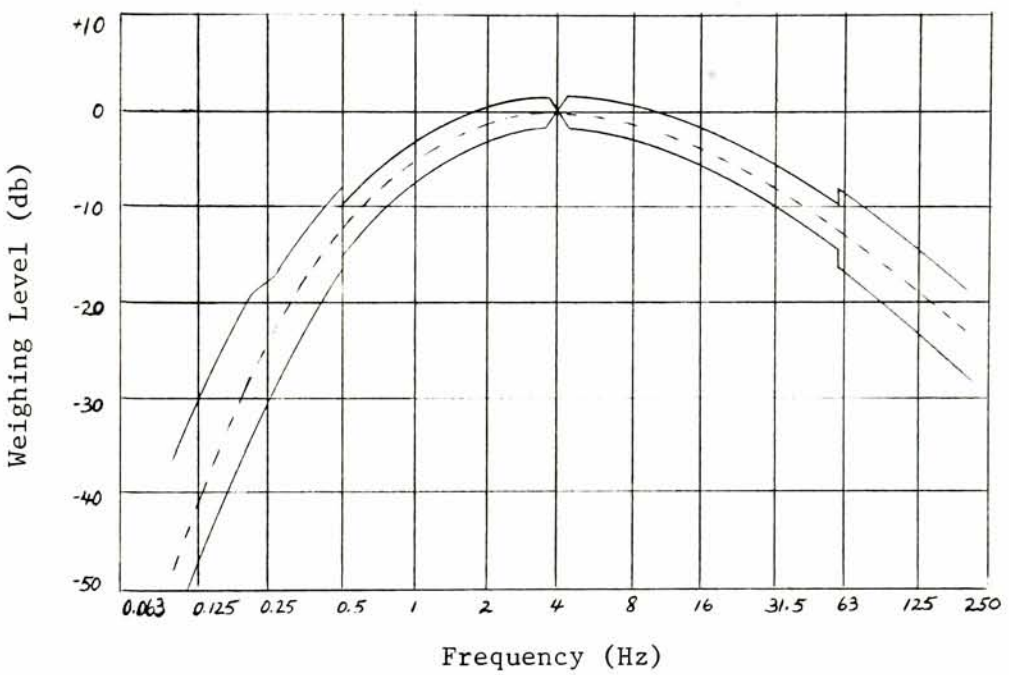

Fig.24 Nationally Standardized Subjective Flutter Weights

preceptible lies approximately between .3 Hz and 200 Hz.

Conceptually, a time base corrector could look like the continuous storage medium depicted in Fig.25. In this figure, the storage elements are the pockets on the circumference of the circle. Data is input to memory by way of the write arm and output by way of the read arm. If these arms are allowed to rotate in a clockwise direction, for example, while maintaining the same angular relationship (in this case, 180°), the system will behave like a delay line with n/2 storage elements and the delay (T) from input to output would be given by:

$$T = \frac{n}{2f_o}$$

where n is the number of storage elements in the delay line, and f_o is the rate at which the arms are allowed to move. Suppose now that the arms were allowed to move at different rates: f_w for the write arm and f_R for the read arm. The angular relationship between the two arms will be contineously changing; however, they are not permitted to overrun one another since the condition will cause either data to be read twice or to be rewritten before it can be read. In any event, a data discontinuity would take place.

The operation of this system as a time base corrector can now be easily understood. Allowing the write arm to move synchronously with the data coming from the tape will store in memory the last n data bits. These are being continuously updated. The write clock (f_w) can be obtained by phase-locking the f_w-generator to the incoming data. The read arm can now be used to extract the data from memory at the read

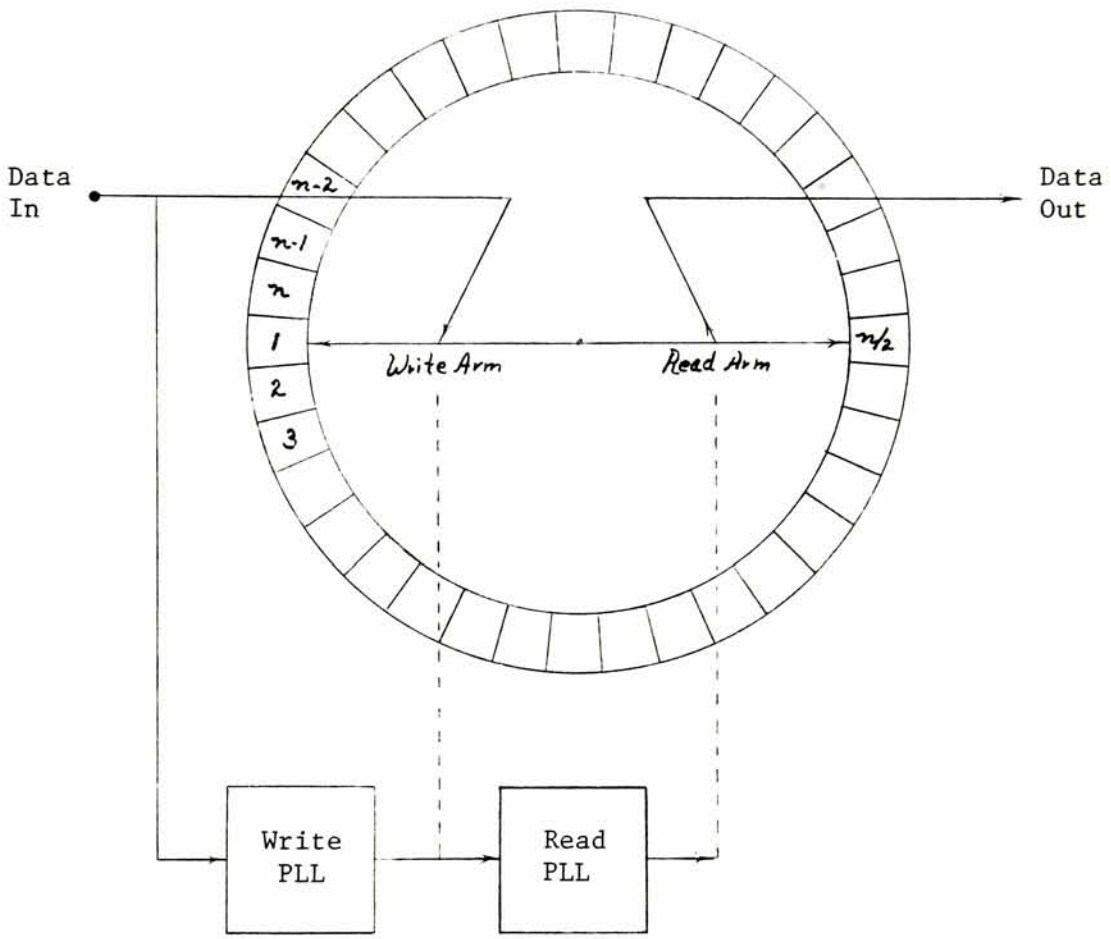

Fig.25 Model of a digital time base corrector

clock rate (f_R). This clock must be chosen to meet the following two characteristics: First of all, the time base stability of the clock will determine the stability of the data. And secondly, the smaller the frequency variation of the clock relative to the write clock, the larger the memory needs to be. This fact was discussed earlier. A good choice, then, is to follow the long term variations of the write clock with the read clock. Hence, this clock can be readily obtained by phase-locking the read clock generator, with a very long time constant, to the write colck. The bandwidth of the read PLL is chosen to be approximately .1 Hz. As perviously noted, this is the beginning of the audible flutter range.

Hardware Description

Fig.26 is a block diagram of a complete time base corrector; it contains the following subdivisions:

Part 1 - Address generator and control logic

Part 2 - Memory and the address multiplex function

Part 3 - Write Phase-Locked Loop

Part 4 - Output Phase-Locked Loop

Each of these subdivisions is, in itself, a block diagram of a circuit schematic (referenced in the upper left-hand corner of each part).

Part 1 is a block diagram of Fig.27. In this figure, the write address is generated by the twelve bit binary counter made up of three 74161 packages labled numbers 1, 2, and 3. This counter is allowed to count to its maximum count and recycle. The read address is generated by a similar counter made up of packages 4, 5 and 6. This counter, like

the write counter, is allowed to recycle after its maximum count as long as the addresses from both the read and the write counters do not overrun each other. If this should happen, a reset mechanism will be triggered which will cause the read counter to be programmed to n/2 when the write counter recycles through zero. Referring to the model, this mechanism sets the arms back to 180°. The mechanism previously referred to consists of a 12 bit comparator which, when the addresses are equal, sets to one the Q output (pin 5) of the FF7474 (package 15). At this point, the system is ready to program; all that is needed is for the write counter to recycle. When this happens, the terminal count output of the write counter will go low causing the 4FF (packages 12 and 13) to emit a pulse synchronously with the read clock, which will cause the read counter to restart its count from the programmed value. It should be noted that this programming mechanism can be started in two other ways. One is by the manual reset switch, and the other is during start up. The start up cycle is used to ensure a quiescent operating point equivalent to a 180° arm separation in our model. Finally, the timing pulses required to operate the multiplexers, the memory, and the latch in Part 2 of Fig.26 are generated from the following edge of the write clock by the 9602 monostable multi-vibrators shown at the bottom left side of Fig.27.

Part 2 is the block diagram of the schematic shown in Fig.28. In this figure, the required electronic circuits needed to multiplex the read and write addresses, as well as the memory, are shown. The multiplexers are the 74S157 (packages 1, 2, 3, and 4) and the memory is the SN745207 (packages 5, 6 and 7). These two packages were chosen

because of their relatively low access time (less than 50 nsec) which ensures a comparatively fast multiplexing time. The SN74S139 is a dual decoder used to decode the two most significant address bits into one of four chip select lines.

Part 3 is the write PLL shown in Fig.29. The dynamic characteristics of this circuit are identical to that of the decoding PLL described in connection with the Ampex-Miller decoder. The only significant difference here is the use of a transition detector at its input to ensure proper operation when the Ampex-Miller decoder is not used.

Part 4, as shown in Fig.26, is the output PLL, the corresponding schematic of which is shown in Fig.30. This phase-locked loop was designed to have three different characteristics, depending on the specific module used. This was motivated by the choice of bandwidth and the tradeoffs involved in their respective tracking ranges. As the PLL's bandwidth is made narrower, so is the corresponding tracking range. At some point, this is likely to present a problem because the low frequency flutter (drift) may cause the input to this loop (f_w) to find itself outside the lock-range of the PLL.[11] The phase detector in this subsystem was designed to be linear from 0 radians to 100π radians, not only to alleviate the tracking problem, but also to permit this type of a loop to perform a dual function. This will be discussed later. The detector itself is made up of the 9316 counters (packages 1, 2, 3, and 4), the 7474 dual D-FF (package 7) and exclusive OR gates (package 5). The voltage control oscillator used is the XR2207 (package 6). This is an excellent device with a very linear voltage to frequency characteristic.

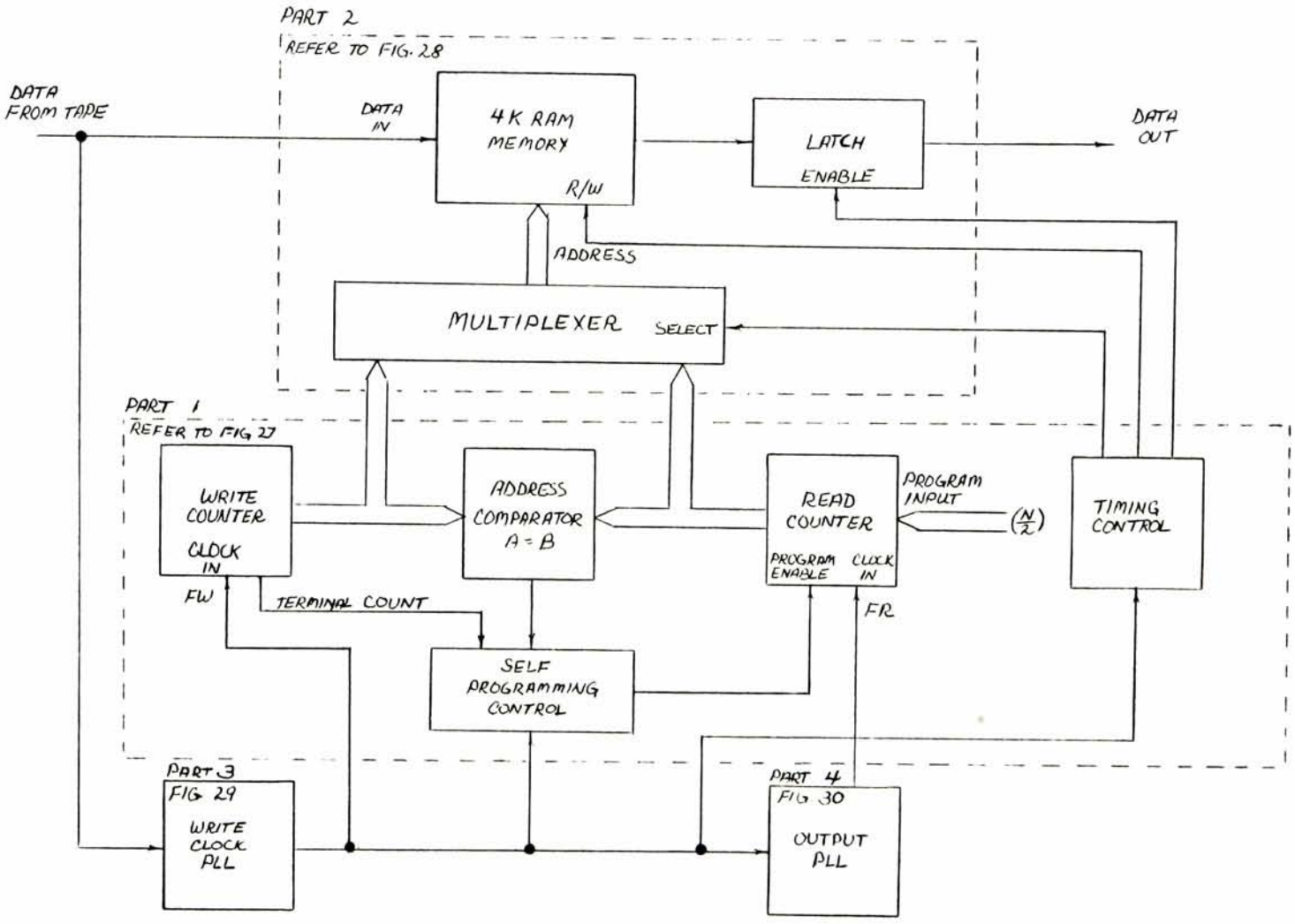

Fig.26 Digital Time Base Corrector
Block Diagram

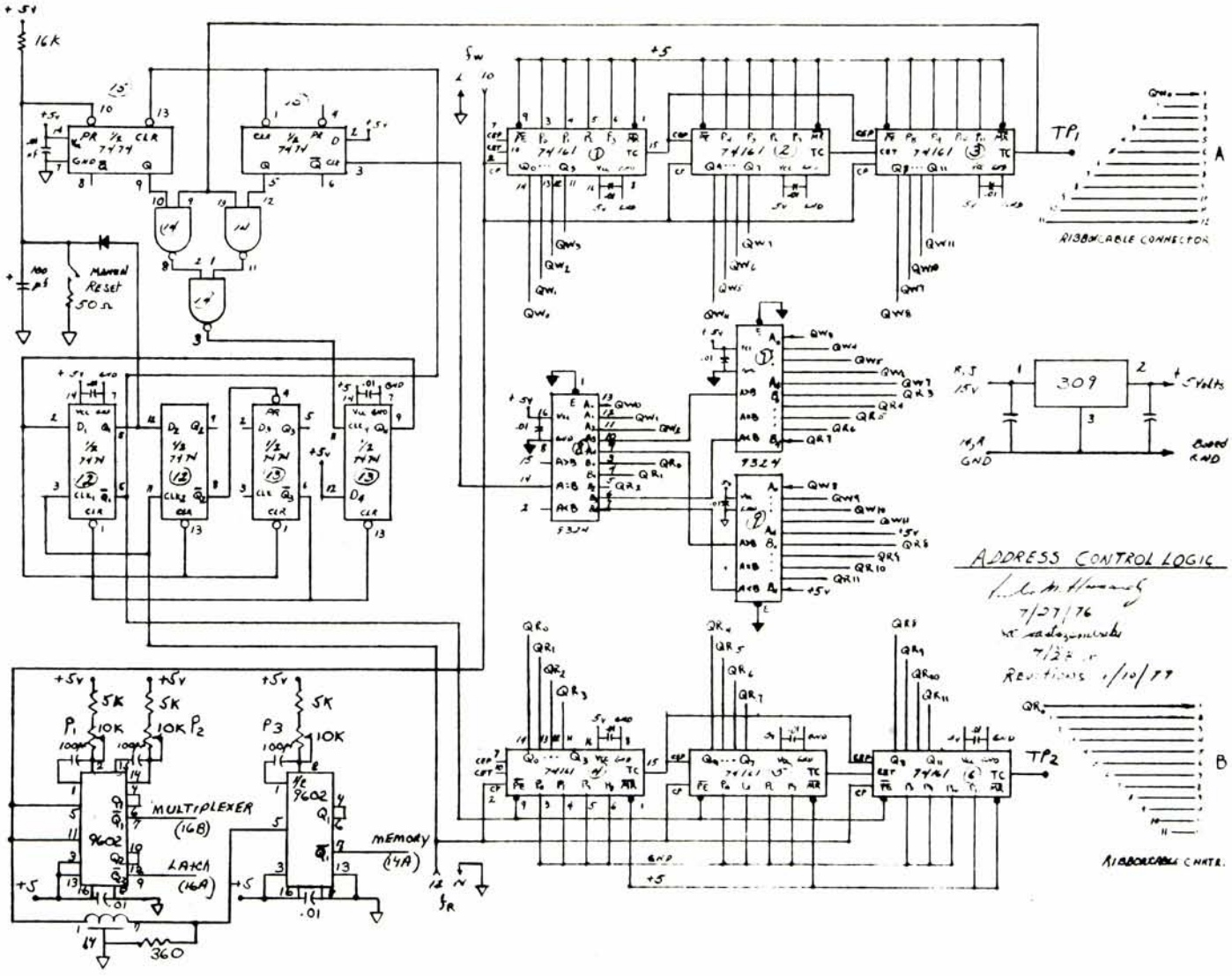

ADDRESS CONTROL LOGIC
7/27/76
MULTIPLEXER (16B)
LATCH (16A)
MEMORY (14A)
RIBBON CABLE CONNECTOR
RIBBON CABLE CNNTR.
TP1
TP2
309
5 Volts
Board GND
Manual Reset

Fig. 27

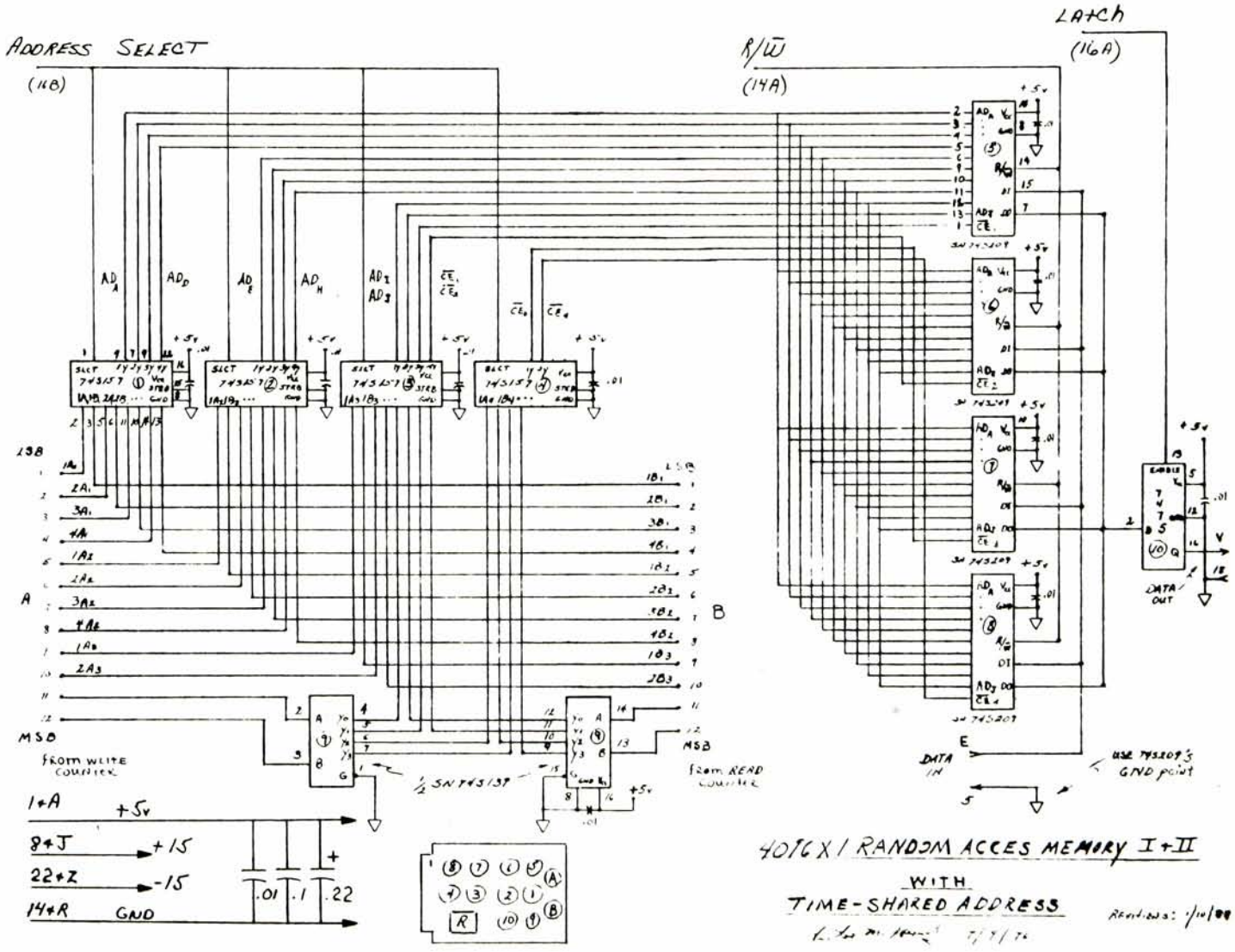
ADDRESS SELECT
(11B)
R/W̄
(14A)
LATCH
(16A)
LSB
MSB
FROM WRITE COUNTER
FROM READ COUNTER
½ SN 74S139
DATA IN
DATA OUT
USE 74S209'S GND point
1+A +5v
8+J +15
22+Z -15
14+R GND
.01
.1
.22
4096 X 1 RANDOM ACCES MEMORY I+II
WITH
TIME-SHARED ADDRESS

Fig. 28

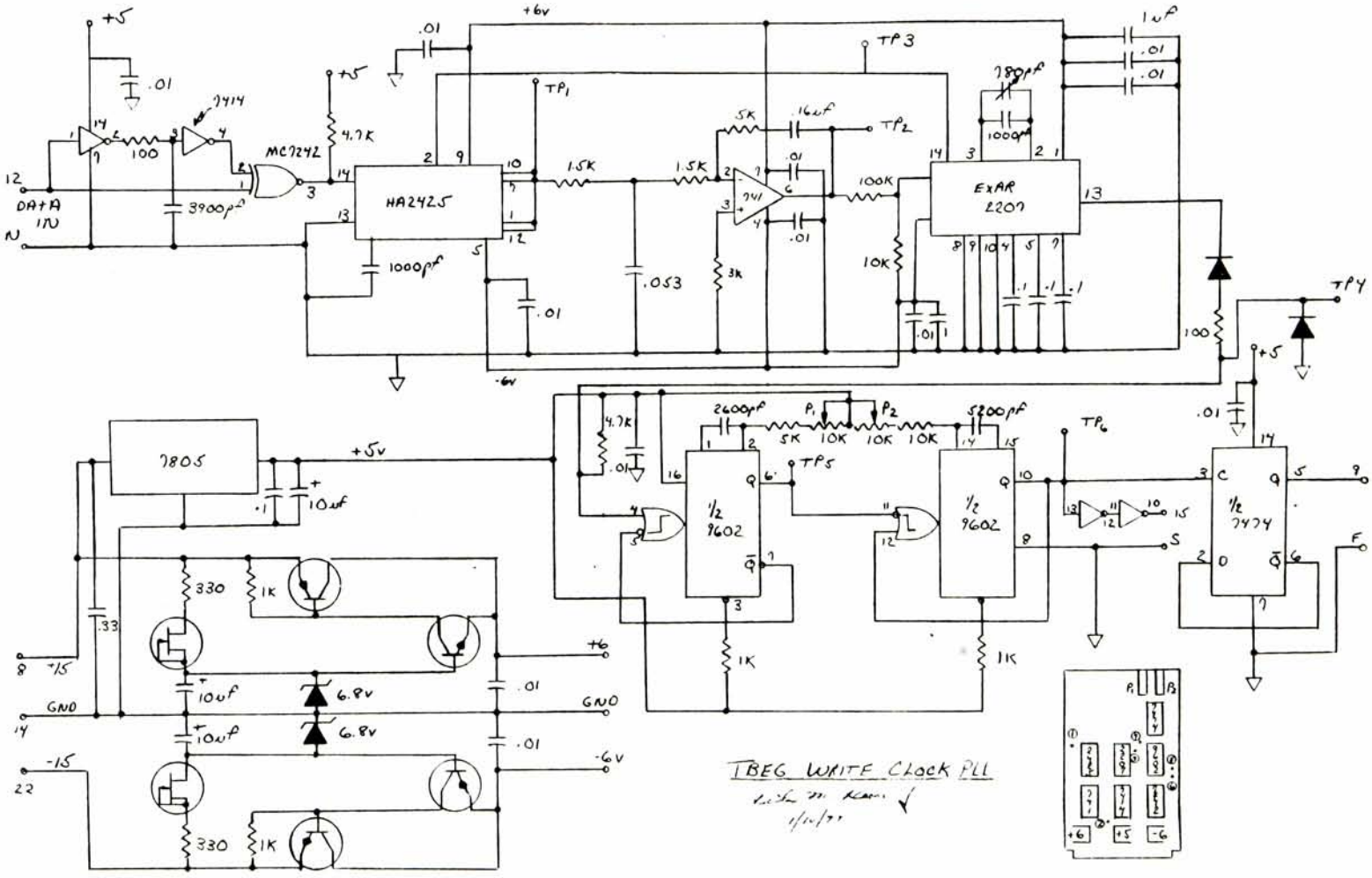

+5
.01
7414
100
3900pf
12
DATA IN
N
MC7242
4.7K
HA2425
1000pf
+6v
TP1
1.5K
.053
.01
-6v
TP3
5K
.16uf
TP2
741
3K
100K
10K
780pf
1000pf
EXAR 2207
1uf
TP4
100
7805
+5v
10uf
.33
330
1K
6.8v
+6
GND
-6v
-15
8
14
22
2600pf
P1
P2
5K
10K
5200pf
TP5
TP6
1/2 9602
1/2 7474
S
F
TBEG WRITE CLOCK PLL

Fig. 29

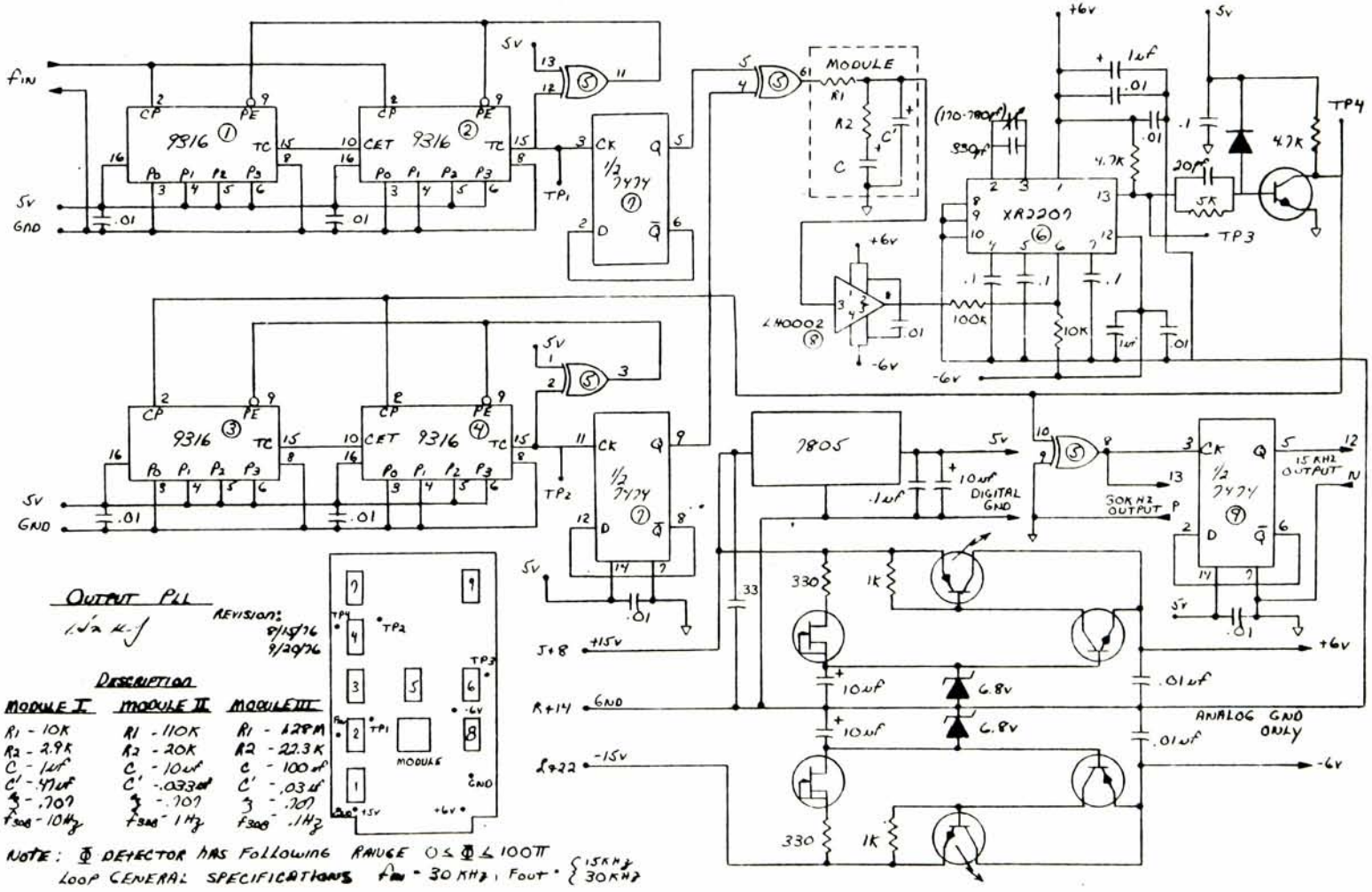

OUTPUT PLL

REVISION: 8/15/76 9/20/76

DESCRIPTION

MODULE I	MODULE II	MODULE III
R1 - 10K	R1 - 110K	R1 - 1.28M
R2 - 2.9K	R2 - 20K	R2 - 22.3K
C - 1uf	C - 10uf	C - 100uf
C' - .47uf	C' - .033uf	C' - .03uf
ζ - .707	ζ - .707	ζ - .707
f_{3DB} - 10Hz	f_{3DB} - 1Hz	f_{3DB} - .1Hz

NOTE: Φ DETECTOR HAS FOLLOWING RANGE $0 \le \Phi \le 100\pi$

LOOP GENERAL SPECIFICATIONS f_{IN} = 30 KHz, F_{OUT} = {15KHz, 30KHz}

Fig. 30

In addition, still another phase-locked loop was implemented in order to study the deleterious effects of flutter. This loop is intended to replace the output PLL in order to convert the time base corrector (TBC) to a time base error generator (TBEG). It will also track the long-term variations of the write clock, but will permit its output frequency to vary while it is still tracking. The schematics for this circuit are shown in Fig.31, where it has been designated "TBEG Read Clock PLL". This figure looks quite similar to Fig.30, but careful observation will reveal that, first of all, the loop has two inputs. One is the write reference clock, and the other is the external flutter input. In order to obtain a satisfactory flutter input-to-output transfer function while maintaining an adequate reference input-to-output phase transfer function, the module was also modified. This is the dual purpose spoken of in the description of Part 4 of Fig.26.

It is relatively easy to show the transfer functions of the input (write) and the output (read) PLL's are:

Input PLL Transfer Function $H_{I\text{-}PLL}(s)$:

$$H_{I\text{-}PLL}(s) = \frac{N(1 + \tau s)\ \omega_n^2}{s^2 + 2\xi\omega_n s + \omega_n^2}$$

Where:

$$\tau = R_2C = 8 \times 10^{-4}$$

$$\xi = 1$$

$$\omega_n = 2\pi(403) \text{ rad/sec}$$

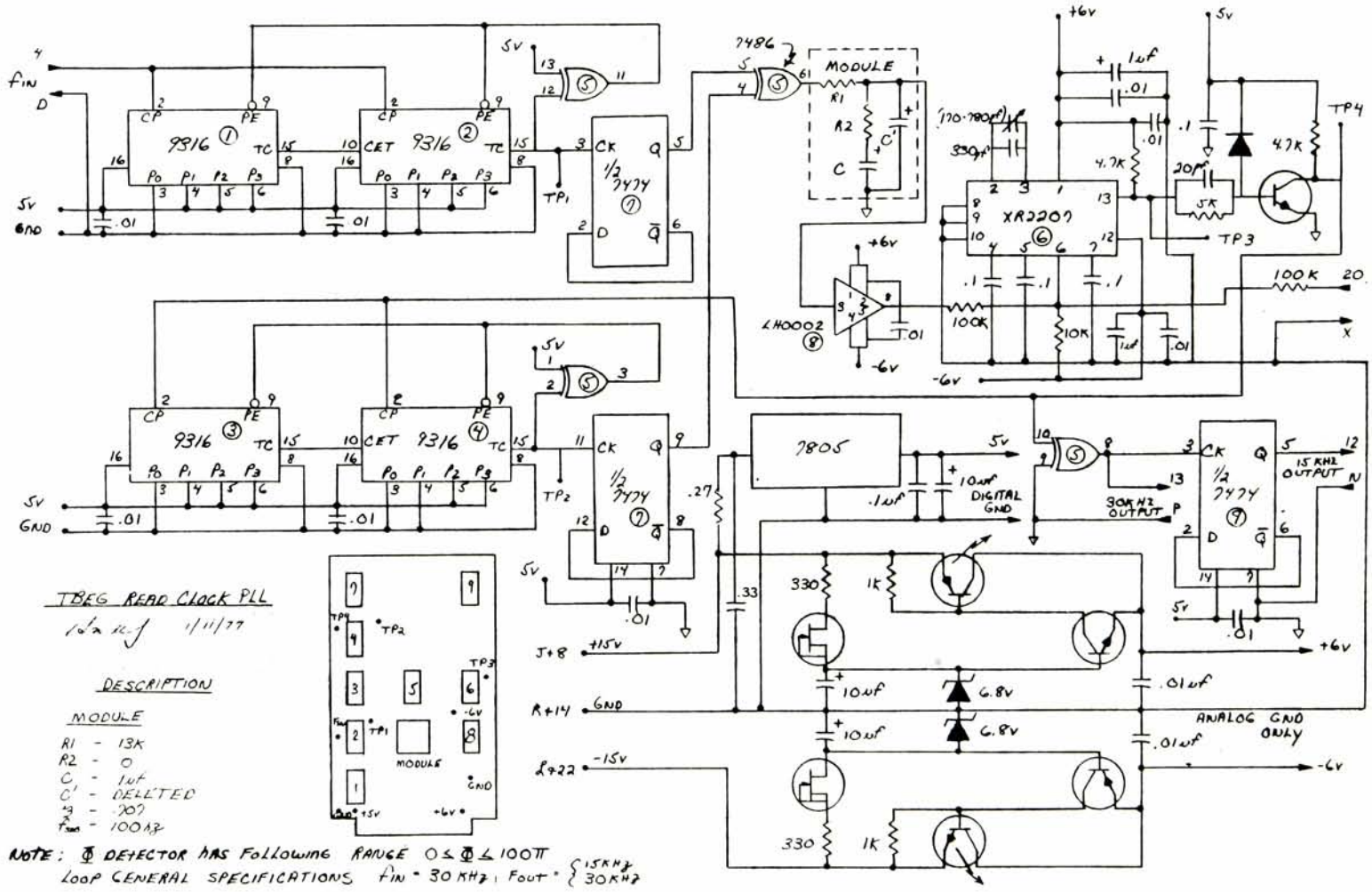

TBEG READ CLOCK PLL
1/11/77
DESCRIPTION
MODULE
R1 - 13K
R2 - 0
C - 1uf
C' - DELETED
Q - 707
Fsub - 100hz
NOTE: Φ DETECTOR HAS FOLLOWING RANGE 0 ≤ Φ ≤ 100π
LOOP GENERAL SPECIFICATIONS fIN = 30 KHz, FOUT = {15KHz 30KHz
9316
1/2 7474
7486
MODULE
XR2207
LH0002
7805
DIGITAL GND
30KHz OUTPUT
15 KHz OUTPUT
ANALOG GND ONLY
J+8 +15v
R+14 GND
L+22 -15v

Fig. 31

Output PLL Transfer Function $H_{O\text{-}PLL}(s)$:

$$H_{O\text{-}PLL}(s) = \frac{\phi_{out}(s)}{\phi_{in}(s)}$$

$$= \frac{s\omega_n\left(2\xi - \frac{\omega_n}{K_o K_\phi}\right) - \omega_n^2}{s^2 + 2\xi\omega_n s + \omega_n^2}$$

Where:

$$\xi = .707$$

$$\omega_n = {}_{3db} = 2\pi(.1)\text{rad/sec}$$

$$K_\phi = \frac{5}{\pi}\frac{\text{volts}}{\text{rads}}$$

$$K_o = 3.2 \times 10 \quad \text{rad/sec volt}$$

The behavior of the time base corrector can be analytically studied if the following assumption is made. Since this system is time variant, it is not possible to obtain a transfer function. However, if we define the term "flutter transfer function", FTF(s), as the amplitude and phase of the ratio of the flutter of the output signal divided by the flutter of the input signal, and further assume the effect of the delays involved to be negligible, a very useful analytical solution can be found which will determine the flutter supressing characteristics of the TBC:

$$FTF(s) = H_{I-PLL}(s) \cdot H_{O-PLL}(s)$$

A plot of the amplitude and phase of the flutter transfer function (FTF) is shown in Fig.32. The low frequency breakpoint is caused by H_{O-PLL}. This is readily observable from the analytical experssion for the FTF. The vertical scale of this figure indicates the amount of flutter rejection in decibles the TBC will deliver to the particular frequency on the horizontal scale. The phase, however, can only be considered a relative measure of the phase shift that a specific flutter component will have with respect to another at a different frequency.

Experimental Results

In order to observe the spectral degradation of a fluttered signal, the test shown in Fig.33 was performed. In this test a known quantity of flutter was generated, and its effect was observed with a high resolution spectrum analyzer. The amount of flutter was calculated from the total change in delay (ΔT) generated by the TBEG and the specific flutter frequency (f_F) as follows:

$$F_{pp}(\%) = 4\pi(100) f_F \Delta T$$

Note: This equation was previously derived for sinusoidal flutter only and is used, as such, throughout this test.

The results of this test are shown in Fig.34. Fig.34-a is the spectrum of the input signal to the TBEG, and Fig.34-b is the output spectrum. The output is a 3 KHz signal with a 1% sinusoidal flutter.

The broadening effect flutter has on the spectrum is readily observable. Time base modulation, like other forms of angle modulation, typically exhibits a line spectrum which broadens as the modulation index becomes larger. The line components of the spectrum are hardly preceptable in Fig. 34-b.

Finally, the test shown in Fig.35 was performed in order to study the flutter-correcting effects of the TBC. The input signal, a 3 KHz square wave, was fluttered with a 100 Hz sinusoidal in order to generate a total peak-to-peak percent flutter equal to 10%. This fluttered signal was then brought to the TBC where it was defluttered. The spectrum of the corresponding input and output signals to the TBC are shown in Fig.36. These results clearly show the supression of the sidebands caused by the unwanted time base modulation.

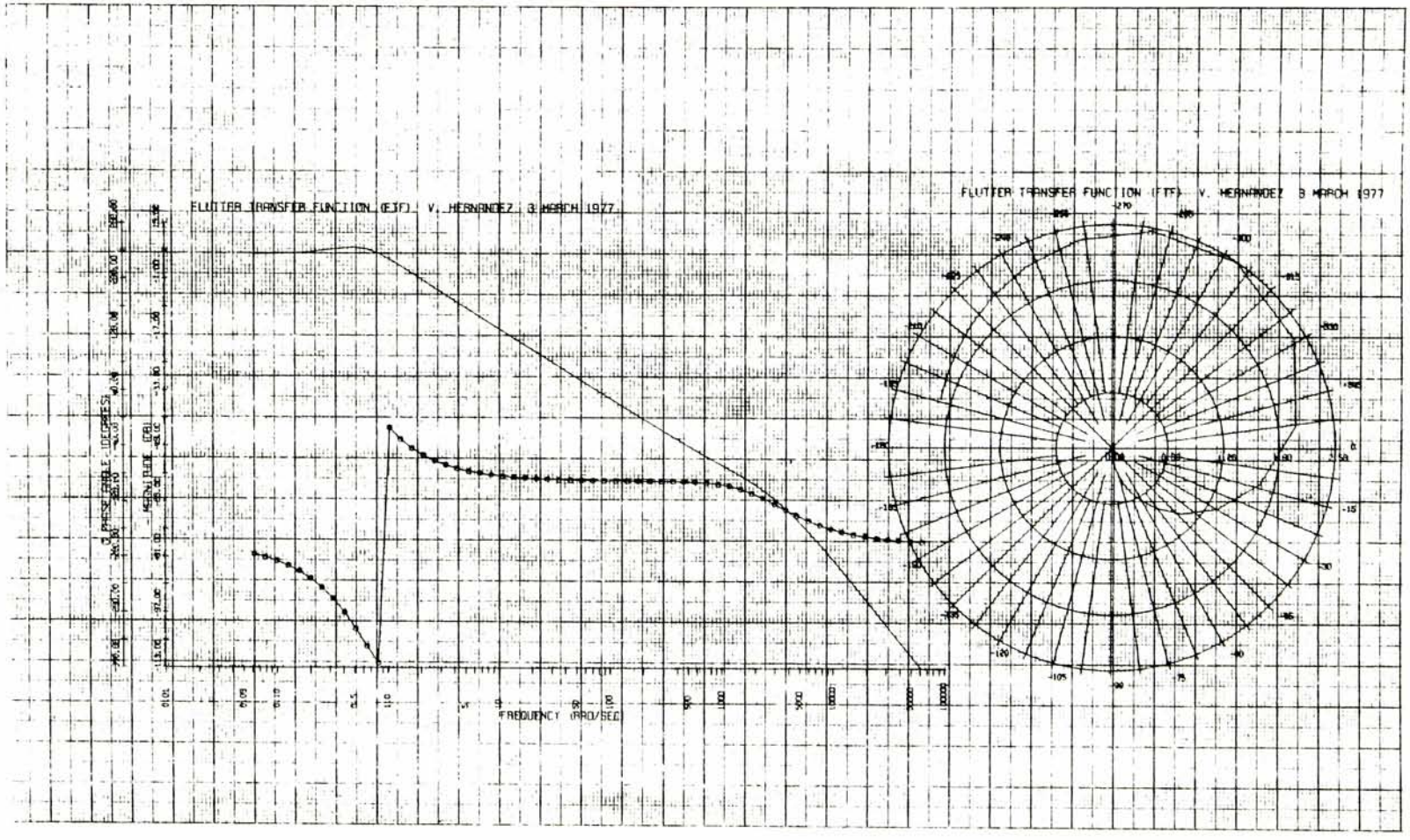
FLUTTER TRANSFER FUNCTION (FTF) V. HERNANDEZ 3 MARCH 1977
FLUTTER TRANSFER FUNCTION (FTF) V. HERNANDEZ 3 MARCH 1977
PHASE ANGLE (DEGREES)
MAGNITUDE (DB)
FREQUENCY (RAD/SEC)

Fig. 32

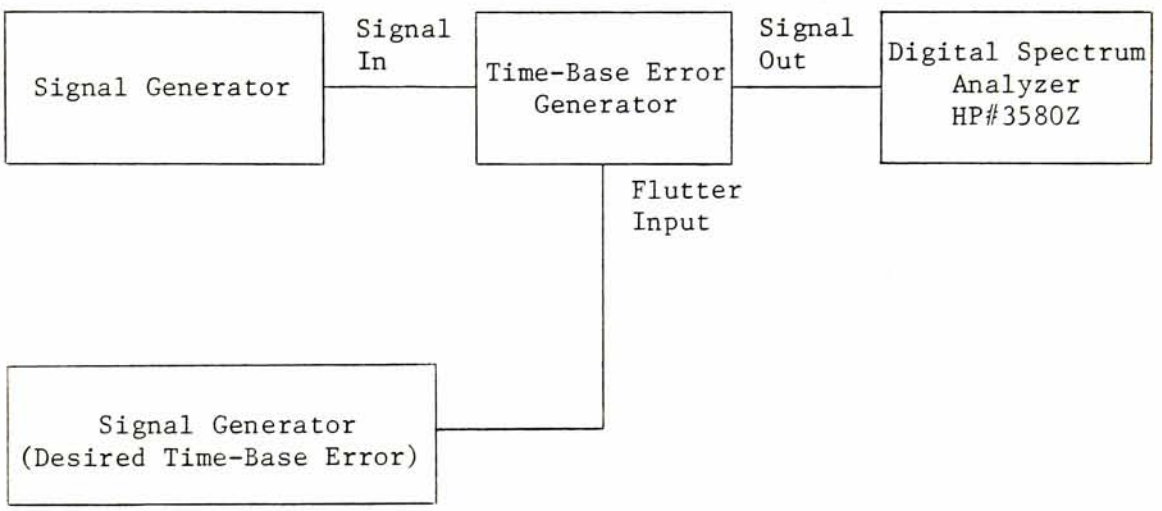

Fig.33 Experimental setup used to study the effect of flutter

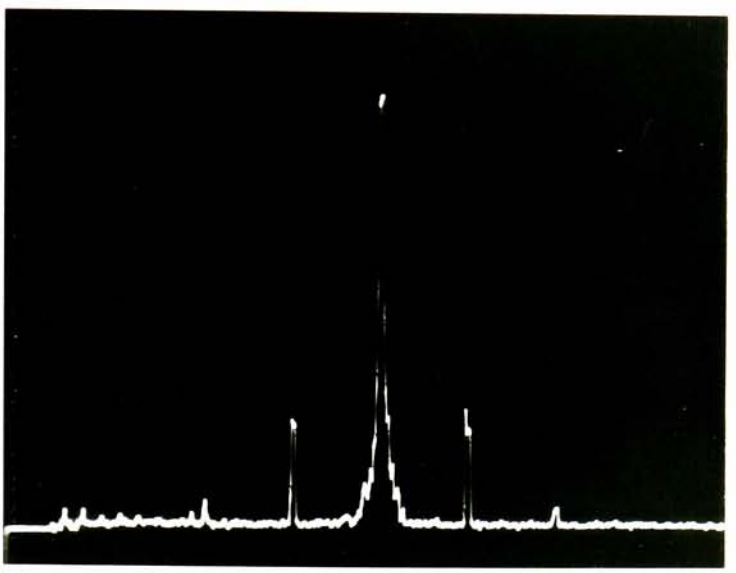

Unfluttered Spectrum

Spectrum Analyzer Settings	
Resolution Bandwidth	3 Hz
Frequency Scan/Division	.5 KHz/cm
Center Frequency	3 KHz
Vertical Scale	10 db/cm
Amplitude Reference Level	-10 db
Input Sensitivity	+10 db
Scan Time/Division	100 sec/cm

Fig.34-a Spectral degrading effects of flutter

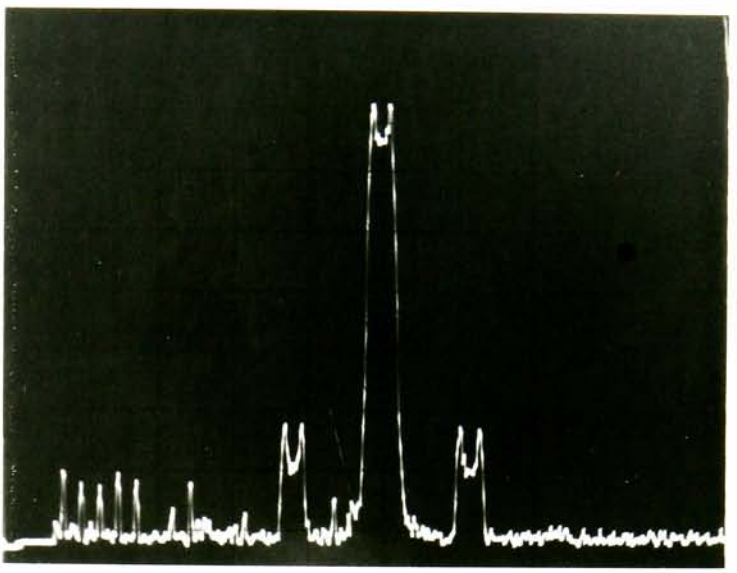

Fluttered Spectrum

$F_{pp}(\%) = 1\%$

$f_{Flutter} = 1$ Hz

Spectrum Analyzer Settings	
Resolution Bandwidth	3 Hz
Frequency Scan/Division	.5 KHz/cm
Center Frequency	3 KHz
Vertical Scale	10 db/cm
Amplitude Reference Level	-10 db
Input Sensitivity	+10 db
Scan Time/Division	100 sec/cm

Fig. 34-b Spectral degrading effects of flutter

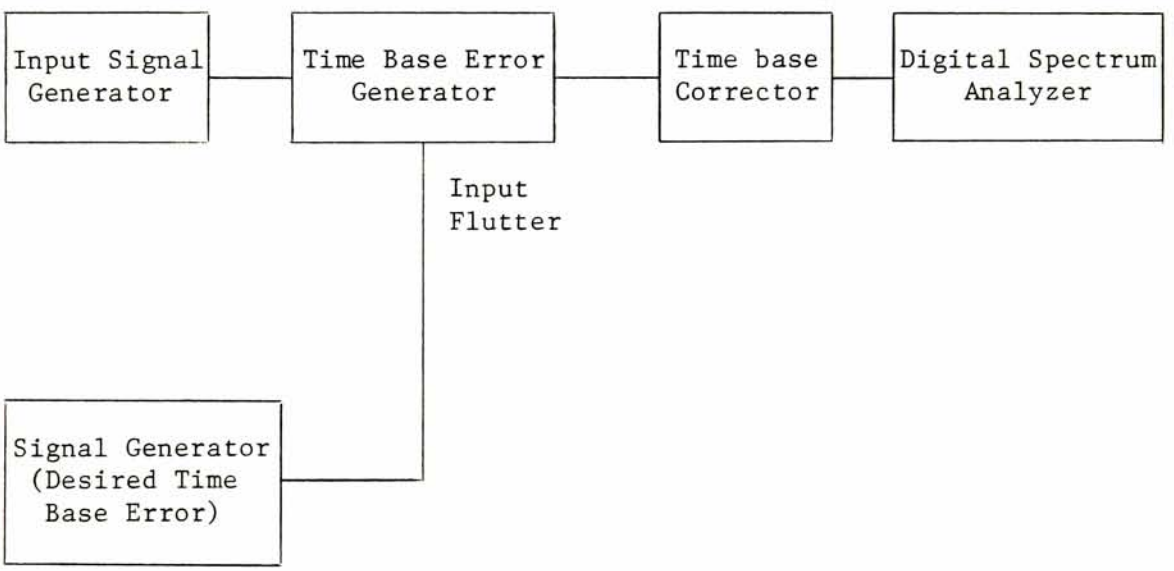

Fig.35 Block diagram of the experimental setup used to observe the flutter supressing effects of the TBC.

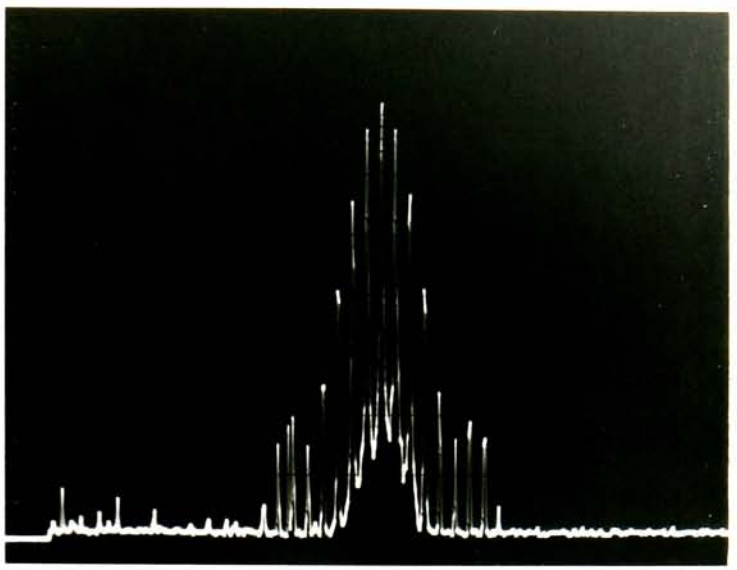

Spectrum of fluttered signal at input to TBC

Flutter: $F_{pp}(\%) = 10\%$

$f_F = 100$ Hz

Spectrum Analyzer Settings	
Resolution Bandwidth	3 Hz
Frequency Scan/Division	.5 KHz/cm
Center Frequency	3 KHz
Vertical Scale	10 db/cm
Amplitude Reference Level	-10 db
Input Sensitivity	+10 db
Scan Time/Division	100 sec/cm

Fig. 36-a Spectral comparison of a fluttered signal before it has been time-base corrected. (Ref: Fig. 36-b, following page)

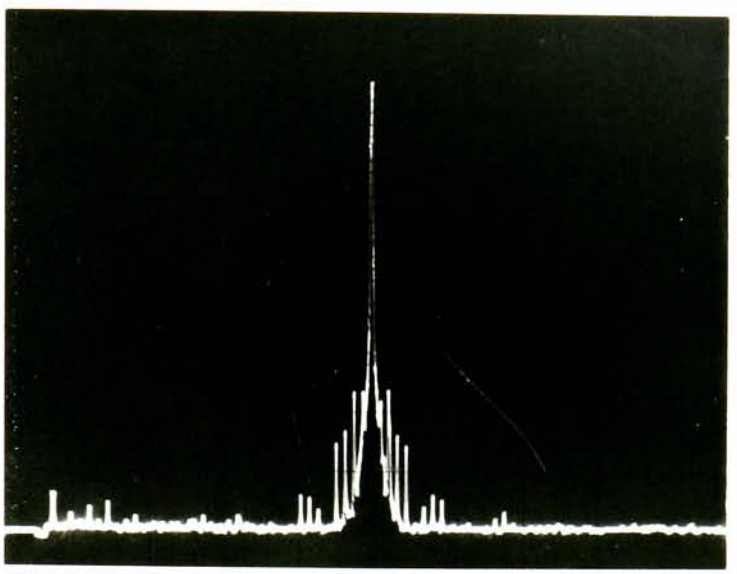

Spectrum of recovered signal at output of TBC

Spectrum Analyzer Settings	
Resolution Bandwidth	3 Hz
Frequency Scan/Division	.5 KHz/cm
Center Frequency	3 KHz
Vertical Scale	10 db/cm
Amplitude Reference Level	-10 db
Input Sensitivity	+10 db
Scan Time/Division	100 sec/cm

Fig. 36-b Spectral comparison of a fluttered signal after it has been time-base corrected. (Ref: Fig. 36-a, preceding page)

CHAPTER V

THE CHANNEL

THE CHANNEL

A study of the performance of the channel, as well as the reason for the particular signal processing choices made, can only be done by first taking a brief look at the record/reproduce process.

Direct Record/Reproduce

A record head is similar to a transformer with a single winding. Signal current flows in the winding, producing a magnetic flux in the core material. To perform as a record head, the core is made in the form of a closed ring, but unlike a transformer core, the ring has a short nonmagnetic gap in it. When the nonmagnetic gap is bridged by magnetic tape, the flux detours around the gap through the tape completing the magnetic path through the core material. Magnetic tape is simply a ribbon of plastic on which tiny particles of magnetic material have been uniformly deposited. When the tape is moved across the record head gap, the magnetic material, or oxide, is subjected to a flux pattern which is prooprtional to the signal current in the head winding. As it leaves the head gap, each tiny particle retains the state of magnetization that was last imposed on it by the protruding flux. Thus, the actual recording takes place at the trailing edge of the record head gap.

To reproduce the signal, the magnetic pattern on the tape is moved across a reproduce head. Again a small nonmagnetic gap in the head core is bridged by the magnetic oxide of the tape. Magnetic lines of flux are shunted through the core, and are proportional to the magnetic gradient of the pattern on the tape which is spanned by the gap. The induced

voltage in the head winding is:

$$e = N\, d\phi \,/\, dt.$$

It is important to note that the reproduced voltage is not proportional to the magnitude of the flux, but to its rate of change.

Suppose the signal to be recorded on the tape is a sine wave voltage described by A sin($2\pi ft$.) Both the current in the record head winding and the flux, ϕ, through the record head core will be proportional to this voltage. If the tape retains this flux pattern and regenerates it in the reproduce head core, the voltage in the reproduce head winding will be

$$e_{repro} \propto \frac{d\phi}{dt}$$

where

$$\frac{d\phi}{dt} = \frac{d}{dt} A \sin(2\pi ft)$$

$$= 2\pi fA \cos(2\pi ft)$$

Thus the reproduce head acts as a differentiator and the reproduce signal is actually the derivative of the recorded signal and not the signal itself. This fact imposes two well-known limitations on the direct record process. The output of the reproduce head is proportional to the signal frequency, and to maintain amplitude fidelity, a 6-db-per-octave rise in the head output must be compensated for in the reproduce amplifier by a process known as <u>equalization</u>. Fig. 37 shows how such a shaped response is applied. The other limitation occurs as the recorded frequency approaches zero. At some point the output voltage from the reproduce head falls below the inherent noise level of the overall recording system.

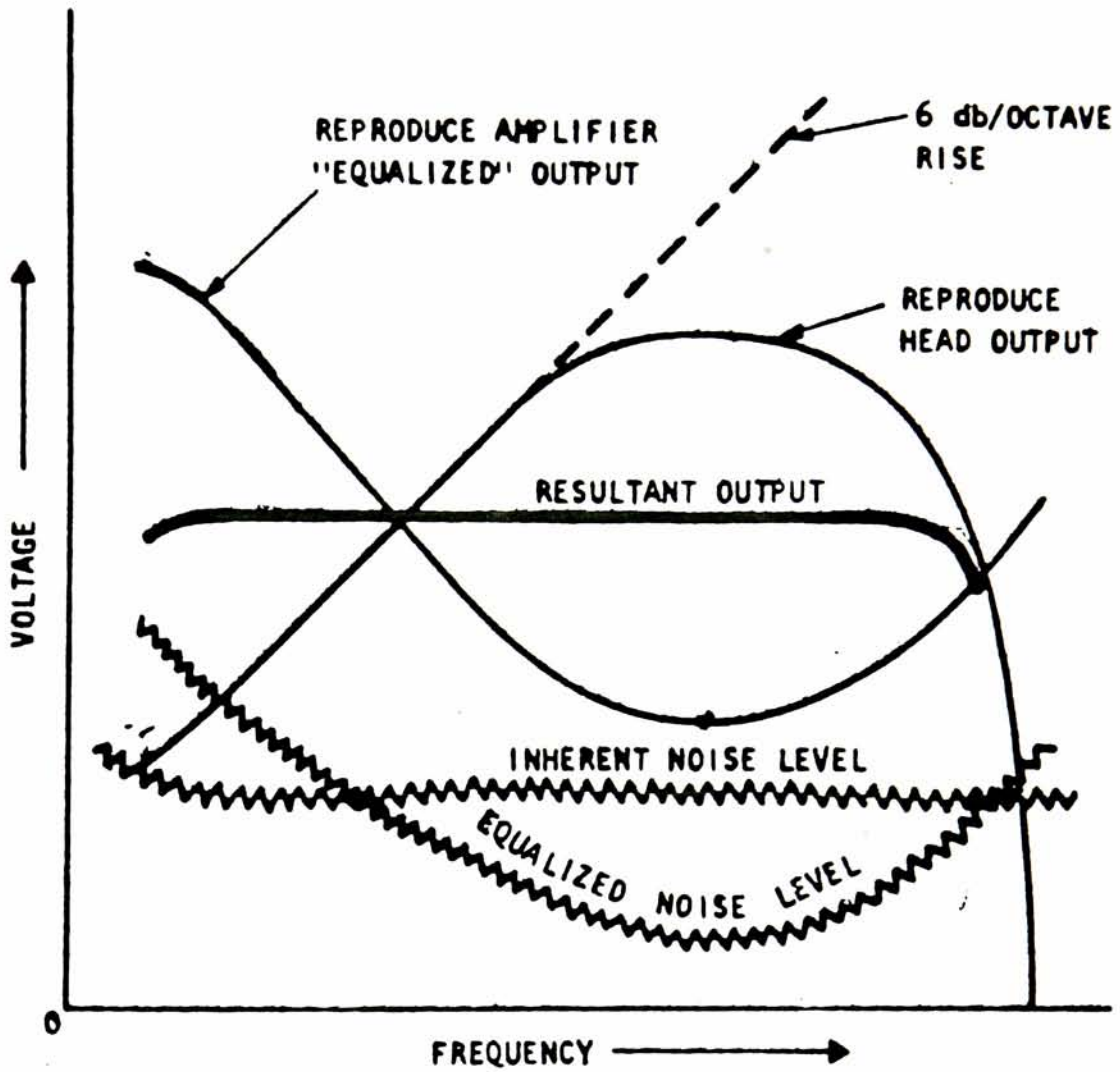

Fig.37 Reproduce Characteristics

So, there is a low-frequency limit in the direct record process, below which reproduction cannot be made.

Bias

Up to now the discussion has assumed that the magnetizable medium responds linearly to the magnetizing force of the record head. As might be expected, this is not the case. Like other magnetic materials, the particles on the tape exhibit a very nonlinear characteristic when exposed to a magnetizing force. A typical magnetization curve, or hysteresis loop, is shown in Fig. 38 . H is the magnetizing force and is determined by the number of turns and the current in the record head-winding. B is the resultant induced magnetization on the tape.

As a demagnitized particle on the tape approaches the record head gap, it carries no residual magnetism. (Point 0, at the origin, Fig.38). Assuming that a cycle of the recorded signal along the tape is very long compared to the gap length, the particle will pass through an essentially constant magnetizing force created by the recording current. Referring to the curve of Fig.38, such a force, (H_R), will carry the particle up the curve to point R, at the center of the gap. As the particle leaves the gap, H falls to zero, but the magnetization of the particle will follow a minor hysteresis loop, RB_R, retaining a residual, or remanent magnetization of B_R. The transfer characteristic of this process is shown graphically in Fig.39 , and its inherent nonlinearity is readily apparent. High distortion in the reproduced signal results unless some corrective action is taken.

Fortunately, there are two fairly linear segments in the transfer

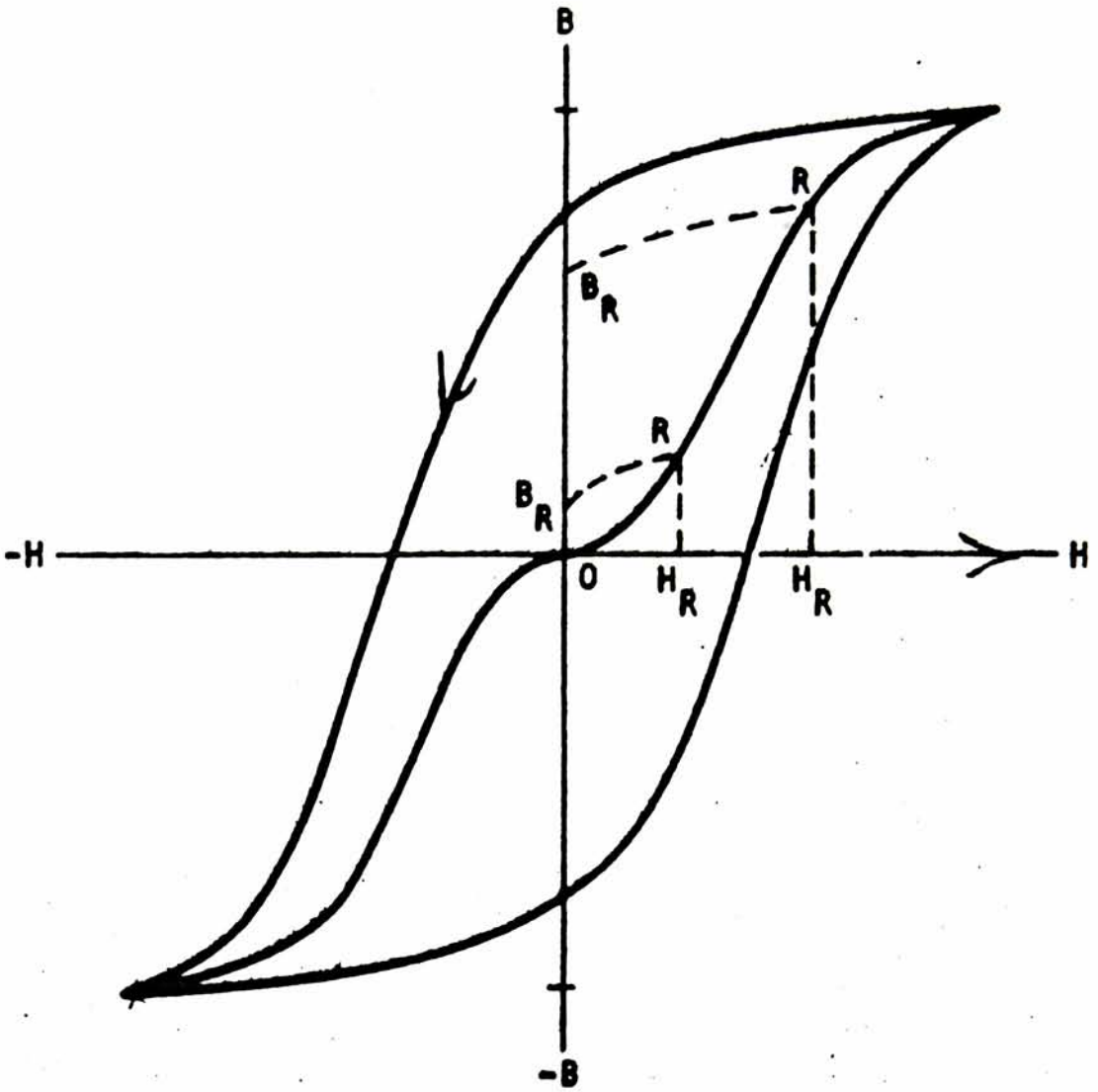

Fig.38 A typical Magnetization Curve, or Hysteresis Loop

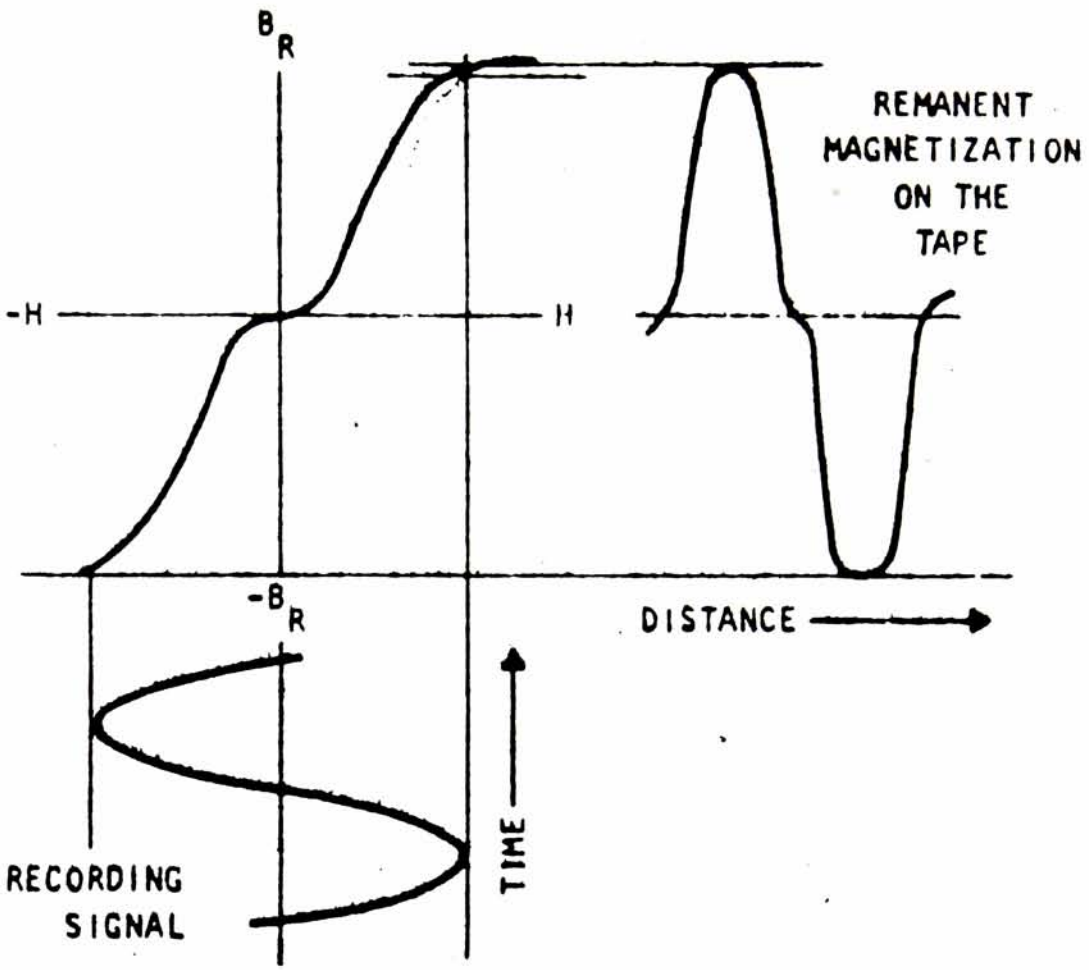

Fig. 39 Head-to-tape transfer characteristic with no bias

characteristic curve, one on each side of the orgin with their centers about half way to saturation. (See Fig.39). If the recording can be confined to one (or both) of these straight sections, low distortion can be realized. Similar to the manner of biasing a vacuum tube into a region of linear operation, some method of "biasing" the recording function into the linear transfer region must be used. Early recorder designers went naturally to a dc bias produced simply by adding a constant dc current to the signal and obtained operation in one or the other of two linear ranges. With the relatively limited range thus available, dc-biased recorders give a very restricted dynamic range, but they are quite improved over zero-bias recording. If both linear sections of the curve are to be used. some means of rapidly switching from one to the other must be devised. This is exactly what a high-frequency ac bias does. There are several theories about how an ac bias performs this function, and no one of them really accounts for all aspects. One of the older and still widely accepted theories, however, is that since the bias itself is not reproducible, because of its high frequency, its switching function is not detectable and the gap between the two linear sections disappears. Fig.40 shows graphically how a low-distortion magnetic signal is thus recorded. Some further reduction in nonlinearity is also obtained in the same way as in push-pull amplifier operation, since nonlinearities are symmetrically disposed around the origin.

Several features of ac bias operation are worth noting: (1) It should be emphasized that the bias and the signal are linearly mixed (or added) together. It is not a modulation process. (2) The proper amplitude for the bias is dependent upon the exact transfer characteristic

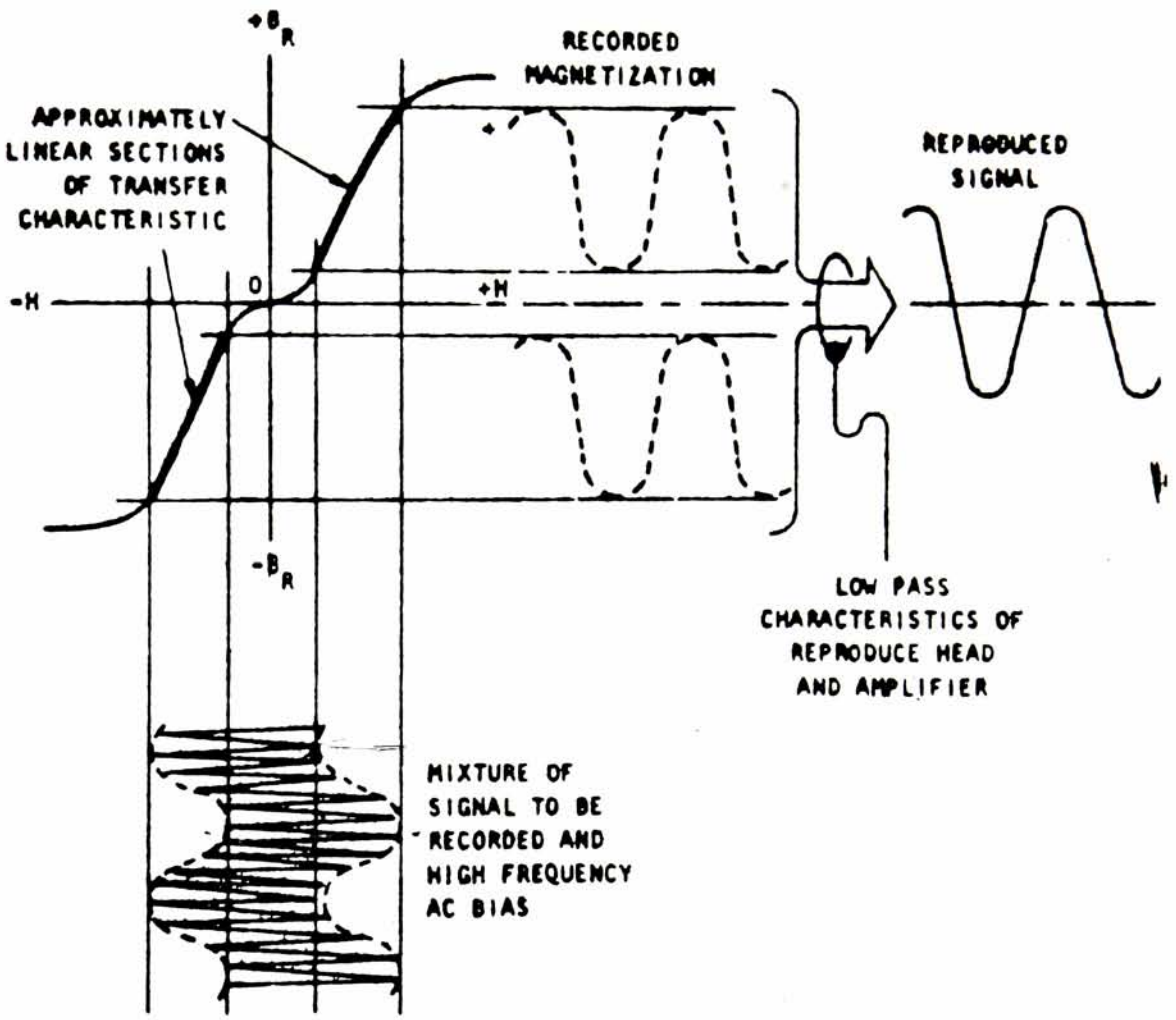

Fig.40 Graphical representation showing how AC bias alternately transfers the signal from one linear section of the curve to the other

of the tape and should be adjusted to reach from center to center of the linear regions. Too much bias will greatly reduce the high-frequency response, while inadequate bias will cause increased distortion of the lower frequencies. (3) Bias frequencies are usually not critical, but should be at least 3.5 times the highest frequency to be recorded to minimize interaction with harmonics of the signal. (4) Care must also be taken to provide a harmonically pure sinewave bias current to minimize distortion products.

In practice, bias currents from 1.0 to 20.0 milliamperes are common and they may be from 5 to 30 times the signal current, depending upon the tape and head characteristics.

High-Frequency Response

Several factors combine to limit the high frequency response of tape recorders, but before these are discussed we should understand what is meant by recorded wavelength, resolution, and packing density.

If a sine wave signal is recorded, the magnetic intensity of the recorded track will vary sinusoidally. The distance along the tape required to record a complete cycle is called the recorded wavelength, or λ, and is directly proportional to tape speed and inversely proportional to signal frequency. For example, a particular recorder quotes 1.2 mHz response at 120-ips. There are several other ways to describe this response. Dividing 1.2 mHz by 120-inches shows the machine is capable of a packing density of 10,000 cycles per inch. Such a signal has a wavelength of 1/10 mil (0.0001 inch), which is the limit of the machine's resolution. Both packing density and resolution can be used

to describe a recorder's response independent of tape speed, and thus are more definitive of a recorder's capability than just a frequency specification at a given speed.

Five factors contribute to the high frequcncy limitation of tape recorders. They are (1) gap effect, (2) recording demagnetization, (3) self-demagnetization, (4) penetration losses, and (5) head losses. As shown in Fig.37, the reproduce head output increases with frequency up to a point and then decreases rapidly to zero. The decrease is primarily the result of gap effect and occurs as the recorded wavelength (λ) becomes shorter and shorter until it eventually equals the reproduce gap dimension itself. At this point there is no magnetic gradient spanned by the gap and thus no output voltage. This is the most serious, single restriction on a tape recorder's high frequency response. Fig.41 shows a graphical representation of the gap effect.

Recording Demagnetization causes a decrease in the reproduced signal level at the shorter wavelengths, and, as the name implies, it occurs in the recording process. Normally, with the longer wavelengths, the particles on the tape are being driven through large symmetrical hysteresis loops by the ac bias while in the influence of the recording field. These loops are offset by the much smaller recording signal and as the particle leaves the field the loops collapse leaving the particle magnetized in proportion to the signal. For shorter wavelengths the recording signal may vary considerably as the particle is leaving the field and a corresponding reduction in the remanent magnetization will result.

Self-demagnetization occurs in the magnetic medium itself when the

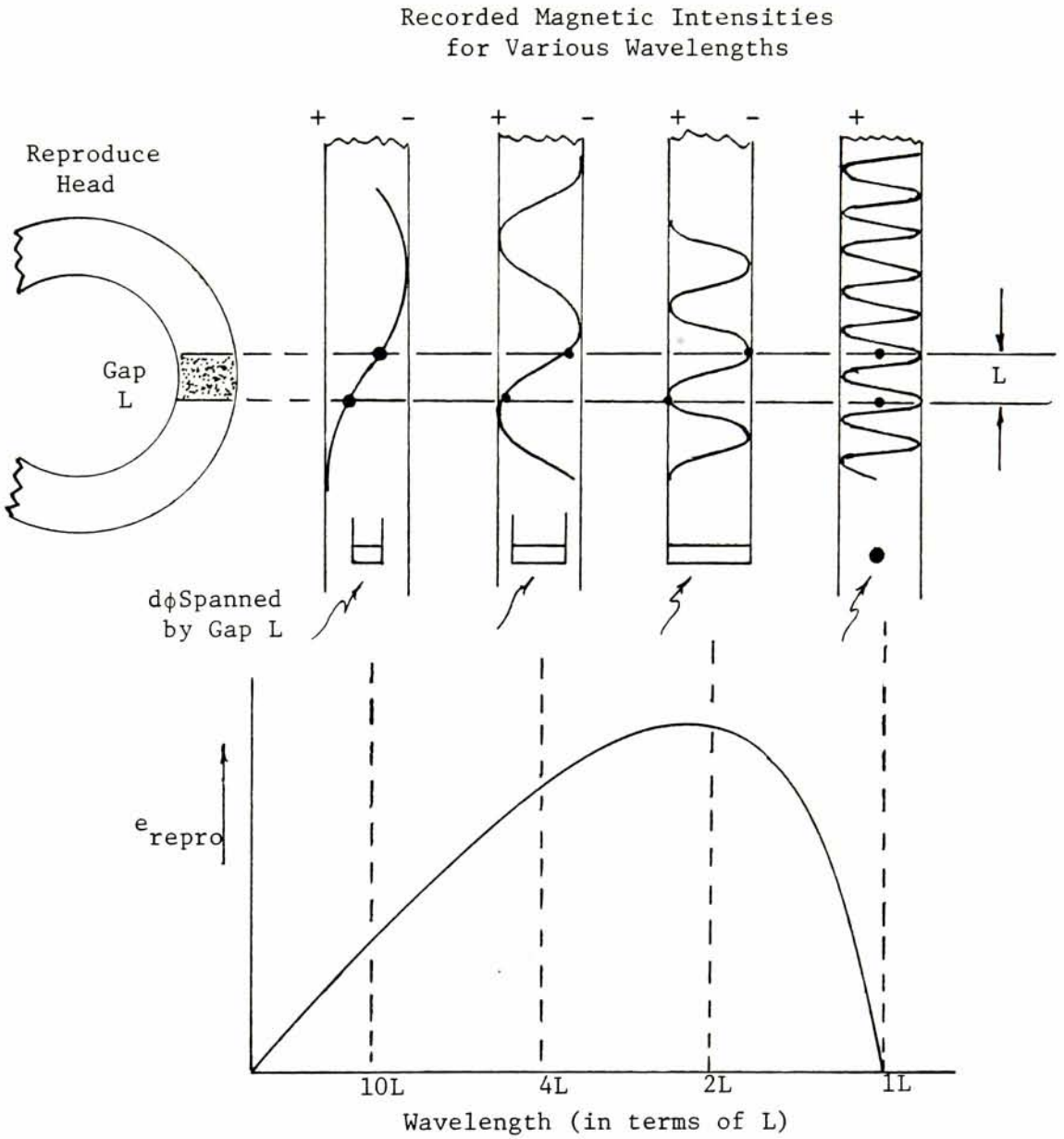

Fig.41 A graphical representation of gap effect

external magnetizing force is removed and is most pronounced when magnetic poles are crowded closer and closer (shorter wavelengths). Actually self-demagnetization is probably the least important of the high frequency limitations.

Penetration losses are wavelength-dependent and cause another reduction in the reproduced signal level. The full depth (or thickness) of the magnetic coating on the tape becomes magnetized at long wavelengths, but as the wavelength decreases the depth of magnetization is reduced and, at very short wavelengths, only the surface layer of particles are effectively magnetized. Thus, the shorter wavelengths influence fewer particles, there is less intensity in the recorded magnetic pattern, and the reproduced output falls off.

The remaining major problem in extending tape recorder response is head losses. Unlike the limitations discussed above, head losses are not wavelength dependent, but like any ac-driven ferromagnetic material, are related strictly to frequency. Both core and winding losses act to reduce the effective recording current at the high signal frequencies. Hysteresis and eddy-current losses in the core material and the distributed capacity of the windings are the major contributors and, of course, they increase with frequency.

Analysis of the Record-Reproduce Process

It was mentioned previously that of the five factors which contribute to the high frequency limitation of a tape channel, the gap effect is the most dominant one. The upper 3db frequency cutoff of the channel can be calculated by relating the gap length to the velocity of the head relative to the tape.

Let f(t) be the signal to be recorded onto a tape moving with a uniform velocity, v, and let s(x) be the head impulse response. Then the resulting magnetic field r(x), as a function of the distance, x, generated by the gap, is given by the convolution integral,

$$r(x) = \int_{t=-\infty}^{\infty} f(t)k\ s(x - vt)dt$$

Where

$f(t) \equiv$ A temporal function describing the signal to be recorded (in amps).

$k \equiv$ Constant of proportionality $\frac{\text{flux lines}}{\text{amps}}$

$S(x) \equiv$ Describes the flux generated by the gap as a function of the distance, x, resulting from an input current impulse. $\frac{\text{flux lines}}{\text{flux lines seconds}}$

$v \equiv$ Head-to-tape velocity $\frac{\text{inches}}{\text{sec.}}$

$t \equiv$ Time in seconds

$r(x) \equiv$ The resultant field left stored on tape as a function of the distance, x (flux lines).

This convolution integral can be solved as follows:

Let

$$\tau = vt$$

Then

$$d = vdt$$

$$r(x) = k \int_{\tau=-\infty}^{\infty} f\left(\frac{\tau}{v}\right) s(x-\tau) \frac{1}{v} d\tau$$

$$= \frac{k}{v} \int_{\tau=-\infty}^{\infty} f\left(\frac{\tau}{v}\right) s(x-\tau) d\tau$$

Let

$$g(\tau) = f\left(\frac{\tau}{v}\right)$$

$$r(x) = \frac{k}{v} \int_{\tau=-\infty}^{\infty} g(\tau) s(x-\tau) d\tau$$

$$= \frac{k}{v} g(\tau) * s(\tau)$$

Taking the Fourier Transform:

$$\mathcal{F}\{r(x)\} = \mathcal{F}\left\{\frac{k}{v} \; g(\tau) * s(\tau)\right\}$$

$$= \frac{k}{v} G(f_x) \; S(f_x)$$

Where f_x is the spacial frequency in the transform domain and

$$\mathcal{F}\{g(\tau)\} = G(f)$$

$$\mathcal{F}\{s(\tau)\} = S(f)$$

$$\mathcal{F}\{r(x)\} = R(f_x)$$

Note that

$$\mathcal{F}\{g(\tau)\} = \mathcal{F}\left\{f\left(\frac{\tau}{v}\right)\right\}$$

$$= vF(vf), \quad F(f) = \mathcal{F}\{f(t)\}$$

Therefore:

$$\mathcal{F}\{r(x)\} = kF(vf_x)S(f_x)$$

$$R(f_x) = kF(vf_x)S(f_x)$$

As noted previously, s(x) is the impulse response of the head. This function describes the field generated by the head along the tape path resulting from an input current impulse to the record head winding. It has units of flux lines out per unit energy in: $\frac{\text{flux lines}}{\text{flux lines sec.}}$

Fig. 42 describes s(x) in greater detail. It should be noted that in this figure, the gap has been assumed to be uniform along the width of the track, since this is usually the case.

$$s(x) = \text{rect}\left(\frac{x}{L}\right)$$

$$s(f_x) = L \text{ sinc}(Lf_x)$$

Letting f(t) be a sinusoidal waveform of frequency f_0:

$$f\left(\frac{x}{v}\right) = \cos\left(2\pi f_0 \frac{x}{v}\right)$$

$$F(vf_x) = \tfrac{1}{2}\,\delta(vf_x - f_0) + \tfrac{1}{2}\,\delta(vf_x + f_0)$$

$$= \tfrac{1}{2}\,\delta\left[\left(f_x - \frac{f_0}{v}\right)v\right] + \tfrac{1}{2}\,\delta\left[\left(f_x + \frac{f_0}{v}\right)v\right]$$

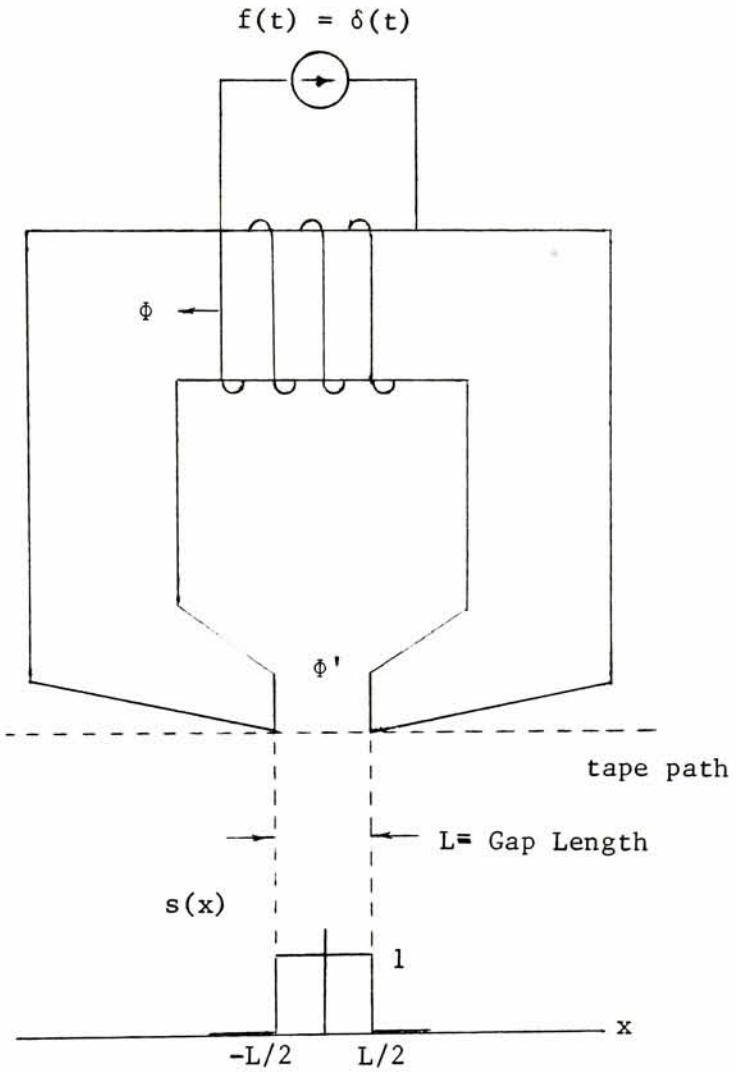

$$s(x) = \text{rect}\,\frac{x}{L}$$

Note: $\Phi = \Phi' = kf(t)$

Fig.42 Impulse response, s(x), of the magnetic head as a function of the distance,(x).

$$R(f_x) = kF(vf_x)\ S(f_x)$$

$$= \frac{kL}{2}\left\{\delta\left[\left(f_x - \frac{f_0}{v}\right)v\right] + \delta\left[\left(f_x + \frac{f_0}{v}\right)v\right]\right\}\mathrm{sinc}(Lf_x)$$

$$= \frac{kL}{2}\left\{\mathrm{sinc}\left[L\left(\frac{f_0}{v}\right)\right] + \mathrm{sinc}\left[L\left(\frac{-f_0}{v}\right)\right]\right\}$$

Note that sinc(x) = sinc(-x)

$$R(f_x) = kL\ \mathrm{sinc}\left(L\ \frac{f_0}{v}\right) \tag{h}$$

Equation (h) describes the energy associated with each spacial frequency of the magnetic field left on the tape by the head gap. As expected, it is a function of the re-coding wave length, λ, where,

$$\lambda = \frac{f_0}{v}$$

The 3db frequency can now be found by setting

$$\mathrm{sinc}\left(L\ \frac{f_0}{v}\right)\Bigg|_{f_0=f_{3db}} = .707$$

Note:

$$\mathrm{sinc}(x)\Big|_{x=.45} = \frac{\sin(\pi x)}{(\pi x)}\Bigg|_{x=.45} = .698 \simeq .7$$

$$L\ \frac{f_{3db}}{v} = .45$$

$$f_{3db} = .45\ \frac{v}{L} \tag{i}$$

Equation (i), therefore, relates the band width of the channel to the velocity and the sizes of the head gap.

It should be noted that this result, derived for the record process only, applies generally to both the record and playback processes simultaneously because, typically, the playback gap is much narrower than the record gap by several orders of magnitude. This implies that the bandwidth limiting factor is the size of the record gap, assuming the same velocity has been chosen for both record and playback. Equation (i) has been verified experimentally with several different types of heads and in the following areas of application: helical-scan video recorders, digital instrumentation recorders and audio recorders.

Implementation of the Channel

The behavior of the complete channel can now be observed. Fig.43 is a block diagram of the complete system in which each of the subsystems previously described are shown interconnected. The broken lines in this figure denote the external rack connections required to operate in one of several modes:

(1) E to E mode (Electronics to Electronics): The signal path does not include the tape.

(2) TBEG Bypass: Bypasses the flutter generating system.

(3) TBC Bypass: Bypasses the flutter correcting system.

In addition, a number of other interconnections are available in order to observe each of the subsystems separately. The normal signal

path, however, is typically shown in solid lines. This signal path is as follows: the input signal is delta-modulated, Ampex-Miller encoded, recorded and reproduced from the tape by way of the record and playback buffers, fluttered, Ampex-Miller decoded, time base corrected and delta demodulated.

Experimental Results

The reason for specific signal processing choices made have already been discussed in detail; however, the primary reason becomes apparent in Fig. 44. This figure is a photograph of the spectrum of a 5 KHz bandlimited Gaussian noise signal after it was delta modulated and Ampex-Miller encoded. This then, is a spectrum of the 5 KHz channel to be recorded on tape. A comparison of this spectrum and the general shape of the unequalized channel response indicated in Fig. 37 as the reproduced head output shows that the signal spectrum closely matches the general shape of the unequalized channel spectral response. Furthermore, most of the signal energy is concentrated in the region of the channel spectrum where the lowest noise power exists and the highest signal response can be achieved. The result, then, is a greater utilization of the channel information spectrum, thereby making more efficient use of the total available channel capacity.

Total Available Channel Capacity (C_T)

The frequency response of the record-reproduce channel increases at 6db/octave. This results because the voltage in the reproduce head winding is proportional to the derivative of the flux on the tape with

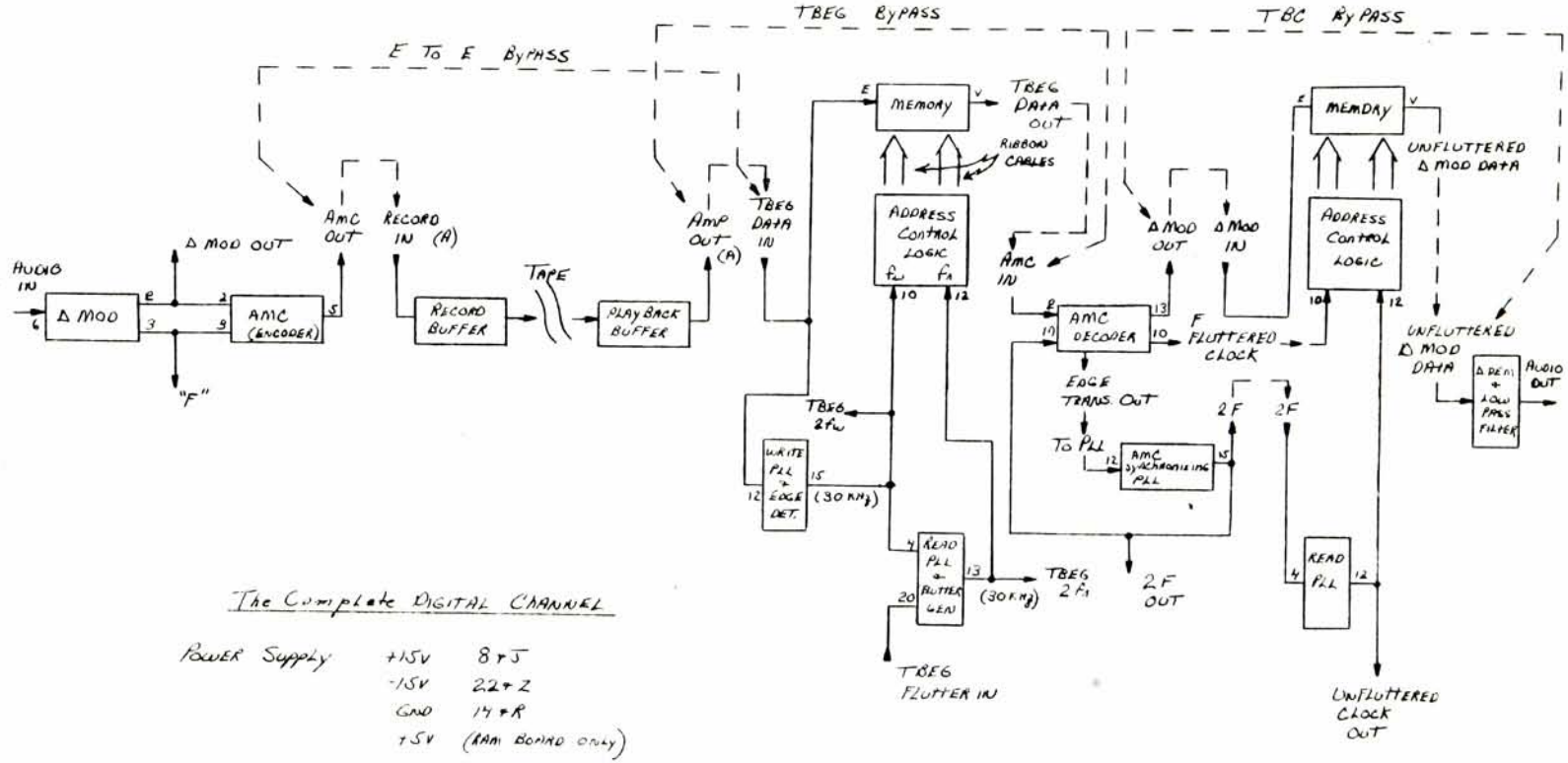

The Complete DIGITAL CHANNEL

POWER SUPPLY	+15V	8 + J
	-15V	22 + Z
	GND	14 + R
	+5V	(RAM BOARD ONLY)

1/4/77

Fig. 43

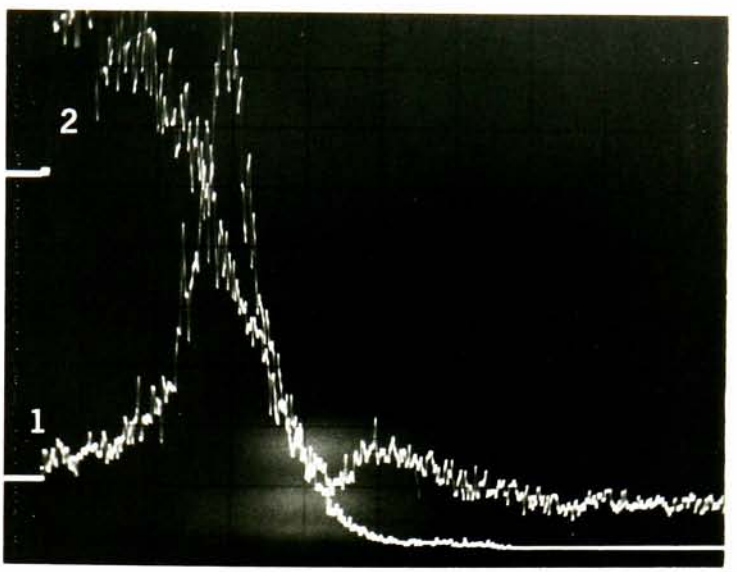

Spectrum Analyzer (HP#3580Z)		
Setting	Trace 1	Trace 2
Resolution Bandwidth	300 Hz	300 Hz
Frequency Scan/Division	2 KHz	2 KHz
Start Frequency	0 Hz	0Hz
Vertical Scale	Linear	Linear
Amplitude Reference Level	-40 db	-30 db
Input Sensitivity	.1 V	.2 V
Scan Time/Division	5 sec/cm	5 sec/cm

Fig.44 Spectrum of the processed signal to be recorded on tape (Trace 1) resulting from a 5 KHz band limited Gaussian noise input (Trace 2)

respect to time. Thus the frequency response of the channel is:

$$|H(f)| = 2|f|$$

Note that the output power spectral density is related to the input power spectral density as follows:

$$S_o(f) = |H^2(f)|S_i(f)$$

Therefore, the signal power associated with the channel is:

$$P_s = \int_{-B}^{B} K_p f^2 df$$

$$= \frac{2K_p B^3}{3}$$

K_p can be readily found by measuring the playback signal power.

$$K_p = \frac{3P_s}{2B^3} \qquad \text{(j)}$$

The average noise power of the channel observed at the output of the playback amplifier is:

$$N_{avg} = \int_{-B}^{B}\left(\frac{N_o}{2}\right)df \qquad \text{(Refer to Fig.37)}$$

$$= N_o B \qquad \text{(k)}$$

Then the differential channel capacity can be calculated employing Shannon's Theorem [13] and by assuming the noise distribution of the

infinitesimal section of the channel under consideration is Gaussian:

$$dC = \log_2\left(1 + \frac{K_p f^2\ df}{\frac{N_o}{2}\ df}\right) df$$

where the differential signal power is:

$$dP = K_p f^2\ df$$

and the differential noise power is:

$$dN = \frac{N_o}{2}\ df$$

The total available channel capacity, C_T, can now be found:

$$C_T = \int_0^B \log_2\left(1 + \frac{K_p f^2\ df}{\frac{N_o}{2}\ df}\right) df$$

$$= \int_0^B \log_2\left(1 + \frac{2K_p f^2}{N_o}\right) df \qquad (1)$$

The upper limit of this integral represents the upper 3db frequency of the channel. Since the highest frequency to be recorded on tape is the fundamental frequency associated with an Ampex-Miller encoded constant digital level, the upper 3db channel cutoff can be set equal to it.

Therefore,

$$B = .45 \frac{v}{L}$$

$$= \tfrac{1}{2} f_s$$

Where:

f_s is the sample frequency of the delta modulator

v is the head-to-tape velocity

L is the head gap length

The relationship

$$.45 \frac{v}{L} = \tfrac{1}{2} f_s \qquad \text{(m)}$$

can now be used to determine the necessary parameters in order to synthesize the channel.

Letting:

$$K_N = \frac{2K_p}{N_o}$$

then equation (1) can be written as follows:

$$C_T = \int_0^B \log_2 (1 + K_N f^2)\, df \qquad \text{(n)}$$

where K_p and N_o can be found experimentally. K_p was defined by equation (j). This equation can be expressed in terms of f_s as follows:

$$K_p = \frac{3P_s}{2B^3}$$

$$= \frac{3P_s}{2\left(\frac{f_s}{2}\right)^3}$$

$$= \frac{12\ P_s}{f_s^{\ 3}}$$

where P_s is the average playback power. This quantity can be determined by recording Gaussian noise of a wider bandwidth than the channel on tape and then measuring the true RMS voltage played back and squaring. The test setup used is shown in Fig. 45. The average power is:

$$P_s = (V_{rms})^2$$

$$= (165 \times 10^{-3})^2$$

$$= 2.7 \times 10^{-2} \text{ watts}$$

K_p is now readily found:

$$K_p = \frac{12p}{f_s^{\ 3}}$$

$$\frac{(12)(2.7 \times 10^{-2})}{(15 \times 10^3)^3}$$

$$= 9.68 \times 10^{-14}$$

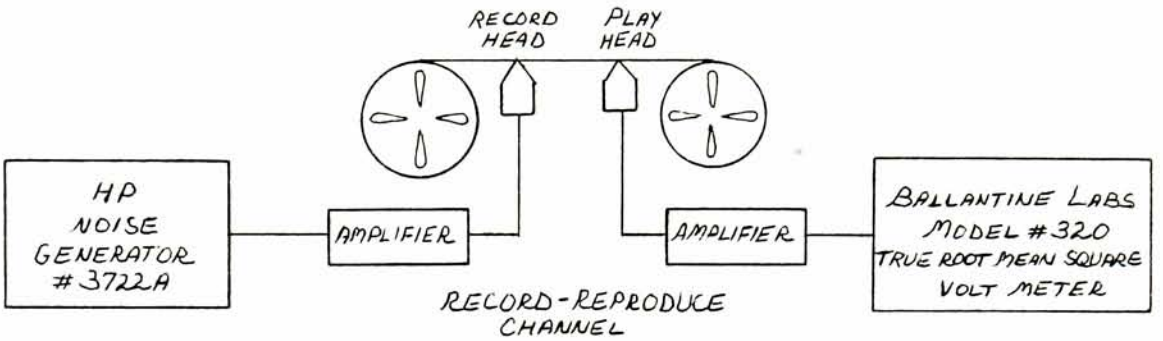

Experimental Data

V_{TP1} = .6 v rms

V_{TP2} = 165 mv rms

$V_{TP2}\Big|_{V_{TP1}=0}$ = 4 mv rms

Fig.45 Test setup to measure the average playback power and average noise power of the record-reproduce channel

Equation (k) is applied to find N_o:

$$N_o = \frac{N_{avg}}{B}$$

N_{avg} is the noise power at the output of the record-reproduce channel. It can be found by measuring the RMS voltage of test point 2 (TP2) with $V_{TP1} = 0$ and squaring:

$$N_{avg} = V_{TP2}^2 \Big|_{V_{TP1} = 0}$$

$$= (4 \times 10^{-3} \text{volts})^2$$

$$= 1.6 \times 10^{-5} \text{watts}$$

N_o is now readily found:

$$N_o = \frac{N_{avg}}{B}$$

$$= \frac{1.6 \times 10^{-5}}{\frac{15K}{2}}$$

$$= (2)(1.06 \times 10^{-9})$$

$$= 2.12 \times 10^{-9}$$

Therefore:

$$K_N = \frac{2K_p}{N_o}$$

$$= \frac{(2)(9.68 \times 10^{-14})}{(2)(1.06 \times 10^{-9})}$$

$$= 9.13 \times 10^{-5}$$

To solve the integral, (n), a new program, MACSYMA, developed at MIT was implemented. This program can perform symbolic as well as numerical manipulations. It can differentiate, integrate, take limits and a series of other mathematical operations.

The results of the program are shown in Fig. 46. In this figure the C_i's are the inputs and the D_i's are the outputs. For instance, C_1 is the input and D_2 is the result. In addition, a check on the indefinate integral was performed by differentiating it. After some simplification, the original function was obtained. This is evident in Fig. 46. It should be noted that when evaluating numerical results using this program, attention should be given to the log funciton. The term "log" is defined as "log to the base e".

C_T can now be computed:

$$C_T = \left\{ F \log_2(F^2 K_N + 1) - 2K_N \left[\frac{F}{K_N} - \frac{\tan^{-1}(FK_N^{\frac{1}{2}})}{(K_N)^{3/2}} \right] \right\} \Bigg|_0^B$$

$$= \left\{ B \log_2(B^2 K_N + 1) - 2K_N \left[\frac{B}{K_N} - \frac{\tan^{-1}(BK_N^{\frac{1}{2}})}{(K_N)^{3/2}} \right] \right\} - \left\{ 0 - 2K_N \left[0 - \frac{\tan^{-1} 0}{(K_N)^{3/2}} \right] \right\}$$

$$= B \log_2(B^2 K_N + 1) - 2B + \frac{\tan^{-1}(BK_N^{\frac{1}{2}})}{(K_N)^{\frac{1}{2}}}$$

Inserting the proper value in this equation yields:

$$C_T = 71.3 \frac{\text{kbits}}{\text{sec}}$$

The actual bit rate achieved was 15 kbits/sec. Therefore, the actual overall channel efficiency is:

$$E(\%) = \frac{C_{achieved}}{C_T} \times 100$$

$$= \frac{15K}{71.3K} \times 100$$

$$= 21\%$$

In order to appreciate this result, consider that the voice modem designed by the Bell Systems Laboratories for implementation in telephone systems achieves a 30% channel efficiency with a data rate of 9.6 kbits/sec.[14] However, this was accomplished using a more sophisticated multilevel coding scheme, rather than a digital one, thereby requiring a higher signal-to-noise ratio to maintain comparable error rates.

Fig. 46

```
This is MACSYMA 262

FIX262 30 DSK MACSYM being loaded
loading done

(C1) LOG(F^2*K[N]+1)/LOG(2);
                                        2
                                  LOG(F  K  + 1)
                                         N
(D1)                              --------------
                                      LOG(2)

(C2) INTEGRATE(D1,F,0,B);

DEFINT FASL DSK MACSYM being loaded
loading done

LIMIT FASL DSK MACSYM being loaded
loading done

RESIDU FASL DSK MACSYM being loaded
loading done

SIN FASL DSK MACSYM being loaded
loading done

SCHATC FASL DSK MACSYM being loaded
loading done
Is  K   positive, negative, or zero?
     N

P;

                                                  ATAN(B SQRT(K ))
                      2                     B                  N
                B LOG(B  K  + 1) - 2 K  (-- - ----------------)
                         N            N  K            3/2
                                          N          K
                                                      N
(D2)            ------------------------------------------------
                                     LOG(2)

(C3) EV(D2,B=7500,K[N]=0.00009132,NUMER);
(D3)                                71281.556

(C4)
     INTEGRATE(D1,F);
Is  K   positive, negative, or zero?
     N

P;
                                                  ATAN(F SQRT(K ))
                      2                     F                  N
                F LOG(F  K  + 1) - 2 K  (-- - ----------------)
                         N            N  K            3/2
                                          N          K
                                                      N
(D4)            ------------------------------------------------
                                     LOG(2)

(C5) DIFF(D4,F);
                                                                  2
                                                                2 F  K
                 2                  1          1                     N
            LOG(F  K  + 1) - 2 K  (-- - --------------) + ---------
                    N           N  K          2              2
                                    N   K  (F  K  + 1)    F  K  + 1
                                         N      N             N
(D5)        ------------------------------------------------------
                                     LOG(2)

(C6) RATSIMP(D5);
                                        2
                                  LOG(F  K  + 1)
                                         N
(D6)                              --------------
                                      LOG(2)

(C7)
```

CHAPTER VI

CONCLUSION

CONCLUSION

In conclusion a summary of the philosophy and results of this study is presented, a list of specific contributions is included, and several suggestions for further research are proposed.

Summary of the Thesis

The primary objective of this study has been to consider the fundamental limiting factors involved in the aquisition and storage of data on a magnetic tape medium and to develop the necessary signal processing solutions to maximize efficient use of the channel. This was accomplished by combining a delta modulator and an Ampex-Miller encoder described in detail in this study. By way of these combined processes, it was seen that the input information spectrum can be made to match the power spectral distribution of the record-reproduce channel.

Additionally, a series of advantages were realized from this coding format. The spectral mapping characteristics of this code resulted in a reduction of the bandwidth necessary to transmit the maximum bit rate of the overall channel. This, in turn, increased the storage packing density of the system. Furthermore, in using this code, the run length of a bit pattern was seen to be unrestricted. Developing a carrier extracting system by exploiting the self-clocking characteristics of the Ampex-Miller code allowed the implementation of a time base correcting system without the need to record a sub-carrier on tape.

In addition to the above, this report considered the following areas: The spectral degrading effects of flutter, the characteristics of the

record-reproduce channel, and the overall channel capacity. During the course of this study, flutter and timing error were proven to be related. It was shown analytically that the channel bandwidth is intrinsically related to the velocity of the tape and size of the head gap. Finally, the overall channel capacity was computed and a significant channel efficiency observed.

In recent years, the development of these signal processing techniques and the advancement in the state of the arts of solid state circuits have made practical the use of the techniques described in this report. A photograph of the actual implementaion of the system is included in order to illustrate the amount of electronic hardware required to implement the channel with the current technology.

The high density recording of wide band information on magnetic media has,in the past, been employed mainly in specialized communication and instrumentation systems where very high channel capacity and storage efficiency had to be achieved. These requirements were generally found in many machine-to-machine communication systems such as computer-to-computer, machine-to-computer, or spacecraft-to-ground station telemetry systems. Although high density information storage and transmission systems are important today, it seems likely that their most salient effect on society will be felt in the not-to-distant future. Like earlier major improvements in communication, the widespread use of high density information storage will undoubtably lead to dramatic changes in man's way of life.

Contributions of the Thesis

The contributions made in this thesis are:

(1) A study of the spectral mapping characteristics of different codes and their associated effect on high density data recording and channel equalization.

(2) A unique carrier extracting and phasing technique which permits data decoding at varying rates.

(3) A study of the deleterious effects of flutter and of the constraints involved in the development of a time base corrector.

(4) An analysis of the bandlimiting effects which result when the incoming data-signal is convolved with the head impulse response. This analysis leads to a relationship which describes the behavior of the channel bandwidth as a function of the size of the head-gap and the velocity of the tape.

(5) The complete channel implementing the above results was built. The shape of the spectral density distribution of the channel response was compared to the response of the unequalized record-reproduce channel. These were observed to be similar, hence removing the need for equalization. Finally, the actual channel capacity was compared to the maximum theoretical channel capacity.

Suggestions for Further Research

To increase the dynamic range, linearity, bandwidth, and efficiency of the channel, the following areas merit further investigation.

(1) Adaptive delta modulation could alleviate the slope overload problem of the delta modulator. This would increase the dynamic range as well as the signal-to-noise ratio of the system.

(2) The use of a Pulse Code Modulation system would increase the overall bandwidth of the system while maintaining the same maximum bit rate.

(3) Other coding schemes may also be possible. Of particular value would be an error-correcting code with spectral characteristics similar to the AMC code discussed in this report.

(4) A number of analog modulation processes are also possible each with unique advantages and disadvantages.

FRONT

BACK

DIGITAL SIGNAL PROCESSING SYSTEM
WITH
TIME BASE CORRECTING CAPABILITY

APPENDIX

APPENDIX I

DECODING PHASE-LOCKED LOOP

General Considerations

"Reproduce" circuits employed in high-density magnetic tape recording machines contain, as do their conventional low-density counterparts, amplitude and phase equalization. Thus, the output from such a circuit, when reproducing high-density digital data recorded in magnetic tape at maximum bit rates, is essentially sinusoidal. A decoding system is used to convert this analog output from the reproduce electronics into a data stream, in the appropriate code, with a synchronized clock. A typical decoding system contains three distinct functional parts: a limiter, which converts the input signal into a logic-compatible square wave; a phase-locked loop (PLL), used to begin reconstruction of the clock signal; and a decoder that reconstructs the output signal in the form of NRZ-L data with a synchronized clock signal by using both PLL and limiter output signals.

The limiter is basically an amplifier with high gain and a relatively fast recovery time. Its function is to amplify the input signal and, instead of allowing it to swing between positive and negative voltages, to clamp, for example, positive excursions to +5 volts and negative ones to 0 volts. A well-designed limiter will generate a square wave at its output and preserve the location of the zero-crossings with input signal amplitudes varying over a range of at least 40 db. This feature makes the bit synchronizer immune to signal-level fluctuations

caused by either tape imperfections or foreign matter at the head-tape interface.

If the data recorder on tape is in a NRZ-L format, the limiter must also perform a "dc-restoring" function. This is simply the generation of a dc voltage that is the short-term average value of the input data. Alternate "ones" and "zeros" produce a zero average voltage. Predominence of either "ones" or "zeros" will cause this short-term average level to shift in either the positive or negative direction. This average level is used as the reference level at the limiter input and allows proper limiting of the data containing long strings of consecutive "ones" or "zeros".

A transition detector (TD) circuit produces a narrow pulse for each positive- or negative-going transition in the limiter output signal. The TD output is used as a reference signal for the PLL. Successive "ones" or "zeros" in the AMC data produce periods of no pulses at the TD output. To keep the PLL-generated clock signal always synchronized with the data, the PLL bandwidth must be made sufficiently narrow. With different codes, different requirements are imposed on the PLL. When tracking a NRZ-L code, a single "divide by two" circuit in the loop is sufficient, whereas two such circuits must be provided for the generation of BI-Φ-L and AMC clocks. Operating this circuit for these two codes further guarantees at least one transition per one or two data cells, respectively. This alleviates the problem of maintaining the PLL in synchronization with the input data, while decoding BI-Φ-L or AMC codes.

The original data is restored in synchronism with the clock by a decoder which receives two outputs: from the PLL, the restored clock

as the output from the PLL's voltage-controlled-oscillator (VCO); and the transition detector output. For BI-Φ-L code and AMC code, the VCO operates at four times the clock rate. By having this higher frequency available, the BI-Φ-L code can be handled in a manner similar to that of the NRZ-L code, where a negative-going transition must follow each and every transition in the data. If the AMC code has been recorded on tape, it can be recovered in a fashion similar to the NRZ-L coded data. There is, however, no direct relationship between the polarity of a clock transition and a data transition. This relationship is established by the decoder (See Chapt. II: "AMC Encoding and Decoding").

Specifications

An actual circuit implementation of this PLL is shown in Fig.I-1. The data transition detector output of the decoder is the input to the PLL circuit. This input is not always present since it is the logic transition of an AMC coded arbitrary data, and hence a continuous phase detector cannot be implemented. Therefore a discrete sample system results.

The phase detector is a sample-and-hold (S/H) circuit, HA2425, which is driven by a voltage controlled oscillator (EXAR 2207). This VCO is operating at 30 KHz, twice the clock rate. The oscillator is wired such that two outputs are available: one is a square wave; the other, a triangular wave. The triangular wave is fed back to the input of the S/H circuit. The filter connecting the output of the S/H to the VCO must be selected quite carefully. The following constraints apply:

1. The PLL should be a TYPE II system because it is desirable to track a frequency offset (ramp in phase) with zero steady state error. This constraint is necessary to ensure tracking tight enough to decode.
2. Since this is a sample data system, we must be aware the information at the output of the phase detector above the Nyquist frequency is aliased and therefore cannot be used. Hence, this constitutes an upper cutoff frequency constraint on this filter.
3. The filter must be chosen such that the loop bandwidth is sufficiently large to accomodate the time-base instability of the transport mechanism. If this is not done, (that is, if the flutter bandwidth is wider than the loop bandwidth), there could be some residual phase error between the input and the output. This would be due to the fact that the loop will not track the phase fluctuations of the input data resulting from flutter frequencies above the PLL cutoff frequency. Decoding errors are then likely to occur.

The filter, then is chosen to have a pole at dc, to ensure a TYPE II system, and to have a gain such that the overall loop gain of the system results in a total PLL bandwidth of 1 KHz. This bandwidth is sufficient to accommodate all of the above constraints since the sample rate will never drop below 3.75 KHz. Therefore, the choice of 1 KHz is well within half the sample rate, and no appreciable transport flutter above 1 KHz is expected.

Finally, the loop was chosen to have a damping factor $\xi = 1$ for optimal TYPE II response. The S/H phase detector is a quadrature phase

detector. Its output is equal to 0 volts when the relative phase of the VCO to the input signal is 90°. Since zero steady-state phase is required and the steady-state phase is 90°, a phase shift network (9602 Circuit) must be introduced to ensure the 2f clock output steady-state phase relative to the input data transition is 0°. The 2f clock is then available for decoding.

PLL Analysis

Refer to Fig.I-2 for the block diagram of the phase-locked loop.

PLL Transfer Function H(s):

$$H(s) = \frac{\theta_o(s)}{\theta_{in}(s)}$$

$$\frac{K_\phi K_o F(s)}{s + \frac{1}{N} K_\phi K_o F(s)} \quad \text{by inspection of Fig.I-2}$$

Filter Transfer Function F(s):

As previously noted, it is desired to have a TYPE II system. This implies the open loop transfer function of the PLL must have poles at the origin (s = 0); by observing the block diagram of the PLL (Fig. I-2), the VCO transfer function (voltage to phase) has a pole at the origin. Hence, the filter must be chosen to have the other.

$$F(s) = \frac{\tau_2 s + 1}{\tau_1 s} \qquad \tau_1 = R_1 C \qquad \tau_2 = R_2 C$$

The complete closed loop transfer function is:

$$H(s) = \frac{K_\phi K_o \left(\frac{\tau_2 s + 1}{\tau_1 s}\right)}{s^2 + \left(\frac{K_\phi K_o \tau_2}{N\tau_1}\right) s + \left(\frac{K_\phi K_o}{N\tau_1}\right)} \tag{1}$$

The denominator of this equation takes on the form of the characteristic equation of a second order system,

$$s^2 + 2\xi\omega_n s + \omega_n^{\ 2}$$

where:

ξ = damping factor

ω_n = natural frequency

By equating, we find:

$$\omega_n = \frac{K_\phi K_o}{N\tau_1} \tag{2}$$

$$\xi = \frac{\tau_2}{2} \frac{K_\phi K_o}{N\tau_1} \tag{3}$$

Finally, from Control Systems, we know:

$$\omega_n = \frac{\omega_{3db}}{\left(1 + 2\xi^2 + \sqrt{2 + 4\xi^2 + 4\xi^4}\right)^{\frac{1}{2}}}$$

Solution:

Let $\xi = 1$

Then $\omega_n = \frac{1}{2.5}\ \omega_{3db}$

Let:

$$\omega_{3db} = 1 \text{ KHz}$$

$$\omega_n = 400 \text{ Hz}$$

From equation (2):

$$\tau_1 = \frac{K_\phi K_o}{N\omega_n^2}$$

From equation (3):

$$\tau_2 = \frac{2\xi}{\omega_n}$$

Experimental Results

From these equations and the following circuit parameters the filter components can be found:

$\xi = 1$	$R_1 = 2$ K
$\omega_n = 400$ Hz	$R_2 = 5$ K
$K_\phi = 1.91$ volts/radians	$C = .16$ μf
$K_o = 3.2 \times 10^3$ radians/sec.volt	
$N = 2$	

Fig.I-3A and B are photographs showing the response of a frequency step (ramp in phase) of the PLL with different scope time-base settings. Trace 1 is the input frequency step; Trace 2 is the error voltage at the output of the S/H; Trace 3 is the input voltage to the VCO. This voltage is proportional to the output frequency and hence it is a good indication of the PLL output frequency. The second trace shows the sample nature of the PLL; however, the sample frequency is sufficiently high so as not to interfere with the behavior of the system. It should

also be noticed that the error voltage (Trace 2) has a steady state value equal to zero, typical of a TYPE II or higher type system. Finally, from the last trace, the damping factor can be seen to be one, as originally intended.

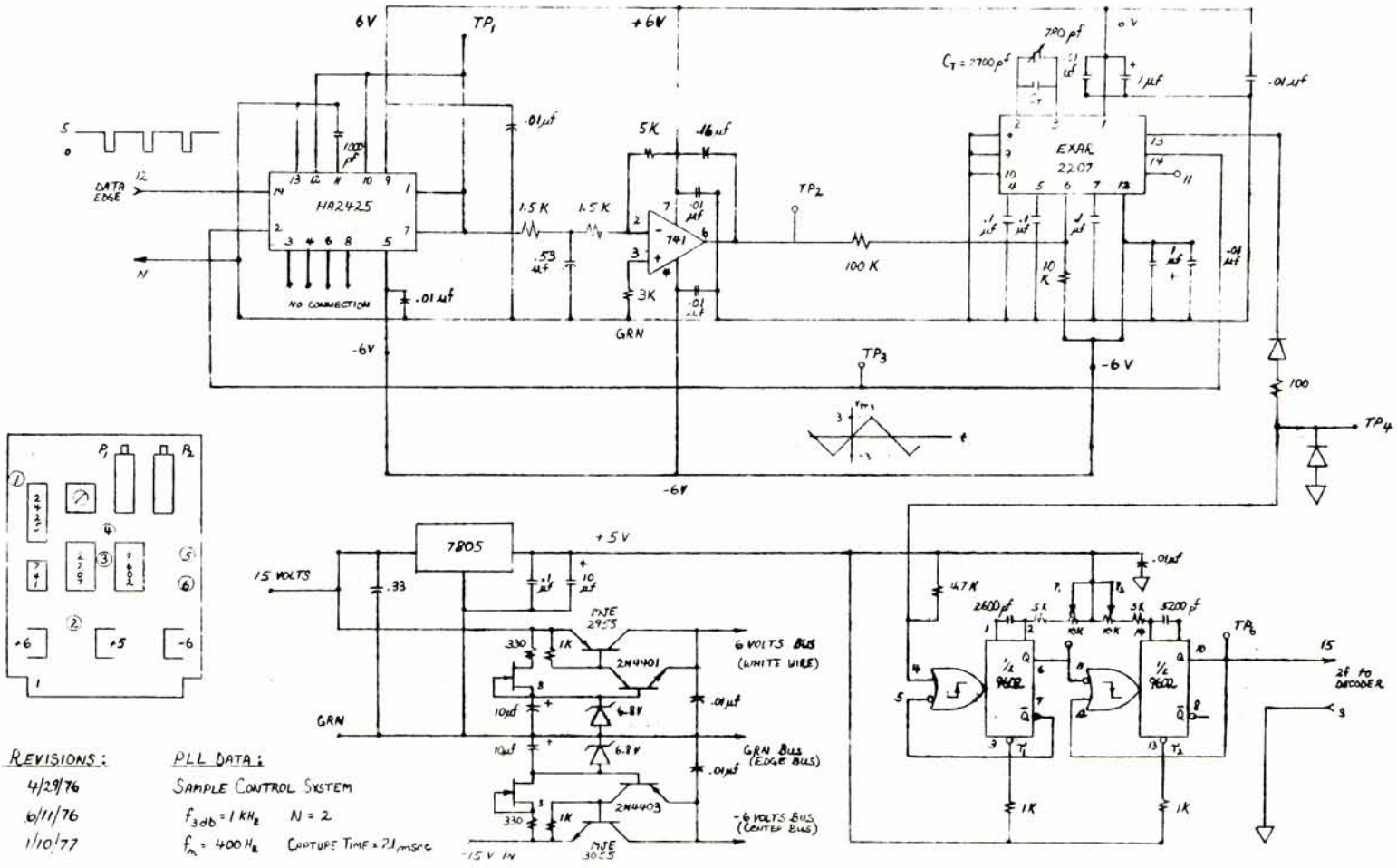

REVISIONS:

4/29/76
6/11/76
1/10/77

PLL DATA:

SAMPLE CONTROL SYSTEM

$f_{3db} = 1\ KH_z$ $N = 2$

$f_m = 400\ H_z$ CAPTURE TIME = 21 msec

Fig. I-1 DECODING PHASE LOCKED LOOP

L. E. A. K. 1/14/76

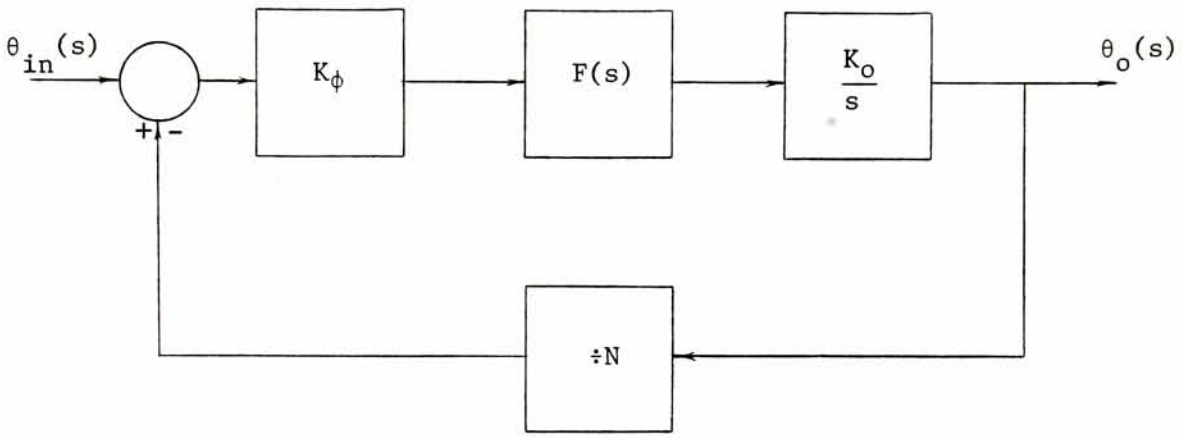

$K_\phi \equiv$ Phase detector gain constant (in volts sec/radian)

$K_o \equiv$ Voltage control oscillator constant (in radians/sec volt)

$F(s) \equiv$ Filter transfer function

$N \equiv$ Feedback gain constant (dimensionless)

Fig. I-2 Phase-locked loop block diagram

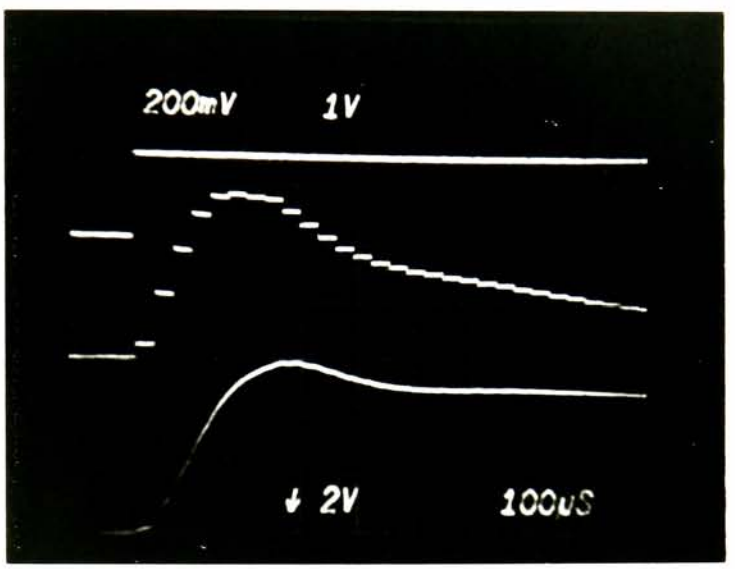

Scope Time Base = 100 μsec/cm

Trace 1 - Input Phase Step
Trace 2 - Error Voltage
Trace 3 - Response of Phase-Locked Loop

Fig. I-3A Step response of the phase-locked loop

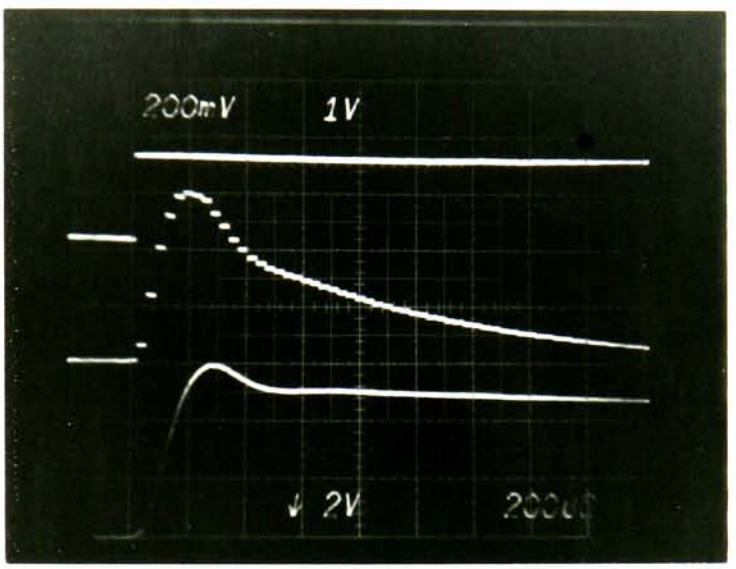

Scope Time Base = 200 μsec/cm

Trace 1 - Input Phase Step
Trace 2 - Error Voltage
Trace 3 - Response of Phase-Locked Loop

Fig.I-3B Step response of the phase-locked loop

BIBLIOGRAPHY

1. Panter, Philip F. Modulation Noise and Spectral Analysis, pp. 679-690, McGraw-Hill Book Co., New York, 1965.

2. Lender, A. "Delta Modulation Study", I.T.T. Internal Lab Report 1565.

3. Taub, Herbert and Schilling, Donald. Principles of Communication Systems, pp. 216-220, McGraw-Hill Book Co., New York, 1971.

4. Spitzer, Charles F. (Ampex Corp.) "Digital Recording of Video Signals up to 50 MHz, Military Airborn Video Recording: Requirements, Utilization and Techniques", Proceedings, SPIE, Vol.36, April 3-5, 1973.

5. Breikss, Ivars P. (Honeywell) "High Density Data Recording", IEEE Spectrum, May, 1975.

6. Jensen, Ted and Starkey, Marvin (Ampex Corp.) "80 MBPS Recording", Journal on Digital Systems (TRW Systems Group), Sept. 1974.

7. Harris, Aubrey. "Time Base Errors and Their Correction in Magnetic Television Recorders", Journal of the SMPTE, July, 1961.

8. IEEE Group on Audio and Eelctroacoustics Standards Committee. "IEEE Standard Method for Measurement of Weighted Peak Flutter of Sound Recording and Reproducing Equipment", 1971.

9. Knight, John G. "The New Standard for Weighted Peak Flutter Measurements", DB Journal, Jan. 1974.

10. Davies, Gomer L. Magnetic Tape Instrumentation, McGraw Hill Book Co., 1961.

11. Gardner, Floyd M. Phase Lock Techniques, John Wiley & Son, Inc., New York, 1966.

12. Ampex Research & Engineering Internal Report, RB67-34, August 1967.

13. Shannon, C.E. "A Mathematical Theory of Communication", Bell Systems Technical Journal, Vol.27, pp. 279-623, 1948.

14. Lucky, R.W.; Salz, J.; and Weldon, E.J., Jr. Principles of Data Communication, McGraw Hill Book Co., New York, 1968.